

Constraining tensor-to-scalar ratio based on VLBI observations: PGWs induced-incoherence approach

F. S. Arani,^{a,b,c} M. Bagheri Harouni^{a,d} Brahim Lamine^{b,c,1} Alain Blanchard^{b,c}

^aDepartment of Physics, University of Isfahan, Hezar Jerib Str., Isfahan 81746-73441, Iran

^bUniversité de Toulouse, UPS-OMP, IRAP, F-31400 Toulouse, France

^cCNRS, IRAP, 14 avenue Edouard Belin, F-31400 Toulouse, France

^dQuantum Optics Group, Department of Physics, University of Isfahan, Hezar Jerib Str., Isfahan 81746-73441, Iran

E-mail: fshojaei@irap.omp.eu, m.bagheri@sci.ui.ac.ir, brahim.lamine@irap.omp.eu

Abstract. In this study, we show that the background of primordial gravitational waves (PGWs) predicted by the inflationary scenario induces a decrease in the spatial coherence length of an electromagnetic (EM) field propagating over cosmological distances, leading the van Citter-Zernike correlations to become eventually unobservable, an effect called as blurring. Since this spatial correlation is observed in VLBI measurements of distant quasars, it imposes a constraint on the level of the primordial gravitational wave background. In this paper, we formulate the interaction between the EM and a generic GW background, and precisely evaluate the blurring effect by considering the primordial gravitational waves background to be in the so-called two-mode squeezed state, which is the standard quantum state predicted by the simplest scenario of inflation. We then exploit a sample of compact radio quasars at redshift range $0.46 \leq z \leq 2.73$ observed by very long baseline interferometry (VLBI) means. These quasars constitute a standard ruler of size 11 pc, based on which the angular size-distance $\theta - z$ relation is determined thanks to the measurement of their spatial coherence. These spatial coherence observations set an upper limit on the squeezing parameters of the PGWs background, which turns into an upper limit for the tensor-to-scalar ratio r_{k_0} . Ultimately, one finds $r_{k_0} < 10^{-6.15}$, four orders of magnitude better than present constraints on this parameter with the CMB. This result is nevertheless compatible with the possible detection of a cosmic background by the pulsar timing array recent observation. Further issues and caveats that potentially affect the results are reviewed. In particular, the possible effect of the quantum-to-classical transition of PGWs is discussed. At last, we promote the idea of using high-precision VLBI measurement of angular size-redshift of distant sources as a new possible way of constraining the background of primordial tensor perturbations.

¹Corresponding author.

Contents

1	Introduction	1
2	PGWs in expansionary Universe	3
2.1	Expansionary Universe	3
2.2	PGWs amplification in expanding Universe	5
2.3	Quantum normalization condition (QNC)	9
3	Quantum mechanical EM-GWs interaction	10
3.1	Hamiltonian formalism for EM-GWs interaction in flat spacetime	10
3.2	Heisenberg equation of the EM field in the presence of GWs	12
4	Loss of spatial coherence induced by two-mode squeezed PGWs	16
4.1	Spatial correlations in the presence of GWs	16
4.1.1	Configuration of a VLBI-type system	16
4.1.2	Equal-time first-order degree of coherence $g^{(1)}(\mathbf{x}_1, t; \mathbf{x}_2, t)$	17
4.2	First-order degree of coherence in the presence of PGWs in two-mode squeezed state	20
4.2.1	Contribution of vacuum fluctuations of GWs in spatial incoherence	22
4.2.2	Contribution of gravitons in two-mode squeezed state in spatial incoherence	24
4.3	The intensity and visibility	25
5	Implication of PGWs background on the VLBI measurements	26
5.1	van Citter-Zernike theorem and Very Long Baseline Interferometry (VLBI)	26
5.2	VLBI measurement of the angular size of standard ruler	28
5.3	Definition of the incoherence parameter $\alpha^{\text{ts}}(z)$ versus redshift	28
5.4	VLBI constraint on the tensor-to-scalar ratio r_{k_0}	30
6	Further discussion and results	32
6.1	Implications for the slow-roll framework	32
6.2	Possible quantum-to-classical transition issue	33
7	Summary and conclusion	33
8	Supplementary materials	34
A	PGWs spectrum and related parameters	34
A.1	Increase parameters $\zeta_E, \zeta_2, \zeta_s, \zeta_1$	34
A.2	Spectral amplitude of PGWs	35
A.3	Characteristic wave numbers K_E, K_H, K_2, K_s and K_1	36
B	Hamiltonian formalism for description of EM-GWs interaction	36
B.1	Derivation of the EM-GWs Hamiltonian $\hat{H}_{\text{em-gw}}$ in the adiabatic limit	37
B.2	Orthogonality relation of the mode functions $\mathbf{f}_{\mathbf{k}}(\mathbf{x}, t)$	38
B.3	Derivation of the interaction Hamiltonian $\hat{H}_{\text{em-gw}}$ in the adiabatic limit	41

C Preliminaries for evaluation of $g^{(1)}(\mathbf{x}_1, t; \mathbf{x}_2, t)$	47
C.1 Mutual intensity of a planar source in the presence of PGWs	47
C.2 Separating different scales k and K in the expression of $g^{(1)}(\mathbf{x}_s^{(\mathbf{k})}, \mathbf{x}_1, t; \mathbf{x}_s^{(\mathbf{k})}, \mathbf{x}_2, t)$	48
C.3 Evaluation of the integral $\int d^3\mathbf{K} \kappa_\gamma^2(\mathbf{K}, \mathbf{k})$	51
C.4 Expression of the time of flight t and distance L versus redshift z	53

1 Introduction

Interferometric methods have found vast applications in testing gravity either at the classical or quantum level. Starting from the famous Michelson-Morley interferometer to rule out the motion through “aether”, light interferometry is now routinely used as a crucial technique to detect the tiniest effects of gravitational waves (GWs) with an incredible precision [1–5]. Whether these ripples in spacetime obey quantum mechanical rules at a fundamental scale, say the Planck scale, is an open question and we lack any direct observational evidence in favor of that [6, 7].

It is believed that space and time when viewed at Planck scales, form a foam-like structure due to quantum fluctuations of the vacuum metric tensor of spacetime [8–10]. Searching for Planck-scale quantum features of spacetime is an old quest and many interferometric schemes based on the phase properties of electromagnetic (EM) radiation of distant objects have been proposed to inquire it [11–16]. For instance, the phase interferometric approach early introduced in [12] inspects the Planck-scale physics through the spacetime foam-induced *phase incoherence* of light emitted from distant objects. It has been perceived that the accumulation of tiny phase-incoherence during the long journey of light through the quantum fluctuations of the vacuum spacetime leads to the loss of the phase of radiation at large distances. This approach was elaborated in [13] to rule out or put stringent limits, on some Planck-scale phenomenological models, by evidence of the diffraction pattern from the Hubble Space Telescope observations of SN 1994D at $z = 5.34$.

However, further studies [17] declared that such effects “are far below what is required in this approach to shed light on the foaminess of spacetime”. Moreover, it turned out that “propagation of spatial correlations is governed by the van Citter-Zernike theorem [18], and spatial correlations are immune to any underlying fuzzy Planck scale”, hence the Planck scale remains inaccessible to interferometer detection with present technology [19]. Albeit, this result leaves room for quantum gravitational effects of length scales much larger than the Planck length.

One important example is the relic background of quantum tensor perturbations naturally generated by the pumping engine of inflation. At the heart of cosmology, the inflationary scenario predicts that quantum fluctuations of the gravitational field present in the very early Universe have evolved and been amplified during the successive expansion of the Universe, and constitute a stochastic background of primordial gravitational waves (PGWs) today [20–32]. Due to its specific generating mechanism, PGWs spectrum span a full range of frequencies, corresponding to wavelengths much larger than the Planck scale. Thereupon, the quest for PGWs has made one of the main targets of today’s and upcoming GWs detectors in different frequency bands: LIGO [33], Advanced LIGO [34, 35], VIRGO [36, 37], GEO [38, 39], AIGO [40, 41], LCGT [42], ET [43, 44] aiming at the frequency range ($10^2 - 10^3$) Hz; the space interferometers, such as the future LISA [45, 46] which is sensitive in the frequency range ($10^{-4} - 10^{-1}$) Hz, BBO [47–49] and DECIGO [50, 51] both sensitive in frequency range (0.1 – 10) Hz; and the pulsar timing arrays [52–56], including PPTA [57–59] and the planned

SKA [60] working in frequency window ($10^{-9} - 10^{-6}$) Hz. Besides, there are potential proposals able to detect the very-high-frequency part of PGWs, among which are the waveguide detector [61–64], the proposed gaussian maser beam detector around GHz [65–67], and the 100 MHz detector [68]. Moreover, the very low-frequency portion of PGWs contributes to the anisotropy and polarization of cosmic microwave background (CMB) [69–75], yielding a magnetic-type polarization of CMB as a distinguished signal of PGWs, which would possibly be sensed using WMAP [76–80], Planck [81, 82], liteBIRD [83], the ground-based ACTPol [84] and the proposed CMBpol [85]. Detection of PGWs would not only confirm the inflationary scenario but also validate the quantum description of gravity at scales much larger than the Planck length.

In the present study, we introduce a new schema to search for the unique imprints of the PGWs on the spatial correlations of the EM emission from furthest objects and show how high-precision measurements of the angular size θ of distant objects using Very Long Baseline Interferometers (VLBI) can exert constraints on PGWs. The VLBI imaging technique takes advantage of the largest possible baselines (from several meters to thousands of kilometers) to precisely determine the location and fine structure of astronomical sources including Active Galactic Nucleis (AGNs) [86–90]. In a typical VLBI experiment, the incoming radiation of a distant source is collected by two or more spatially separated telescopes (see Fig. 2). The existence of spatial correlations throughout the projected baseline of the interferometer leads to the appearance of an interference pattern (non-vanishing visibility), which is used to determine the geometrical properties of the object, such as its angular diameter.

Noticeably, VLBI imaging has found great attention in constraining cosmology. For instance, the Event Horizon Telescope (EHT) which is a VLBI array imaging supermassive black holes (SMBHs) on event horizon scales, allows tests of deviation from general relativity by performing high precision measurements of the Kerr metric [91, 92]. Moreover, the Megamaser Cosmology Project (MCP) which is based on the VLBI sub-milliarcsecond angular mapping of compact objects, has provided an independent laboratory to constrain the Hubble constant, H_0 , in parallel to other surveys such as CMB [93], likewise putting updated constraints on the mass of SMBHs [94]. In particular, capability of VLBI method in accurate measurement of the angular size-redshift $\theta - z$ of intermediate-luminosity radio quasars has led to specify AGNs as astrophysical standard rulers with intrinsic size $\ell_m \sim 11.03$ pc, that can be used to constrain cosmological parameters [95–97]. Recently, the capability of stellar interferometry as a potential tool to detect GWs in the lower frequency range ($10^{-6} - 10^{-4}$) Hz is investigated [98]. However, to our best knowledge, VLBI measurements of the angular size-redshift have not yet been used to constrain the background of PGWs. Here, we promote the idea of employing stellar interferometric methods to constrain the underlying gravitational background of PGWs. We show how VLBI measurements of the angular size-redshift may put new constraints on the inflationary parameters, in particular the tensor-to-scalar ratio r_{k_0} .

It is worth mentioning that, in the literature, there are numerous schema that focus on graviton-induced *decoherence* (GID) of light [99, 100] or particles [101, 102]. As a matter of fact, due to negligibly small coupling strength between gravity and radiation or matter fields, one usually needs a huge interaction time to observe the GID effect, provided that the system is completely isolated from other environmental effects that may lead to decoherence. In contrast, spatial correlations of a source are known to be immune to the typical environment-induced-decoherence. In particular, van Citter-Zernike theorem implies that the correlation length of initially spatial-incoherent sources grows with distance [18]. However, we show that

PGWs background acts as a competitive mechanism that tends to reduce spatial correlation length. Hence, sources with cosmological distances that have had enough time to interact with the underlying gravitational background seem proper candidates to explore the underlying quantum gravitational effects.

The paper is organized as follows. Sec. 2 provides a brief introduction to the expansionary Universe, the generation of two-mode squeezed PGWs from vacuum fluctuations, and the definition of the related quantities of PGWs. In Sec. 3, a self-contained investigation of the EM-GWs interaction at the quantum level is included, followed by solving the Heisenberg equation of motion of the EM field. This will help us investigate the two-point correlation function of the EM radiation in Sec. 4, where the loss of correlations induced by two-mode squeezed PGWs is evaluated and characteristic length scales are defined. Sec. 5 is devoted to the definition of the visibility and the coherence criteria that can be established with the help of current VLBI measurements. Eventually, we assess the coherence criteria based on the angular diameter-distance $\theta - z$ measurement of a set of compact radio-quasars, which are suggested as standard rulers, and try to constrain the underlying PGWs background based on that. In particular, we obtain interesting constraint on the tensor-to-scalar ratio, namely $r_{k_0} \leq 10^{-6.15}$, five orders of magnitude better than present constraints. In Sec. 6, further possible topics and caveats that can be addressed within the present method are discussed, followed by a summary and conclusion in Sec. 7. A complete supplementary material containing the details of the derivation of the equations and their subtleties is provided in Apps. A-C. Throughout the paper, we explicitly write c , \hbar , and G in all equations. Table 1 contains the list symbols and notations involved in the present study.

2 PGWs in expansionary Universe

2.1 Expansionary Universe

The spatially flat expanding Universe is often described by the Friedmann–Lemaître–Robertson–Walker (FLRW) metric assuming a power-law scale factor $a(\eta) \propto \eta^\alpha$, where η is the conformal time. Each successive expanding stage is specified with a different index α . The whole expansion history can be described by [103]

$$a(\eta) = \begin{cases} \ell_0 |\eta|^{1+\beta} & , \quad -\infty \leq \eta \leq \eta_1 \\ a_z (\eta - \eta_p)^{1+\beta_s} & , \quad \eta_1 \leq \eta \leq \eta_s \\ a_e (\eta - \eta_e) & , \quad \eta_s \leq \eta \leq \eta_2 \\ a_m (\eta - \eta_m)^2 & , \quad \eta_2 \leq \eta \leq \eta_E \\ \ell_H |\eta - \eta_a|^{-\gamma} & , \quad \eta_E \leq \eta \leq \eta_H \end{cases} \quad (2.1)$$

where η_H is the conformal time today and $a(\eta)$ has the dimensionality of length [103, 104].

Usually the inflation index β is related to the scalar spectral index of primordial perturbations according to $n_s = 2\beta + 5$ [23, 105, 106]. n_s is a parameter introduced under the assumption that scalar perturbation spectrum obeys a power-law behavior near the pivot scale k_0 , with $n_s = 1$ referred to as the Harrison-Zeldovich spectrum. The *Planck2018* release favor $n_s \simeq 0.9649 \pm 0.0044$ [107], corresponding to $\beta \simeq -2.018 \pm 0.0022$. However, the exact relation between β and n_s depends crucially on the specific inflationary potential through the (first order) slow-roll parameter ϵ_V (see Sec. 6.1). In this study, we consider β as a free parameter of the model. However, for the sake of illustration, we mostly take $\beta = -2.0$.

Table 1. List of symbols and notations.

symbol	description
η	conformal time
$a(\eta)$	scale factor in conformal time
$\mathcal{H}(\eta)$	Hubble parameter in conformal time
$(\Omega_K/c, \mathbf{K})$	GWs four wave vector
(K, Θ_K, Φ_K)	GWs wave vector in spherical coordinates
$e_{ij}^\gamma[\hat{\mathbf{K}}]$	polarization tensor
$\hat{S}_{\mathbf{K}}(\zeta_K)$	two-mode squeezing operator
$\hat{R}_{\mathbf{K}}(\theta_K)$	rotation operator
$\zeta_K = r_K e^{2i\phi_K}$	squeezing parameter
(r_K, ϕ_K)	squeezing amplitude and phase
θ_K	rotation parameter
$\zeta_1, \zeta_s, \zeta_2, \zeta_E$	increase parameters
A	initial amplitude of tensor perturbations at $K = K_H$ scale
(A_s, n_s)	scalar power spectrum and spectral index
(A_T, n_T)	tensor power spectrum and spectral index
ϵ_V	slow-roll parameter
T_{reh}	reheating temperature
k_0	pivot scale
r_{k_0}	tensor-to-scalar ratio at the pivot scale
K_E, K_H, K_2, K_s, K_1	characteristic wave numbers
$(\omega_k/c, \mathbf{k})$	EM four wave vector
$(\mathbf{x}_s, \mathbf{x}_r)$	sender and receiver's locations
\mathbf{x}_P	observation point
$(\mathbf{x}_1, \mathbf{x}_2)$	location of two detectors on the Earth
$V = L_x L_y L_z$	the EM-GW interaction volume
$(\bar{\epsilon}, \bar{\mu})$	permittivity and permeability tensors
$\nu_k(\mathbf{x}, t)$	temporal mode function of the EM field
$\mathbf{f}_k(\mathbf{x}, t)$	spatial mode function of the EM field
$\mathbf{A}(\mathbf{x}, t)$	vector potential of the EM field
α_k	electromagnetic field expansion coefficient
$\hat{\mathbf{u}}_{\mathbf{k}}$	EM field polarization unit vector
ϵ_{ijr}	Levi-Civita symbol
$n_k(\mathbf{x}, t)$	refractive index corresponding to the GW's medium
ϑ_s	angle between the baseline and the source's orientation
θ	angular diameter of the source
σ	planar source
(ρ, ϕ)	polar coordinates of the the surface element $d\sigma$ with respect to origin
$(\theta_{\mathbf{k}}, \phi_{\mathbf{k}})$	spatial angles of electromagnetic mode \mathbf{k}
L	distance of the source
z	redshift of the source

The parameter β_s describes the expansion during the reheating stage starting right after the end of inflation and may be related to the equation of state (EoS) parameter during the

reheating stage, w_{reh} , and to the inflationary model parameters. In the literature, usually, $\beta_s = 1$ is chosen, which may correspond to a quadratic inflation potential with EoS parameter $w_{reh} = 0$ [104, 108]. As discussed in App. (A.3), β_s affects only the high-frequency part of the PGWs spectrum, which will leave a negligible effect on the incoherence of the EM field that we study in this paper. Hence we mostly adopt the value $\beta_s = 1$ in our investigations.

The parameter γ determines the late expansion of the Universe governed by dark energy Λ . Throughout later numerical investigations, we take $\gamma = 1$ which would correspond to a pure de Sitter acceleration phase [109]. On the other hand, the present scale factor is conveniently chosen $a(\eta_H) = \ell_H$, so that the condition $|\eta_H - \eta_a| = 1$ turns out [109]. The constant ℓ_H is determined by $\ell_H = \gamma/H_0$ as a result of Eq. (2.1). Here, $H_0 = 67.4 \text{ km s}^{-1} \text{ Mpc}^{-1}$ is the present Hubble constant [110].

Considering β and β_s as free parameters, there remain 12 constants in Eq. (2.1), 8 of which are reduced by the continuity of $a(\eta)$ and its derivative at four jointing points η_1, η_s, η_2 and η_E , resulting in 4 independent parameters. One usually expresses these 4 parameters in terms of increase of the scale factor during various stages, namely, $\zeta_1 \equiv a(\eta_s)/a(\eta_1)$, $\zeta_s \equiv a(\eta_2)/a(\eta_s)$, $\zeta_2 \equiv a(\eta_E)/a(\eta_2)$, and $\zeta_E \equiv a(\eta_H)/a(\eta_E)$. For the accelerating stage in the simple Λ CDM model, one has $\zeta_E = 1 + z_E \sim 1.33$, where z_E is the redshift when the accelerating stage begins. For the matter-dominated stage one has $\zeta_2 = (1 + z_{eq})\zeta_E^{-1} \sim 2547$ with $z_{eq} = 3387$ [110] being the redshift at matter-radiation equality (see App. A.3). The increase of scale factor during the reheating and radiation-dominated stages, namely ζ_1 and ζ_s , generally depend on the reheating temperature T_{reh} at which the radiation stage begins (see Appendix A for details). Big Bang Nucleosynthesis (BBN) and the energy scale at the end of inflation put lower and upper bounds on T_{reh} as $T_{reh} \geq 10 \text{ MeV}$ and $T_{reh} \leq 10^{16} \text{ GeV}$, respectively [111]. However, the CMB data modify the lower bound on the reheating temperature $T_{reh} \geq 6 \times 10^3 \text{ GeV}$ [111], and gravitinos generation has given the upper bound $T_{reh} \leq 10^7 \text{ GeV}$ [112]. As discussed in App. A.3, T_{reh} does not play a significant role in the incoherence of the EM field, since it only changes the high-frequency part of the PGWs spectrum (see Fig. 1). However, the value of T_{reh} could affect the range of other parameters, including β, β_s, ζ_1 , when considering specific inflationary scenarios (see [113] for example). In this paper, we mainly adopt $T_{reh} = 10^8 \text{ GeV}$ for the sake of illustration. The specific T_{reh} -dependence of ζ_s is determined by Eq. (A.3), though ζ_1 is usually regarded as a free parameter. So far, four parameters ($\beta, \beta_s, T_{reh}, \zeta_1$) determine the expansion of the Universe. The introduction of primordial perturbations adds extra degrees of freedom, namely the scalar and tensor power spectrum, $A_{s,T}$, and the scalar and tensor spectral indices, $n_{s,T}$, at some pivot scale k_0 , among which we only treat A_T (or equivalently the tensor-to-scalar ratio r_{k_0}) as free parameter and use the current constraints on A_s and n_s made by *Planck2018* observations (see Sec. 2.3).

2.2 PGWs amplification in expanding Universe

Inflationary-generated PGWs originate from tensor perturbations of the FLRW metric during the inflationary era. Starting from the vacuum state, they have been amplified during the expansion of the Universe. The super-adiabatic amplification leads vacuum tensor perturbations to evolve into a two-mode squeezed (TS) state with an enormously large number of gravitons [114, 115]. Dynamics of the tensorial perturbations are governed by the perturbed Hilbert-Einstein action in FLRW Universe [116]

$$S[h_{ij}] \simeq \frac{M_{\text{Pl}}^2 c^2}{8\hbar} \int d\eta d^3\mathbf{x} a^2(\eta) \left(h^{ij'} h'_{ij} - \partial^k h^{ij} \partial_k h_{ij} \right), \quad (2.2)$$

where $M_{\text{Pl}}^2 = \hbar c / (8\pi G)$ is the reduced Planck mass. Here, $'$ denotes the derivative with respect to conformal time η , and spatial indices are raised and lowered with the help of the unit tensor δ_{ij} , assuming the metric signature $(-, +, +, +)$. To decouple time and spatial variables, it is convenient to introduce the Fourier transform of the metric perturbation $h_{ij}(\mathbf{x}, \eta)$ by

$$h_{ij}(\mathbf{x}, \eta) = \frac{\sqrt{2\hbar}}{M_{\text{Pl}}c} \sum_{\gamma=+, \times} \int_{\mathbf{K} \in \mathbb{R}^3} \frac{d^3\mathbf{K}}{(2\pi)^{3/2}} e_{ij}^\gamma(\hat{\mathbf{K}}) h_{\mathbf{K}}^\gamma(\eta) e^{i\mathbf{k}\cdot\mathbf{x}}, \quad (2.3)$$

where $\mathbf{K} = K\hat{\mathbf{K}}$ denotes the conformal wave vector, $e_{ij}^\gamma(\hat{\mathbf{K}})$ stands for the polarization tensor and $\gamma = +, \times$ represents the polarization state of tensor perturbations. Since the tensor field $h_{ij}(\mathbf{x}, \eta)$ is real, one has $e_{ij}^\gamma(\hat{\mathbf{K}}) = e_{ij}^{\gamma*}(\hat{\mathbf{K}})$ and $h_{-\mathbf{K}}^\gamma(\eta) = h_{\mathbf{K}}^{\gamma*}(\eta)$. This property implies that, in the Fourier space, all degrees of freedom are not independent, since the metric perturbation $h_{ij}(\mathbf{x}, \eta)$ is a real quantity while $h_{\mathbf{K}}^\gamma(\eta)$ is complex. Note that, throughout the paper, we shall use upper-case letters $K = (\Omega_K/c, \mathbf{K})$ to represent the four-momentum of GWs, while lower-case letters $k = (\omega/c, \mathbf{k})$ will be used to represent the four-momentum of the EM field. The polarization tensor $e_{ij}^\gamma(\hat{\mathbf{K}})$ fulfills the following conditions

$$K^i e_{ij}^\gamma(\hat{\mathbf{K}}) = 0 \quad , \quad e_{ii}^\gamma(\hat{\mathbf{K}}) = 0 \quad \text{and} \quad e_{ij}^{\gamma*}(\hat{\mathbf{K}}) e_{ij}^{\gamma'}(\hat{\mathbf{K}}) = 2\delta_{\gamma\gamma'}. \quad (2.4)$$

Additionally, the two independent polarization states $\gamma = +, \times$ can be expressed in terms of two unit vectors $(\hat{\mathbf{n}}, \hat{\mathbf{m}})$ orthogonal to the propagation direction $\hat{\mathbf{K}}$ and to each other. In terms of the Euler's angles (Θ_K, Φ_K) , one may specify $(\hat{\mathbf{K}}, \hat{\mathbf{n}}, \hat{\mathbf{m}})$ by

$$\hat{\mathbf{K}} = \begin{pmatrix} \sin \Theta_K \cos \Phi_K \\ \sin \Theta_K \sin \Phi_K \\ \cos \Theta_K \end{pmatrix}, \quad \hat{\mathbf{n}} = \begin{pmatrix} \cos \Theta_K \cos \Phi_K \\ \cos \Theta_K \sin \Phi_K \\ -\sin \Theta_K \end{pmatrix}, \quad \hat{\mathbf{m}} = \begin{pmatrix} -\sin \Phi_K \\ \cos \Phi_K \\ 0 \end{pmatrix}, \quad (2.5)$$

and the polarization tensors are written as [117]

$$\begin{cases} \hat{e}_{ij}^+[\hat{\mathbf{K}}] = \hat{n}_i \hat{n}_j - \hat{m}_i \hat{m}_j, \\ \hat{e}_{ij}^\times[\hat{\mathbf{K}}] = \hat{m}_i \hat{n}_j + \hat{n}_i \hat{m}_j, \end{cases} \quad (2.6)$$

which satisfy Eq. (2.4). Inserting the field expansion Eq. (2.3) into the action Eq. (2.2) and taking variation with respect to the Fourier field amplitude $h_{\mathbf{K}}^\gamma(\eta)$ determines dynamics of the tensor perturbations inside the expanding Universe according to

$$h_{\mathbf{K}}^{\gamma''}(\eta) + 2\mathcal{H}(\eta)h_{\mathbf{K}}^{\gamma'}(\eta) + K^2 h_{\mathbf{K}}^\gamma(\eta) = 0, \quad (2.7)$$

where $\mathcal{H}(\eta) \equiv \frac{a'(\eta)}{a(\eta)}$ is the conformal Hubble parameter. Eq. (2.7) can be solved for a given $a(\eta)$. This procedure has been extensively studied in the literature to obtain an analytical expression for the tensor perturbations (for instance see [118]). Especially, the solution of Eq. (2.7) in two asymptotic regimes is interesting: $K \gg 2\pi\mathcal{H}$ and $K \ll 2\pi\mathcal{H}$, corresponding to short-wavelength (sub-Hubble) and long-wavelength (super-Hubble) regimes, respectively. In the former case, the amplitude of the wave experiences a decay as $h_{\mathbf{K}}^\gamma(\eta) \propto 1/a(\eta)$, while in the latter case, the amplitude stays constant during the whole long-wavelength regime [22].

or our discussion, we chose the formalism and notations that was previously introduced for the quantization of scalar perturbations in [114, 115]. Following the same procedure that

is presented in detail in [115], one ends up with the following Hamiltonian governing the evolution of tensor perturbations

$$\hat{H} = \hbar \sum_{\gamma=+, \times} \int_{\mathbf{K} \in \mathfrak{R}^{3+}} d^3\mathbf{K} \left[K(\hat{b}_{\mathbf{K}, \gamma} \hat{b}_{\mathbf{K}, \gamma}^\dagger + \hat{b}_{-\mathbf{K}, \gamma} \hat{b}_{-\mathbf{K}, \gamma}^\dagger) - i \frac{a'}{a} (\hat{b}_{\mathbf{K}, \gamma} \hat{b}_{-\mathbf{K}, \gamma} - \hat{b}_{\mathbf{K}, \gamma}^\dagger \hat{b}_{-\mathbf{K}, \gamma}^\dagger) \right]. \quad (2.8)$$

Here, $(\hat{b}_{\mathbf{K}, \gamma}, \hat{b}_{\mathbf{K}, \gamma}^\dagger)$ denote the bosonic operators of mode (\mathbf{K}, γ) of tensor perturbations. The advantage of using half Fourier space is that the opposite momenta in $\mathbf{K} \in \mathfrak{R}^{3+}$ are independent and their corresponding operators commute. Hamiltonian Eq. (2.8) is the generator of the two-mode squeezed states as previously investigated in the context of quantum optics [119, 120]. Thus, interaction with the pumping field of the expanding Universe leads the vacuum of tensor perturbations to get energy and evolve into a two-mode squeezed state [22, 114, 115]. For our later use in subsequent sections, here we adopt the Schrödinger picture. Thus, the quantum field operator of tensor perturbations at all times is determined by its initial value, i.e.,

$$\begin{aligned} \hat{h}_{ij}(\mathbf{x}, \eta_{\text{ini}}) = \mathcal{C} \sum_{\gamma=+, \times} \int_{\mathbf{K} \in \mathfrak{R}^{3+}} \frac{d^3\mathbf{K}}{(2\pi)^{3/2}} \frac{e^{i\gamma_j(\hat{\mathbf{K}})}}{\sqrt{2\Omega_K}} \left\{ (\hat{b}_{\mathbf{K}, \gamma}(\eta_{\text{ini}}) + \hat{b}_{-\mathbf{K}, \gamma}^\dagger(\eta_{\text{ini}})) e^{i\mathbf{K} \cdot \mathbf{x}} \right. \\ \left. + (\hat{b}_{\mathbf{K}, \gamma}^\dagger(\eta_{\text{ini}}) + \hat{b}_{-\mathbf{K}, \gamma}(\eta_{\text{ini}})) e^{-i\mathbf{K} \cdot \mathbf{x}} \right\}, \end{aligned} \quad (2.9)$$

where $\mathcal{C} = \sqrt{16\pi c \ell_{\text{Pl}}}$, and η_{ini} denotes some initial time during the inflationary epoch, before the initiation of super-adiabatic amplification. The quantum state of inflationary-generated PGWs at a given conformal time η , governed by the Hamiltonian Eq. (2.8), turns out to be given by

$$|\text{TS}(\eta)\rangle \equiv \prod_{\mathbf{K} \in \mathfrak{R}^{3+}} \hat{S}_{\mathbf{K}}(\zeta_K(\eta)) \hat{R}_{\mathbf{K}}(\theta_K(\eta)) |0_{\mathbf{K}}, 0_{-\mathbf{K}}\rangle, \quad (2.10)$$

which is basically a two-mode squeezed state (hereafter denoted by TS state). Here, because the opposite momenta are not independent degrees of freedom, the multiplication is taken over half Fourier space $\mathbf{K} \in \mathfrak{R}^{3+}$. The two-mode squeezing operator $\hat{S}_{\mathbf{K}}(\zeta_K(\eta))$ and the rotation operator $\hat{R}_{\mathbf{K}}(\theta_K(\eta))$ are defined by (see [115] for details)

$$\begin{aligned} \hat{S}_{\mathbf{K}}(\zeta_K(\eta)) &\equiv \exp \left[\zeta_K^*(\eta) \hat{b}_{-\mathbf{K}} \hat{b}_{\mathbf{K}} - \zeta_K(\eta) \hat{b}_{-\mathbf{K}}^\dagger \hat{b}_{\mathbf{K}}^\dagger \right], \\ \hat{R}_{\mathbf{K}}(\theta_K(\eta)) &\equiv \exp \left[-i\theta_K(\eta) (\hat{b}_{\mathbf{K}}^\dagger \hat{b}_{\mathbf{K}} + \hat{b}_{-\mathbf{K}}^\dagger \hat{b}_{-\mathbf{K}}) \right], \end{aligned} \quad (2.11)$$

where the squeezing parameter is defined by $\zeta_K(\eta) \equiv r_K(\eta) e^{2i\phi_K(\eta)}$ with (r_K, ϕ_K) being the squeezing amplitude and angle, respectively, and the rotation angle is defined by $\theta_K(\eta)$. Also note that we shall use the symbol r_K to represent the squeezing amplitude of the PGWs mode K , while the symbol r_{k_0} is reserved for the tensor-to-scalar ratio at the pivot scale k_0 . The evolution of the squeezing and rotation parameters are determined by [115]

$$\begin{aligned} \frac{dr_K}{d\eta} &= \frac{a'}{a} \cos(2\phi_K), \\ \frac{d\phi_K}{d\eta} &= -K - \frac{a'}{a} \coth(2r_K) \sin(2\phi_K), \\ \frac{d\theta_K}{d\eta} &= -K - \frac{a'}{a} \tanh(2r_K) \sin(2\phi_K). \end{aligned} \quad (2.12)$$

Note that, the equation of motion for the squeezing parameters $(r_K(\eta), \phi_K(\eta))$ are decoupled from the rotation angle $\theta_K(\eta)$, and the latter can be determined once $(r_K(\eta), \phi_K(\eta))$ are determined. Indeed, one may see from Eq. (2.12) that $\hat{R}_{\mathbf{K}}(\theta_K(\eta))|0_{\mathbf{K}}, 0_{-\mathbf{K}}\rangle = |0_{\mathbf{K}}, 0_{-\mathbf{K}}\rangle$, which means that the variable θ_K is not involved in the dynamics of perturbations, as it should be by invariance under rotation.

Equivalently, the three parameters (r_K, ϕ_K, θ_K) may be represented by two complex variables $(u_K(\eta), v_K(\eta))$ defined by [114, 115]

$$\begin{aligned} u_K(\eta) &\equiv e^{i\theta_K(\eta)} \cosh r_K(\eta), \\ v_K(\eta) &\equiv e^{-i\theta_K(\eta)+2i\phi_K(\eta)} \sinh r_K(\eta), \end{aligned} \quad (2.13)$$

which satisfy the normalization $|u_K(\eta)|^2 - |v_K(\eta)|^2 = 1$. The use of $(u_K(\eta), v_K(\eta))$ is most favored in the literature, especially when investigating quantum features of cosmological perturbations [121]. In the present study, we use these two sets of parameters interchangeably.

In the following, we consider the approximate solution to the system of equations (2.12) in the super-Hubble regime $K \ll 2\pi\mathcal{H}$, when the mode K has been amplified sufficiently and the squeezing amplitude is high so that $r_K \gg 1$. The equations (2.12) in the long wavelength regime $K \ll 2\pi\mathcal{H}$ can be approximated by

$$\begin{aligned} r'_K(\eta) &= \frac{a'}{a} \cos(2\phi_K), \\ \phi'_K(\eta) &= -\frac{a'}{a} \coth(2r_K) \sin(2\phi_K) \end{aligned} \quad (2.14)$$

For super-Hubble scales, the squeezing amplitude r_K is very large, so that $\coth(2r_K) \rightarrow 1$. Hence, the equation for ϕ_K yields the following solution

$$\phi'_K(\eta) = -\frac{a'}{a} \sin(2\phi_K) \quad \Rightarrow \quad \tan(\phi_K) \propto \frac{1}{a^2(\eta)}, \quad (2.15)$$

which implies $\tan(\phi_K) \rightarrow 0$ during the long-wavelength regime. The squeezing angle ϕ_K tends to either values 0 or π , both resulting in $\cos(2\phi_K) \rightarrow 1$. Hence the equation of motion for $r_K(\eta)$ reduces to $r'_K(\eta) = a'/a$ with the simple solution $r_K(\eta) = \ln a(\eta)/a_*(K)$, where $a_*(K) \equiv a(\eta_*(K))$ denote the value of the scale factor at the initial moment of horizon-crossing, $\eta_*(K)$, when the long-wavelength regime initiates for a given mode K . The initial value for r_K is chosen as $r_K(\eta_*) = 0$. If one denoted by $\eta_{**}(K)$ the time when the mode leaves the long-wavelength regime and re-enters the Hubble horizon and $K \geq 2\pi\mathcal{H}$, the final value of the squeezing amplitude is determined by

$$e^{r_K} = \frac{a_{**}(K)}{a_*(K)}, \quad (2.16)$$

where $a_{**}(K) = a(\eta_{**}(K))$ denotes the value of scale factor when the mode re-enters the horizon (see [22] for more details). Considering the model of successive expansion of the Universe introduced in Sec. 2.1, one may show that the squeezing factor at present, $e^{r_K(\eta_H)}$, is related to the present spectral amplitude $h(K, \eta_H)$ according to $e^{r_K(\eta_H)} = \frac{1}{8\sqrt{\pi\gamma}} \frac{\ell_H}{\ell_{\text{Pl}}} \left(\frac{K_H}{K}\right) h(K, \eta_H)$,

and is given by (see App. A.2)

$$e^{r_K(\eta_H)} = \frac{1}{8\sqrt{\pi}} \frac{\ell_H}{\ell_{\text{Pl}}} \left(\frac{K_H}{K} \right) \begin{cases} A \left(\frac{K}{K_H} \right)^{2+\beta} & , \quad K \leq K_E \\ A \left(\frac{K}{K_H} \right)^{\beta-1} \frac{1}{(1+z_E)^3} & , \quad K_E \leq K \leq K_H \\ A \left(\frac{K}{K_H} \right)^{\beta} \frac{1}{(1+z_E)^3} & , \quad K_H \leq K \leq K_2 \\ A \left(\frac{K}{K_H} \right)^{1+\beta} \left(\frac{K_H}{K_2} \right) \frac{1}{(1+z_E)^3} & , \quad K_2 \leq K \leq K_s \\ A \left(\frac{K}{K_H} \right)^{1+\beta-\beta_s} \left(\frac{K_s}{K_H} \right) \left(\frac{K_H}{K_2} \right) \frac{1}{(1+z_E)^3} & , \quad K_s \leq K \leq K_1 \end{cases} \quad (2.17)$$

where the characteristic wave numbers K_E, K_H, K_2, K_s and K_1 are determined once the increase parameters $\zeta_1, \zeta_s, \zeta_2$ and ζ_E are fixed (see App. A.3). The coefficient A determines the initial perturbation amplitude that can be assessed by theoretical or observational normalization conditions, as discussed below.

2.3 Quantum normalization condition (QNC)

In the CMB literature, it is convenient to express the contribution of tensor perturbations around the pivot scale k_0 in terms of the so-called tensor-to-scalar ratio, $r_{k_0} \equiv \frac{A_T(k_0)}{A_s(k_0)}$ with $A_{T,s}(k_0)$ being the tensor and scalar power spectrum at the pivot scale k_0 , respectively. We remind that throughout the paper, the pivot scale is exceptionally denoted by k_0 and the symbol r_{k_0} is reserved for the tensor-to-scalar ratio, not to be confused with the squeezing amplitude r_K . We shall take $k_0 = 0.002 \text{ Mpc}^{-1}$ in our calculations [110]. The perturbation field h_{ij} at the initial moment (that is to say before exiting the horizon during the inflationary era) can be treated as a quantum field in its vacuum state, possessing half energy quanta $\frac{1}{2} \hbar \Omega_K$ in each mode K . This assumption imposes a criteria on the initial amplitude A , called the quantum normalization condition (QNC) [22, 103, 122], which translates into a condition on the tensor-to-scalar ratio r_{k_0} . As a result of QNC, it can be shown that one ends up with the following theoretical constraint between the previously discussed parameters $(\beta, \beta_s, T_{\text{reh}}, \zeta_1, r_{k_0})$ [103],

$$A = \sqrt{A_s r_{k_0}} \left(\frac{K_H}{k_0} \right)^{\beta} \zeta_E^{\frac{2+\gamma}{\gamma}} = 8\sqrt{\pi} \left(\frac{\ell_{\text{Pl}} H_0}{c} \right) \gamma^{-(2+\beta)} \zeta_1^{\frac{\beta_s-\beta}{1+\beta_s}} \zeta_s^{-\beta} \zeta_2^{\frac{1-\beta}{2}} \zeta_E^{1+\frac{1+\beta}{\gamma}} \quad (2.18)$$

Upper bounds $A_s \lesssim 2.1 \times 10^{-9}$ and $r_{k_0} < 0.056$ have been obtained by *Planck2018* using TTTEEE + lowE + lensing + BAO [123]. Taking r_{k_0} as free parameter, one may convert Eq. (2.18) to express ζ_1 in terms of the other parameters, namely

$$\zeta_1(\beta, \beta_s, \zeta_s, r_{k_0}) = \left[\frac{c(A_s(k_0)r_{k_0})^{1/2}}{8\sqrt{\pi}\ell_{\text{Pl}}H_0} \left(\frac{K_H}{k_0} \right)^{\beta} \gamma^{2+\beta} \zeta_s^{\beta} \zeta_2^{\frac{\beta-1}{2}} \zeta_E^{\frac{1-\beta}{\gamma}} \right]^{\frac{1+\beta_s}{\beta_s-\beta}}, \quad (2.19)$$

and the expansionary model Eq. (2.1) is fully described by four independent parameters $(\beta, \beta_s, T_{\text{reh}}, r_{k_0})$. The spectral amplitude $h(K, \eta_H)$ and the corresponding squeezing factor $e^{r_K(\eta_H)}$ are shown in figure 1 panel (a) and panel (b), respectively, for different values of the parameters $(\beta, \beta_s, T_{\text{reh}}, r_{k_0})$ (see App. A.2). It can be seen that changing the reheating parameters β_s and T_{reh} changes only the high-frequency part of the spectrum, i.e. $K_s < K < K_1$, which contains only a small amount of squeezing, with respect to the ultra-low frequency part. On the other hand, changing β and r_{k_0} affect almost the whole frequency range of the spectrum.

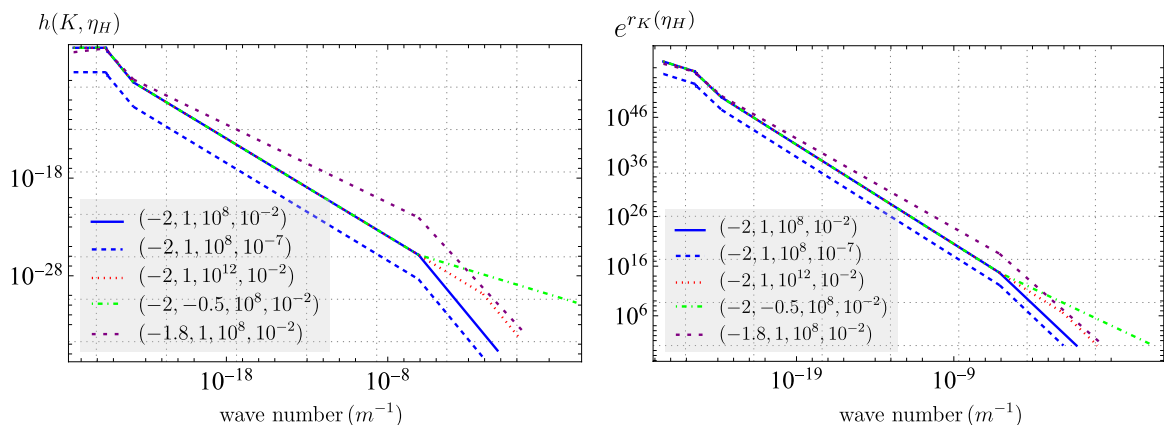


Figure 1. *Panel (a):* today PGWs spectral amplitude $h(K, \eta_H)$ and *panel (b):* the corresponding squeezing factor $e^{r_K(\eta_H)}$, versus the physical wave number $0.01K_E \leq K \leq K_1$ for different values of the parameters $(\beta, \beta_s, T_{\text{reh}}/\text{GeV}, r_{k_0})$.

3 Quantum mechanical EM-GWs interaction

After reviewing the generation of PGWs in TS state in the expanding Universe, in this section, we include a self-contained investigation of the EM-GWs interaction at the quantum level, where we derive and solve the Heisenberg equation governing a single-mode EM field propagating through a quantum background of GWs. This step helps us investigate the Glauber's correlation functions of the EM field in the presence of such quantum background, in the next sections.

3.1 Hamiltonian formalism for EM-GWs interaction in flat spacetime

The imprint of GWs on light is comprehensively studied in the literature, either at classical [117] or quantum level [99, 100, 124, 125]. In the following, we proceed by adopting the formalism presented in [100]. For practical purposes, it seems natural to consider a situation that a single-mode EM field, possessing wave vector \mathbf{k} and frequency ω_k , propagates through the flat Minkowski spacetime and interacts with tensor perturbations $h_{ij}(\mathbf{x}, t)$. The EM field is emitted from a source located at \mathbf{x}_s and reaches a receiver located at \mathbf{x}_r . Quantum mechanical interaction of a continuum of GWs with a single-mode EM field, in the adiabatic approximation where $\omega_k \ll \Omega_K$, can be described by the following total Hamiltonian (see App. B)

$$\hat{H}_{\text{tot}}(\mathbf{x}_s, \mathbf{x}_r, t) = \hat{H}_{\text{em}}^{(0)} + \hat{H}_{\text{gw}}^{(0)} + \hat{H}_{\text{int}}(\mathbf{x}_s, \mathbf{x}_r, t). \quad (3.1)$$

Here, $\hat{H}_{\text{em}}^{(0)}$ and $\hat{H}_{\text{gw}}^{(0)}$ account for free evolution of each sub-system, according to

$$\begin{aligned} \hat{H}_{\text{em}}^{(0)} &= \hbar\omega_k \hat{a}_{\mathbf{k}}^\dagger \hat{a}_{\mathbf{k}}, \\ \hat{H}_{\text{gw}}^{(0)} &= \hbar \sum_{\gamma=+, \times} \int d^3\mathbf{K} \Omega_K \hat{b}_{\mathbf{K}, \gamma}^\dagger \hat{b}_{\mathbf{K}, \gamma}, \end{aligned} \quad (3.2)$$

where $(\hat{a}_{\mathbf{k}}, \hat{a}_{\mathbf{k}}^\dagger)$ are the ladder operators of the EM field satisfying the usual bosonic commutation relation $[\hat{a}_{\mathbf{k}}, \hat{a}_{\mathbf{k}'}^\dagger] = \delta^{(3)}(\mathbf{k} - \mathbf{k}')$. The interaction Hamiltonian is determined by (see

App. B for the details of derivation)

$$\begin{aligned} \hat{H}_{\text{int}}(\mathbf{x}_s, \mathbf{x}_r, t)/\hbar &= -\frac{1}{2} \left(\frac{\hbar\omega_k}{E_{\text{Pl}}} \right) \frac{\sqrt{16\pi c^3}}{(2\pi)^{3/2}} \sum_{\gamma=+, \times} \int d^3\mathbf{K} \frac{F_\gamma(\hat{\mathbf{K}}, \hat{\mathbf{k}})}{\sqrt{2\Omega_K}} \\ &\times \left(\hat{b}_{\mathbf{K}, \gamma} e^{-i\Omega_K t} g(\mathbf{K} \cdot (\mathbf{x}_r - \mathbf{x}_s)) + \hat{b}_{\mathbf{K}, \gamma}^\dagger e^{i\Omega_K t} g^*(\mathbf{K} \cdot (\mathbf{x}_r - \mathbf{x}_s)) \right) \hat{a}_{\mathbf{k}}^\dagger \hat{a}_{\mathbf{k}}, \end{aligned} \quad (3.3)$$

which explicitly depends on the sender and receiver spatial points \mathbf{x}_s and \mathbf{x}_r . Here, the spatial factor $g(\mathbf{K} \cdot (\mathbf{x}_r - \mathbf{x}_s))$ is defined by

$$\begin{aligned} g(\mathbf{K} \cdot (\mathbf{x}_r - \mathbf{x}_s)) &\equiv \frac{1}{V} \int_{\mathbf{x}_s}^{\mathbf{x}_r} d^3\mathbf{x} e^{i\mathbf{K} \cdot \mathbf{x}} \\ &= e^{i\mathbf{K} \cdot \mathbf{x}_s} \prod_{i=1}^3 \frac{e^{iK_i(x_r^i - x_s^i)} - 1}{iK_i(x_r^i - x_s^i)}. \end{aligned} \quad (3.4)$$

with $V \equiv (x_r - x_s)(y_r - y_s)(z_r - z_s) = L_x L_y L_z$ being the interaction volume. One may easily check that for small detectors where the spatial extend of the EM probe is small compared to the GW's wavelength, $K_i(x_r^i - x_s^i) \equiv K_i L_i \ll 1$, the spatial factor $|g(\mathbf{K} \cdot (\mathbf{x}_r - \mathbf{x}_s))|$ tends to unity and the Hamiltonian reduces to that of [126]. However, this factor becomes especially important when we consider the EM propagation through cosmological distances hence we keep it in our investigation. The spatial factor Eq. (3.4) that appears in the Hamiltonian Eq. (3.3) is a generalization of the result of [127] to the case of three-dimensional propagation of the EM probe. The spatio-temporal dependence of the interaction Hamiltonian stems from the spatio-temporal dependence of GWs field $\hat{h}_{ij}(\mathbf{x}, t)$.

Note that the Hamiltonian Eq. (3.3) is obtained in the adiabatic approximation, meaning that $\Omega_K \ll \omega_k$ and $K \ll k$, which is valid concerning the PGWs spectrum $K_E \leq K \leq K_1$ and EM field of radio-frequency $\omega_k \sim \text{GHz}$ used in the VLBI technique. In this approximation, each mode \mathbf{k} of the EM field is scattered only to itself. In general, the momentum conservation implies that the mode \mathbf{k} of the field can be scattered to another mode \mathbf{k}' such that $\mathbf{k}' = \mathbf{k} \pm \mathbf{K}$. However, as far as we consider the adiabatic approximation $K \ll k$, we may ignore higher-order scattering processes. Consequently, the interaction Hamiltonian Eq. (3.3) includes only terms like $\hat{a}_{\mathbf{k}} \hat{a}_{\mathbf{k}}^\dagger$ and $\hat{a}_{\mathbf{k}}^\dagger \hat{a}_{\mathbf{k}}$ which preserve the number of photons in the EM field. Other terms such as $\hat{a}_{\mathbf{k}} \hat{a}_{-\mathbf{k}}$ and $\hat{a}_{\mathbf{k}}^\dagger \hat{a}_{-\mathbf{k}}^\dagger$ which are responsible for the production of photons from GWs are suppressed.

Moreover, the *detector pattern function* $F_\gamma(\hat{\mathbf{K}}, \hat{\mathbf{k}})$ defined by

$$F_\gamma(\hat{\mathbf{K}}, \hat{\mathbf{k}}) \equiv e_{ij}^\gamma[\hat{\mathbf{K}}] \hat{\mathbf{k}}_i \hat{\mathbf{k}}_j, \quad (3.5)$$

accounts for the geometrical configuration of the EM-GWs system (see Eq. (7.21) of [117] for definition of the detector pattern function). Here, $\hat{\mathbf{k}}_i$ represents the unit vector in the direction of the i -th component of \mathbf{k} .

Quantization of GWs in flat spacetime gives rise to the following expression for the field operator [100]

$$\hat{h}_{ij}(\mathbf{x}, t) = \mathcal{C} \sum_{\gamma=+, \times} \int \frac{d^3\mathbf{K}}{(2\pi)^{3/2}} \frac{e_{ij}^\gamma[\hat{K}]}{\sqrt{2\Omega_K}} \left(\hat{b}_{\mathbf{K}, \gamma} e^{-i(\Omega_K t - \mathbf{K} \cdot \mathbf{x})} + \hat{b}_{\mathbf{K}, \gamma}^\dagger e^{i(\Omega_K t - \mathbf{K} \cdot \mathbf{x})} \right), \quad (3.6)$$

where $\mathcal{C} = \sqrt{16\pi c} \ell_{\text{Pl}} = \sqrt{16\pi c^3} (\hbar/E_{\text{Pl}})$ as in Eq. (2.9). The explicit time-dependence in Eq. (3.5) implies that the field operator $\hat{h}_{ij}(\mathbf{x}, t)$, as well as the interaction Hamiltonian Eq. (3.3), are basically written in the *Heisenberg picture* where free time evolution of the ladder operators, $\hat{b}_{\mathbf{K},\gamma}(t) = \hat{b}_{\mathbf{K},\gamma} e^{-i\Omega_{\mathbf{K}} t}$ and $\hat{b}_{\mathbf{K},\gamma}^\dagger(t) = \hat{b}_{\mathbf{K},\gamma}^\dagger e^{i\Omega_{\mathbf{K}} t}$, are explicitly included. The Hamiltonian in the Schrödinger picture is achieved by disregarding the time evolution of the field operators, which results in the following expression for the interaction Hamiltonian in the *Schrödinger picture*

$$\begin{aligned} \hat{H}_{\text{int}}^{(S)}(\mathbf{x}_s, \mathbf{x}_r)/\hbar &= -\frac{1}{2} \left(\frac{\hbar\omega_k}{E_{\text{Pl}}} \right) \frac{\sqrt{16\pi c^3}}{(2\pi)^{3/2}} \sum_{\gamma=+,\times} \int d^3\mathbf{K} \frac{F_\gamma(\hat{\mathbf{K}}, \hat{\mathbf{k}})}{\sqrt{2\Omega_{\mathbf{K}}}} \\ &\times \left(\hat{b}_{\mathbf{K},\gamma} g(\mathbf{K} \cdot (\mathbf{x}_r - \mathbf{x}_s)) + \hat{b}_{\mathbf{K},\gamma}^\dagger g^*(\mathbf{K} \cdot (\mathbf{x}_r - \mathbf{x}_s)) \right) \hat{a}_{\mathbf{k}}^\dagger \hat{a}_{\mathbf{k}}, \end{aligned} \quad (3.7)$$

The Hamiltonian Eq. (3.7) describes the interaction between the EM and GWs fields through the intensity-dependent coupling (proportional to $\hat{a}_{\mathbf{k}}^\dagger \hat{a}_{\mathbf{k}}$) between the EM field and GWs, and is reminiscent of the optomechanical coupling in cavity optomechanics [128]. This analogy turns out to be useful in formulating quantum dynamics of the EM field.

Before proceeding, let us remind that the interaction Hamiltonian (3.7) assumes the flat Minkowski spacetime as the spacetime metric. Let us justify this approximation in our cosmological context. Actually, the EM-GWs interaction occurs in the fabric of FLRW spacetime, and both fields interact with FLRW spacetime in addition to the EM-GWs interaction. For the EM field, the expansion of the Universe leads to the EM frequency redshift according to $\omega_k \rightarrow \omega_k/(1+z)$ with z being the redshift of the source. Moreover, the time of flight of the EM field through cosmological background as well as the distance of the source located at the redshift z must be modified accordingly (see App. B.3). We will return to this point in Sec. 5.3 where we consider spatial correlations of a set of radio-quasars located at redshift range $0.46 \leq z \leq 2.76$. On the other hand, as it was pointed out in Sec. 2.2, when the modes re-enter the Hubble horizon and the short-wavelength regime starts, the spectral amplitude $h(K, \eta)$ suffers a decay, as a result of the expansion of the Universe [22, 23, 103]. However, one may easily show from Eq. (2.12) that the squeezing amplitude $r_K(\eta)$ stays approximately constant, meaning that the mean number of gravitons in the TS state does not change with the expansion of the Universe during the sub-Hubble regime. Consequently, we may proceed by considering the (flat) Minkowski spacetime as the background on which EM and GWs interplay, and eventually enter the effect of Universe expansion on the EM frequency shift as well as on the interaction time (or time of flight) of the EM source and its distance from the Earth. We assume that the squeezing parameters do not evolve during the interaction time, and the squeezing factor is determined by Eq. (2.17) throughout the EM-GWs interaction.

With the help of Hamiltonian Eq. (3.7), we now proceed to the derivation of the Heisenberg equation of motion for the EM field operators.

3.2 Heisenberg equation of the EM field in the presence of GWs

To proceed, we first initialize the *time evolution operator* generated by the Hamiltonian Eq. (3.1). When written in the Schrödinger picture, the total Hamiltonian becomes time-

independent, which lets us write the time evolution operator of the total system as

$$\begin{aligned}\hat{U}(\mathbf{x}_s, \mathbf{x}_r, t) &= e^{-\frac{i}{\hbar} \int_0^t dt' \hat{H}_{\text{tot}}^{(S)}(\mathbf{x}_s, \mathbf{x}_r)} = e^{-\frac{i}{\hbar} t \hat{H}_{\text{tot}}^{(S)}(\mathbf{x}_s, \mathbf{x}_r)} \\ &= \exp \left[-i(\omega_k t) \hat{a}_{\mathbf{k}}^\dagger \hat{a}_{\mathbf{k}} - i \sum_{\gamma} \int d^3 \mathbf{K} (\Omega_K t) \hat{b}_K^\dagger \hat{b}_K \right. \\ &\quad \left. + \frac{i}{2\pi} \left(\frac{\hbar \omega_k}{E_{\text{Pl}}} \right) \sum_{\gamma} \int d^3 \mathbf{K} \frac{F_{\gamma}(\hat{\mathbf{K}}, \hat{\mathbf{k}})}{K^{3/2}} \left(\hat{b}_K g(\mathbf{K} \cdot (\mathbf{x}_r - \mathbf{x}_s)) + \hat{b}_K^\dagger g^*(\mathbf{K} \cdot (\mathbf{x}_r - \mathbf{x}_s)) \right) (\Omega_K t) \right].\end{aligned}\quad (3.8)$$

Here, for the sake of abbreviation we use the notation $K \equiv (\mathbf{K}, \gamma)$. In the second line, Eq. (3.2) and Eq. (3.6) are inserted. To break up \hat{U} into separate exponential factors, we follow the trick introduced in [129] for a single-mode optomechanical interaction, and generalize it to the case of continuum of GWs modes with a space-dependent Hamiltonian. We define the unitary operator \hat{T} as

$$\hat{T} \equiv e^{-\hat{a}_{\mathbf{k}}^\dagger \hat{a}_{\mathbf{k}} \sum_{\gamma} \int d^3 \mathbf{K} \kappa_{\gamma}(\mathbf{K}, \mathbf{k}) \left(\hat{b}_K^\dagger g^*(\mathbf{K} \cdot (\mathbf{x}_r - \mathbf{x}_s)) - \hat{b}_K g(\mathbf{K} \cdot (\mathbf{x}_r - \mathbf{x}_s)) \right)}, \quad (3.9)$$

Here, we have defined

$$\kappa_{\gamma}(\mathbf{K}, \mathbf{k}) \equiv \frac{1}{2\pi} \left(\frac{\hbar \omega_k}{E_{\text{Pl}}} \right) K^{-3/2} F_{\gamma}(\hat{\mathbf{K}}, \hat{\mathbf{k}}), \quad (3.10)$$

which can be interpreted as a measure of the EM-GWs coupling strength. By performing straightforward algebra, one may show that

$$\begin{aligned}\hat{T} \hat{b}_K \hat{T}^\dagger &= \hat{b}_K + \hat{a}_{\mathbf{k}}^\dagger \hat{a}_{\mathbf{k}} \kappa_{\gamma}(\mathbf{K}, \mathbf{k}) g^*(\mathbf{K} \cdot (\mathbf{x}_r - \mathbf{x}_s)), \\ \hat{T} \hat{b}_K^\dagger \hat{T}^\dagger &= \hat{b}_K^\dagger + \hat{a}_{\mathbf{k}}^\dagger \hat{a}_{\mathbf{k}} \kappa_{\gamma}(\mathbf{K}, \mathbf{k}) g(\mathbf{K} \cdot (\mathbf{x}_r - \mathbf{x}_s)), \\ \hat{T} \hat{a}_{\mathbf{k}}^\dagger \hat{a}_{\mathbf{k}} \hat{T}^\dagger &= \hat{a}_{\mathbf{k}}^\dagger \hat{a}_{\mathbf{k}},\end{aligned}\quad (3.11)$$

which is a generalization of the result of [130] to the case of the detector of arbitrary size, for which $KL \sim 1$. For a unitary operator \hat{T} and a given function $f(\{\hat{X}_i\})$ of some operators \hat{X}_i , one has the property $\hat{T} f(\{\hat{X}_i\}) \hat{T}^\dagger = f(\{\hat{T} \hat{X}_i \hat{T}^\dagger\})$. With the help of this property, the time evolution operator may be written as

$$\begin{aligned}\hat{U} &= \hat{T}^\dagger \left(\hat{T} \hat{U} \hat{T}^\dagger \right) \hat{T} = e^{-i\omega_k \hat{a}_{\mathbf{k}}^\dagger \hat{a}_{\mathbf{k}} t} e^{i(\hat{a}_{\mathbf{k}}^\dagger \hat{a}_{\mathbf{k}})^2 \sum_{\gamma} \int d^3 \mathbf{K} \kappa_{\gamma}^2(\mathbf{K}, \mathbf{k}) \left| g(\mathbf{K} \cdot (\mathbf{x}_r - \mathbf{x}_s)) \right|^2 (\Omega_K t)} \\ &\quad \times e^{\hat{a}_{\mathbf{k}}^\dagger \hat{a}_{\mathbf{k}} \sum_{\gamma} \int d^3 \mathbf{K} \kappa_{\gamma}(\mathbf{K}, \mathbf{k}) \left(\hat{b}_K^\dagger g^*(\mathbf{K} \cdot (\mathbf{x}_r - \mathbf{x}_s)) - \hat{b}_K g(\mathbf{K} \cdot (\mathbf{x}_r - \mathbf{x}_s)) \right)} \\ &\quad \times e^{-i \sum_{\gamma} \int d^3 \mathbf{K} \hat{b}_K^\dagger \hat{b}_K (\Omega_K t)} e^{-\hat{a}_{\mathbf{k}}^\dagger \hat{a}_{\mathbf{k}} \sum_{\gamma} \int d^3 \mathbf{K} \kappa_{\gamma}(\mathbf{K}, \mathbf{k}) \left(\hat{b}_K^\dagger g^*(\mathbf{K} \cdot (\mathbf{x}_r - \mathbf{x}_s)) - \hat{b}_K g(\mathbf{K} \cdot (\mathbf{x}_r - \mathbf{x}_s)) \right)} \\ &\quad \times e^{i \int d^3 \mathbf{K} \hat{b}_K^\dagger \hat{b}_K (\Omega_K t)} e^{-i \int d^3 \mathbf{K} \hat{b}_K^\dagger \hat{b}_K (\Omega_K t)}.\end{aligned}\quad (3.12)$$

Note that terms containing $\hat{a}_{\mathbf{k}}^\dagger \hat{a}_{\mathbf{k}}$ commute with each other, and in the last line we inserted the unit operator $\mathcal{I} = e^{i \int d^3 \mathbf{K} \hat{b}_K^\dagger \hat{b}_K (\Omega_K t)} e^{-i \int d^3 \mathbf{K} \hat{b}_K^\dagger \hat{b}_K (\Omega_K t)}$. By rearranging the terms and using the Baker–Campbell–Hausdorff formula, one may find the time evolution operator as follows

$$\begin{aligned}\hat{U}(\mathbf{x}_s, \mathbf{x}_r, t) &= e^{iE(\mathbf{x}_s, \mathbf{x}_r, t) (\hat{a}_{\mathbf{k}}^\dagger \hat{a}_{\mathbf{k}})^2} e^{\hat{a}_{\mathbf{k}}^\dagger \hat{a}_{\mathbf{k}} \sum_{\gamma} \int d^3 \mathbf{K} \kappa_{\gamma}(\hat{\mathbf{K}}, \hat{\mathbf{k}}) \left(\hat{b}_K^\dagger \nu_{\mathbf{K}}(\mathbf{x}_s, \mathbf{x}_r, t) - \hat{b}_K \nu_{\mathbf{K}}^*(\mathbf{x}_s, \mathbf{x}_r, t) \right)} \\ &\quad \times e^{-i\omega_k t \hat{a}_{\mathbf{k}}^\dagger \hat{a}_{\mathbf{k}}} e^{-i \sum_{\gamma} \int d^3 \mathbf{K} \hat{b}_K^\dagger \hat{b}_K \Omega_K t},\end{aligned}\quad (3.13)$$

In the above expression, we have defined

$$\begin{aligned}\nu_{\mathbf{K}}(\mathbf{x}_s, \mathbf{x}_r, t) &\equiv \left(1 - e^{-i\Omega_K t}\right) g^*(\mathbf{K} \cdot (\mathbf{x}_r - \mathbf{x}_s)), \\ E(\mathbf{x}_s, \mathbf{x}_r, t) &\equiv \sum_{\gamma} \int d^3\mathbf{K} \kappa_{\gamma}^2(\mathbf{K}, \mathbf{k}) |g(\mathbf{K} \cdot (\mathbf{x}_r - \mathbf{x}_s))|^2 \left(\Omega_K t - \sin(\Omega_K t)\right).\end{aligned}\quad (3.14)$$

Note that the spatial dependence of the time evolution operator is inherited from the spatial dependence of the underlying GWs background, through the spatial factors $g(\mathbf{K} \cdot (\mathbf{x}_r - \mathbf{x}_s))$. With the help of Eq. (3.4) we obtain

$$|g(\mathbf{K} \cdot (\mathbf{x}_r - \mathbf{x}_s))|^2 = \prod_{i=1}^3 \left(\frac{\sin(\frac{K_i L_i}{2})}{(\frac{K_i L_i}{2})}\right)^2. \quad (3.15)$$

where $L_i \equiv x_r^i - x_s^i$ with $i = 1, 2, 3$. One may check that in the small-detector limit $K_i L_i \ll 1$ one obtain $|g(\mathbf{K} \cdot (\mathbf{x}_r - \mathbf{x}_s))|^2 \rightarrow 1$, and Eq. (3.13) and Eq. (3.14) reduce to that of [126] and Eq. (3) of [129] for the analog optomechanical system.

With the help of $\hat{U}(\mathbf{x}_s, \mathbf{x}_r, t)$, both Schrödinger and Heisenberg dynamics can be perused. We proceed by choosing the Heisenberg picture, where the equation of motion for the EM field operators can be solved without effort, thanks to the well-established cavity opto-mechanical investigations. Time-evolution of the EM field operator $\hat{a}_{\mathbf{k}}(\mathbf{x}_s, \mathbf{x}_r, t)$ can be obtained from $\hat{U}(\mathbf{x}_s, \mathbf{x}_r, t)$ according to

$$\begin{aligned}\hat{a}_{\mathbf{k}}(\mathbf{x}_s, \mathbf{x}_r, t) &= \hat{U}^\dagger(\mathbf{x}_s, \mathbf{x}_r, t) \hat{a}_{\mathbf{k}} \hat{U}(\mathbf{x}_s, \mathbf{x}_r, t) \\ &= \left(e^{i \int d^3\mathbf{K} \hat{b}_K^\dagger \hat{b}_K \Omega_K t} e^{i\omega_k t} \hat{a}_{\mathbf{k}}^\dagger \hat{a}_{\mathbf{k}} e^{-\hat{a}_{\mathbf{k}}^\dagger \hat{a}_{\mathbf{k}} \sum_{\gamma} \int d^3\mathbf{K} \kappa_{\gamma}(\hat{\mathbf{K}}, \hat{\mathbf{k}}) \left(\hat{b}_K^\dagger \nu_{\mathbf{K}}(\mathbf{x}_s, \mathbf{x}_r, t) - \hat{b}_K \nu_{\mathbf{K}}^*(\mathbf{x}_s, \mathbf{x}_r, t) \right)} \right) \\ &\quad \times e^{-iE(\mathbf{x}_s, \mathbf{x}_r, t) (\hat{a}_{\mathbf{k}}^\dagger \hat{a}_{\mathbf{k}})^2} \hat{a}_{\mathbf{k}} \left(e^{iE(\mathbf{x}_s, \mathbf{x}_r, t) (\hat{a}_{\mathbf{k}}^\dagger \hat{a}_{\mathbf{k}})^2} \right. \\ &\quad \left. \times e^{\hat{a}_{\mathbf{k}}^\dagger \hat{a}_{\mathbf{k}} \sum_{\gamma} \int d^3\mathbf{K} \kappa_{\gamma}(\hat{\mathbf{K}}, \hat{\mathbf{k}}) \left(\hat{b}_K^\dagger \nu_{\mathbf{K}}(\mathbf{x}_s, \mathbf{x}_r, t) - \hat{b}_K \nu_{\mathbf{K}}^*(\mathbf{x}_s, \mathbf{x}_r, t) \right)} e^{-i\omega_k t} \hat{a}_{\mathbf{k}}^\dagger \hat{a}_{\mathbf{k}} e^{-i \sum_{\gamma} \int d^3\mathbf{K} \hat{b}_K^\dagger \hat{b}_K \Omega_K t} \right).\end{aligned}\quad (3.16)$$

In the above equation, $\hat{a}_{\mathbf{k}}$ stands for the annihilation operator of photons at the initial time $t = 0$ when EM-GWs interaction initiates. Using the formula $e^{\hat{A}} \hat{B} e^{-\hat{A}} = \hat{B} + [\hat{A}, \hat{B}] + \frac{1}{2!} [\hat{A}, [\hat{A}, \hat{B}]] + \dots$, one may show that

$$\begin{aligned}(1) : & e^{-iE(\mathbf{x}_s, \mathbf{x}_r, t) (\hat{a}_{\mathbf{k}}^\dagger \hat{a}_{\mathbf{k}})^2} \hat{a}_{\mathbf{k}} e^{iE(\mathbf{x}_s, \mathbf{x}_r, t) (\hat{a}_{\mathbf{k}}^\dagger \hat{a}_{\mathbf{k}})^2} = e^{2iE(\mathbf{x}_s, \mathbf{x}_r, t) \left(\hat{a}_{\mathbf{k}}^\dagger \hat{a}_{\mathbf{k}} + \frac{1}{2} \right)} \hat{a}_{\mathbf{k}}, \\ (2) : & e^{-\hat{a}_{\mathbf{k}}^\dagger \hat{a}_{\mathbf{k}} \sum_{\gamma} \int d^3\mathbf{K} \kappa_{\gamma}(\hat{\mathbf{K}}, \hat{\mathbf{k}}) \left(\hat{b}_K^\dagger \nu_{\mathbf{K}}(\mathbf{x}_s, \mathbf{x}_r, t) - \hat{b}_K \nu_{\mathbf{K}}^*(\mathbf{x}_s, \mathbf{x}_r, t) \right)} e^{2iE(\mathbf{x}_s, \mathbf{x}_r, t) \left(\hat{a}_{\mathbf{k}}^\dagger \hat{a}_{\mathbf{k}} + \frac{1}{2} \right)} \hat{a}_{\mathbf{k}} \\ & \quad \times e^{\hat{a}_{\mathbf{k}}^\dagger \hat{a}_{\mathbf{k}} \sum_{\gamma} \int d^3\mathbf{K} \kappa_{\gamma}(\hat{\mathbf{K}}, \hat{\mathbf{k}}) \left(\hat{b}_K^\dagger \nu_{\mathbf{K}}(\mathbf{x}_s, \mathbf{x}_r, t) - \hat{b}_K \nu_{\mathbf{K}}^*(\mathbf{x}_s, \mathbf{x}_r, t) \right)} \\ & = e^{2iE(\mathbf{x}_s, \mathbf{x}_r, t) \left(\hat{a}_{\mathbf{k}}^\dagger \hat{a}_{\mathbf{k}} + \frac{1}{2} \right)} \hat{a}_{\mathbf{k}} e^{\sum_{\gamma} \int d^3\mathbf{K} \kappa_{\gamma}(\mathbf{K}, \mathbf{k}) \left(\hat{b}_K^\dagger \nu_{\mathbf{K}}(\mathbf{x}_s, \mathbf{x}_1, t) - \hat{b}_K \nu_{\mathbf{K}}^*(\mathbf{x}_s, \mathbf{x}_r, t) \right)}, \\ (3) : & e^{i\omega_k t \hat{a}_{\mathbf{k}}^\dagger \hat{a}_{\mathbf{k}}} e^{2iE(\mathbf{x}_s, \mathbf{x}_r, t) \left(\hat{a}_{\mathbf{k}}^\dagger \hat{a}_{\mathbf{k}} + \frac{1}{2} \right)} \hat{a}_{\mathbf{k}} e^{\sum_{\gamma} \int d^3\mathbf{K} \kappa_{\gamma}(\hat{\mathbf{K}}, \hat{\mathbf{k}}) \left(\hat{b}_K^\dagger \nu_{\mathbf{K}}(\mathbf{x}_s, \mathbf{x}_r, t) - \hat{b}_K \nu_{\mathbf{K}}^*(\mathbf{x}_s, \mathbf{x}_r, t) \right)} e^{-i\omega_k t \hat{a}_{\mathbf{k}}^\dagger \hat{a}_{\mathbf{k}}} \\ & = e^{2iE(\mathbf{x}_s, \mathbf{x}_r, t) \left(\hat{a}_{\mathbf{k}}^\dagger \hat{a}_{\mathbf{k}} + \frac{1}{2} \right)} \hat{a}_{\mathbf{k}} e^{-i\omega_k t} e^{\sum_{\gamma} \int d^3\mathbf{K} \kappa_{\gamma}(\hat{\mathbf{K}}, \hat{\mathbf{k}}) \left(\hat{b}_K^\dagger \nu_{\mathbf{K}}(\mathbf{x}_s, \mathbf{x}_r, t) - \hat{b}_K \nu_{\mathbf{K}}^*(\mathbf{x}_s, \mathbf{x}_r, t) \right)}.\end{aligned}\quad (3.17)$$

Thus, Eq. (3.16) can be written as follows

$$\hat{a}_{\mathbf{k}}(\mathbf{x}_s, \mathbf{x}_r, t) = e^{-\sum_{\gamma} \int d^3\mathbf{K} \kappa_{\gamma}(\hat{\mathbf{K}}, \hat{\mathbf{k}}) \left(\hat{b}_K^\dagger \nu_{\mathbf{K}}(\mathbf{x}_s, \mathbf{x}_r, t) - \hat{b}_K \nu_{\mathbf{K}}^*(\mathbf{x}_s, \mathbf{x}_r, t) \right)} e^{2iE(\mathbf{x}_s, \mathbf{x}_r, t) \left(\hat{a}_{\mathbf{k}}^\dagger \hat{a}_{\mathbf{k}} + \frac{1}{2} \right)} e^{-i\omega_k t} \hat{a}_{\mathbf{k}}, \quad (3.18)$$

where we have defined

$$\eta_{\mathbf{K}}(\mathbf{x}_s, \mathbf{x}_r, t) \equiv (1 - e^{i\Omega_{\mathbf{K}}t}) g^*(\mathbf{K} \cdot (\mathbf{x}_r - \mathbf{x}_s)). \quad (3.19)$$

Note that in the above equations, $(\hat{a}_{\mathbf{k}}, \hat{a}_{\mathbf{k}}^\dagger)$ stand for the EM ladder operators at the initial moment (before the EM-GWs interaction takes place). Expression (3.18) is a generalization of the result of [129, 130] to the case of a continuum of GWs modes, where the spatial-dependence of the field operators is included, i.e., without the small detector approximation ($KL \ll 1$), and with a general geometric configuration encoded in the detector pattern function $F_\gamma(\hat{\mathbf{K}}, \hat{\mathbf{k}})$.

Now, from the general definition of the displacement operator corresponding to a bosonic oscillator, $\hat{D}(\alpha) \equiv e^{\alpha \hat{a}^\dagger - \alpha^* \hat{a}}$, one may identify the *displacement operator* associated to GW of mode K as follows

$$\hat{D}_K(-\kappa_\gamma(\mathbf{K}, \mathbf{k}) \eta_{\mathbf{K}}(\mathbf{x}_s, \mathbf{x}_r, t)) \equiv \exp\left(-\kappa_\gamma(\mathbf{K}, \mathbf{k}) \eta_{\mathbf{K}}(\mathbf{x}_s, \mathbf{x}_r, t) \hat{b}_K^\dagger + \kappa_\gamma(\mathbf{K}, \mathbf{k}) \eta_{\mathbf{K}}^*(\mathbf{x}_s, \mathbf{x}_r, t) \hat{b}_K\right). \quad (3.20)$$

Now, if one formally discretizes the integration over GWs modes in Eq. (3.18) according to $\int d^3\mathbf{K} \rightarrow \frac{(2\pi)^3}{V} \sum_{\mathbf{K}}$, $\hat{a}_{\mathbf{k}}(\mathbf{x}_s, \mathbf{x}_r, t)$ is identified as follows

$$\hat{a}_{\mathbf{k}}(\mathbf{x}_s, \mathbf{x}_r, t) = \left[\prod_{\gamma, \mathbf{K}} \hat{D}_K(-\kappa_\gamma(\mathbf{K}, \mathbf{k}) \eta_{\mathbf{K}}(\mathbf{x}_s, \mathbf{x}_r, t)) \right] e^{2iE(\mathbf{x}_s, \mathbf{x}_r, t) (\hat{a}_{\mathbf{k}}^\dagger \hat{a}_{\mathbf{k}} + \frac{1}{2})} e^{-i\omega_{\mathbf{k}}t \hat{a}_{\mathbf{k}}}, \quad (3.21)$$

The quantity inside the brackets is nothing but the tensor product of the displacement operator of each GW mode. Hence, each mode interacts with the EM field independently of the other modes. The appearance of the displacement operator of the tensor field in the EM field dynamics can be justified by our intuition about the opto-mechanical system. In a cavity opto-mechanical system of length L , a single-mode EM field couples with the vibrational mode of the end mirror of the cavity, and the radiation pressure leads the mirror to vibrate. Vibration of the end mirror causes a change in the cavity length, ΔL , which induces the resonant frequency of the the cavity to vary as

$$\omega_k = \frac{n\pi}{L} \quad \rightarrow \quad \frac{n\pi}{L + \Delta L} = \frac{n\pi}{L(1 + \frac{\Delta L}{L})} = \omega_k \left(1 - \frac{\Delta L}{L}\right), \quad (3.22)$$

In the last equality, one may identify the strain field, $h \equiv \frac{\Delta L}{L}$, and the analogy becomes evident. In the EM-GWs analogous case, the strain field of GWs leads the EM frequency to change, and the appearance of the displacement operator of GWs in the evolution of the EM field can be understood from the analogy with the vibrational mode in cavity opto-mechanical system.

One interesting aspect that can be deduced from Eq. (3.21) is the *decoherence* induced by GWs, as previously studied in [100] in the small-detector approximation. However, in the following, we focus on the *incoherence* of the EM field, e.g., the loss of spatial correlations of the EM field caused by GWs. Before doing so, it is beneficial to separate the contribution of the opposite momenta \mathbf{K} and $-\mathbf{K}$ in Eq. (3.21). This step makes the investigation of the two-mode squeezed PGWs easier. To separate the contribution of the opposite momenta, one may start from the interaction Hamiltonian Eq. (3.7) and rewrite it as

$$\hat{H}_{\text{int}}^{(S)}(\mathbf{x}_s, \mathbf{x}_r) \equiv \hat{H}_{\text{int}}^{(S,+)}(\mathbf{x}_s, \mathbf{x}_r) + \hat{H}_{\text{int}}^{(S,-)}(\mathbf{x}_s, \mathbf{x}_r), \quad (3.23)$$

where $\hat{H}_{\text{int}}^{(S,\pm)}$ are given by Eq. (3.7) with integral limits $\mathbf{K} \in \mathfrak{R}^{3\pm}$, respectively. In this manner, the two Hamiltonians corresponding to each half-Fourier space commute,

$[\hat{H}_{\text{int}}^{(S,+)}(\mathbf{x}_s, \mathbf{x}_r), \hat{H}_{\text{int}}^{(S,-)}(\mathbf{x}_s, \mathbf{x}_r)] = 0$. One may easily check that the operator \hat{T} introduced in Eq. (3.9) can be factorized into *positive* and *negative* commuting parts, $\hat{T} \equiv \hat{T}^{(+)} \otimes \hat{T}^{(-)}$ where $[\hat{T}^{(+)}, \hat{T}^{(-)}] = 0$, and each part is the same as Eq. (3.9) with the integral range $\mathbf{K} \in \mathfrak{R}^{3\pm}$. Similarly, the time evolution operator $\hat{U}(\mathbf{x}_s, \mathbf{x}_r, t)$ can be factorized into positive and negative parts, namely $\hat{U}(\mathbf{x}_s, \mathbf{x}_r, t) = \hat{U}^{(+)}(\mathbf{x}_s, \mathbf{x}_r, t) \otimes \hat{U}^{(-)}(\mathbf{x}_s, \mathbf{x}_r, t)$. Following the same steps, one ends up with the following expression for $\hat{a}_{\mathbf{k}}(\mathbf{x}_s, \mathbf{x}_r, t)$

$$\hat{a}_{\mathbf{k}}(\mathbf{x}_s, \mathbf{x}_r, t) = \left[\prod_{\gamma, \mathbf{K} \in \mathfrak{R}^{3+}} \hat{D}_{\mathbf{K}, \gamma}(-\kappa_{\gamma}(\mathbf{K}, \mathbf{k}) \eta_{\mathbf{K}}(\mathbf{x}_s, \mathbf{x}_r, t)) \otimes \hat{D}_{-\mathbf{K}, \gamma}(-\kappa_{\gamma}(\mathbf{K}, \mathbf{k}) \eta_{-\mathbf{K}, \gamma}(\mathbf{x}_s, \mathbf{x}_r, t)) \right] \times e^{2iE(\mathbf{x}_s, \mathbf{x}_r, t) \left(\hat{a}_{\mathbf{k}}^{\dagger} \hat{a}_{\mathbf{k} + \frac{1}{2}} \right)} e^{-i\omega_{\mathbf{k}} t} \hat{a}_{\mathbf{k}}, \quad (3.24)$$

which is a direct product of \mathbf{K} and $-\mathbf{K}$ modes, as one could expect from Eq. (3.21). With the help of Eq. (3.24), we are equipped to investigate spatial correlations of the EM field emitted from distant objects, in the presence of the two-mode squeezed PGWs background.

4 Loss of spatial coherence induced by two-mode squeezed PGWs

4.1 Spatial correlations in the presence of GWs

To investigate the effect of PGWs background on the EM field spatial correlations, we first describe the experimental setup depicted in Fig. 2, which presents the physical concept of spatial correlations of the EM field based on which the angular size of extended objects is measured.

4.1.1 Configuration of a VLBI-type system

Fig. 2 panel (a) shows a typical Michelson stellar interferometer setup. The EM field radiated from two distant edges of a planar source, σ , of radius a (for example a star), each of which denoted by the wave vectors \mathbf{k} and \mathbf{k}' , illuminate two mirrors M_1 and M_2 , located at \mathbf{x}_1 and \mathbf{x}_2 , respectively. For simplicity, we take the origin of coordinates at the center of the planar source, and \mathbf{x}_1 and \mathbf{x}_2 denote the location of each mirror (or telescope) with respect to the center of the planar disc. The signals are then combined at point P at zero difference-time (note that two paths $\overline{M_1 P}$ and $\overline{M_2 P}$ are equal). Panel (b) represents an equivalent situation where the mirrors are replaced by detectors, and the interference pattern is produced by combining the signals at the output of each detector. This is a typical VLBI configuration. In the practical situation of a VLBI instrument, the orientation of the source with respect to the detector baseline makes an angle ϑ_s , as is shown in panel (b). It causes a *geometrical delay time* $\tau_g = (\mathbf{x}_1 - \mathbf{x}_2) \cdot \mathbf{k}/c$ that is often compensated in order to achieve equal-time correlations [131], so that the configuration reduces to the simplified one of panel (a) or (c), where there is no delay time. Panel (c) shows the symmetric configuration, corresponding to the Michelson setup panel (a). In the figure, $\mathbf{K} = (K, \Theta_K, \Phi_K)$ represents the GWs wave vector in polar coordinates. We assume that the planar source lies in the $x-y$ plane, and the two detectors are symmetrically located around the z -axis, with positions $\mathbf{x}_1 = (-\frac{d}{2}, 0, L)$ and $\mathbf{x}_2 = (\frac{d}{2}, 0, L)$. From now on, d and L represent the (transverse) separation of two detectors and the distance of the source with respect to the Earth. The angle θ represents the angular diameter subtended by the source defined by $\theta \equiv \frac{2a}{L}$, when viewed from $M_1 M_2$ on the Earth.

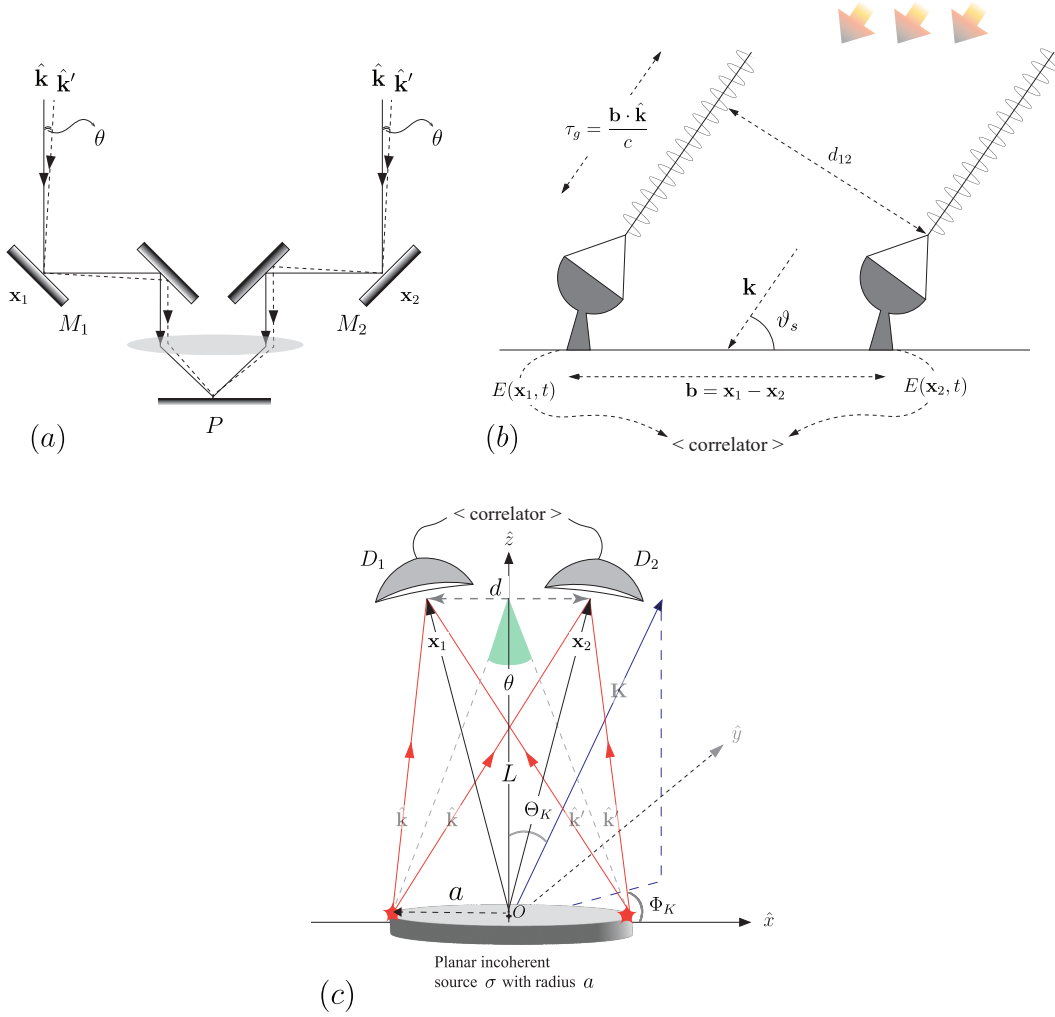


Figure 2. Configuration of the system. *Panel (a)*: a typical Michelson stellar interferometer consisting of two mirrors M_1 and M_2 located at positions $\mathbf{x}_1 = (-\frac{d}{2}, 0, L)$ and $\mathbf{x}_2 = (\frac{d}{2}, 0, L)$. The EM field emitted from two distant edges of an extended source σ , possessing wave vectors \mathbf{k} and \mathbf{k}' , illuminates the mirrors and the intensity is observed in the focal plane of a lens, at point P . *Panel (b)*: Equivalent representation in a VLBI-type configuration in which the mirrors M_1 and M_2 of the Michelson stellar interferometer are replaced by detectors D_1 and D_2 . The interference pattern is produced by beating the signals received by the two detectors, thanks to a correlator. *Panel (c)*: representation of the symmetric configuration and different physical quantities that are used in the text. The angle $\theta \equiv \frac{2a}{L}$ stands for the angular diameter of the source as seen from the VLBI apparatus on the Earth.

4.1.2 Equal-time first-order degree of coherence $g^{(1)}(\mathbf{x}_1, t; \mathbf{x}_2, t)$

For the Michelson stellar interferometer shown in Fig 1 panel (a), the electric field of the incoming light is collected by two mirrors M_1 and M_2 located at \mathbf{x}_1 and \mathbf{x}_2 , at time t . The total electric field received at point P is thus determined by $\hat{E}(\mathbf{x}_P, t) = \hat{E}^{(+)}(\mathbf{x}_P, t) + \hat{E}^{(-)}(\mathbf{x}_P, t)$, where the positive and negative frequency parts of the electric field are defined by

$$\hat{E}^{(+)}(\mathbf{x}_P, t) = \hat{E}^{(+)}(\mathbf{x}_1, t - \tau_1) + \hat{E}^{(+)}(\mathbf{x}_2, t - \tau_2), \quad (4.1)$$

and its Hermitian conjugate. Here, τ_i accounts for the time delay of the EM signal through the arm $\overline{M_i P}$, with $i = 1, 2$, and $\hat{E}^{(+)}(\mathbf{x}_i, t - \tau_i)$ stands for the electric field at the location of the i -th mirror at the delay time $t - \tau_i$. In the symmetric setup one has $\tau_1 = \tau_2$, which is also true in VLBI measurement thanks to the geometric delay line that ensures equal time correlation. Since we neglect the effect of the GWs background during the time delays τ_i (practically $\tau_i \lll t$), we can proceed by setting $t - \tau_1 = t - \tau_2 \equiv t$. Therefore, t will refer to the time at which the EM signal arrives at the detectors, which can also be called the time of flight or the interaction time. The expression of the intensity at point P now reads

$$I(\mathbf{x}_P, t) = \langle \hat{E}^{(-)}(\mathbf{x}_P, t) \hat{E}^{(+)}(\mathbf{x}_P, t) \rangle, \quad (4.2)$$

In the first approach, we consider the simplified case where only two wave vectors \mathbf{k} and \mathbf{k}' , coming from two distant edges of the extended source, illuminate the detectors (see panel (c) of Fig 2). This simplified picture lets us grasp the phenomenon of incoherence induced by PGWs. However, it is straightforward to generalize this picture to the case of the continuous electromagnetic emission from all surface elements of the extended source, possessing wave vector $\mathbf{k} \in \sigma$. This step is left to App. C, where we show that under the adiabatic approximation $K \ll k$ and up to $\mathcal{O}(\theta^2) \simeq 10^{-16}$ (for the typical quasar considered in this paper), the incoherence induced by two-mode squeezed state is identical for all wave vectors $\mathbf{k} \in \sigma$. Here, $\theta \equiv \frac{2a}{L}$ stands for the angular diameter subtended by the source. We now proceed by limiting our consideration to two EM modes \mathbf{k} and \mathbf{k}' . Thus, the positive and negative frequency parts of the electric field at the location of each mirror are specified by

$$\hat{E}^{(+)}(\mathbf{x}_s, \mathbf{x}_i, t) = \mathcal{E}_{\mathbf{k}} \left(\hat{a}_{\mathbf{k}}(\mathbf{x}_s^{(\mathbf{k})}, \mathbf{x}_i, t) e^{i\mathbf{k} \cdot \mathbf{x}_i} + \hat{a}_{\mathbf{k}'}(\mathbf{x}_s^{(\mathbf{k}')}, \mathbf{x}_i, t) e^{i\mathbf{k}' \cdot \mathbf{x}_i} \right), \quad i = 1, 2 \quad (4.3)$$

and its Hermitian conjugate. Here, $\mathcal{E}_{\mathbf{k}}$ represents the electric field amplitude of mode \mathbf{k} of the EM field and can be considered equal with $\mathcal{E}_{\mathbf{k}'}$ without losing generality, assuming a uniform radiation intensity from the source. In Eq. (4.3), the $\mathbf{x}_s^{(\mathbf{k})}$ -dependence of the annihilation operator $\hat{a}_{\mathbf{k}}(\mathbf{x}_s^{(\mathbf{k})}, \mathbf{x}_i, t)$ is written explicitly to emphasis that EM dynamics in the presence of GWs depends on the initial and final spatial points in space (see Sec. 3.2 for details). Note that, in general, each mode $\mathbf{k} \in \sigma$ is emitted from a different location $\mathbf{x}_s^{(\mathbf{k})}$ on the source. The evolution of the EM field through GW background is determined by Eq. (3.24). Plugging Eq. (3.24) into Eq. (4.3) and using Eqs. (4.1, 4.2), one obtains the following expression for the intensity at point \mathbf{x}_P

$$I(\mathbf{x}_P, t) = |\mathcal{E}_{\mathbf{k}}|^2 \left\{ \langle \hat{n}_{\mathbf{k}}(\mathbf{x}_s^{(\mathbf{k})}, \mathbf{x}_1, t) \rangle + \langle \hat{n}_{\mathbf{k}'}(\mathbf{x}_s^{(\mathbf{k}')}, \mathbf{x}_1, t) \rangle + \langle \hat{n}_{\mathbf{k}}(\mathbf{x}_s^{(\mathbf{k})}, \mathbf{x}_2, t) \rangle + \langle \hat{n}_{\mathbf{k}'}(\mathbf{x}_s^{(\mathbf{k}')}, \mathbf{x}_2, t) \rangle \right. \\ \left. + 2\Re \left[\left\langle \hat{a}_{\mathbf{k}}^\dagger(\mathbf{x}_s^{(\mathbf{k})}, \mathbf{x}_1, t) \hat{a}_{\mathbf{k}}(\mathbf{x}_s^{(\mathbf{k})}, \mathbf{x}_2, t) \right\rangle e^{-i\mathbf{k} \cdot (\mathbf{x}_1 - \mathbf{x}_2)} + \mathbf{k} \longleftrightarrow \mathbf{k}' \right] \right\}. \quad (4.4)$$

where $\hat{n}_{\mathbf{k}}(\mathbf{x}_s^{(\mathbf{k})}, \mathbf{x}_i, t) \equiv \hat{a}_{\mathbf{k}}^\dagger(\mathbf{x}_s^{(\mathbf{k})}, \mathbf{x}_i, t) \hat{a}_{\mathbf{k}}(\mathbf{x}_s^{(\mathbf{k})}, \mathbf{x}_i, t)$ represents photon number operator of mode \mathbf{k} . Note that, as it was explained in Sec. 3.2, the Hamiltonian Eq. (3.3) preserves the number of photons as a result of the adiabatic conditions $\Omega_K \ll \omega_k$ and $K \ll k$. Hence,

$$\hat{n}_{\mathbf{k}}(\mathbf{x}_s^{(\mathbf{k})}, \mathbf{x}_i, t) \equiv \hat{n}_{\mathbf{k}}(\mathbf{x}_s^{(\mathbf{k})}) \quad , \quad i = 1, 2 \quad (4.5)$$

with $\hat{n}_{\mathbf{k}}(\mathbf{x}_s^{(\mathbf{k})})$ being the photon number operator of mode \mathbf{k} emitted from $\mathbf{x}_s^{(\mathbf{k})}$ at initial time. In Eq. (4.4), cross-correlations of type $\propto \langle \hat{a}_{\mathbf{k}}^\dagger \hat{a}_{\mathbf{k}'} \rangle = \langle \hat{a}_{\mathbf{k}}^\dagger \rangle \langle \hat{a}_{\mathbf{k}'} \rangle$ between independent

modes \mathbf{k} and \mathbf{k}' vanish, assuming that each mode of the EM field is in thermal state and $\langle \hat{a}_{\mathbf{k}} \rangle = 0$. The first line in Eq. (4.4) represents the contribution of each mode in the intensity at each point \mathbf{x}_i , while the second line shows the role of correlations in each mode, in the interference pattern. In absence of GWs, the annihilation operator simply reduces to the free field case $\hat{a}_{\mathbf{k}(\mathbf{k}')}(\mathbf{x}_s^{(\mathbf{k})}, \mathbf{x}_i, t) \rightarrow e^{-i\omega_{\mathbf{k}}t} \hat{a}_{\mathbf{k}(\mathbf{k}')}$ (see Eq. (3.21)) and Eq. (4.4) recasts to the free-field expression. The quantity inside the brackets is closely related to the equal-time first-order degree of coherence which is usually defined by [132]

$$g^{(1)}(\mathbf{x}_s^{(\mathbf{k})}, \mathbf{x}_1, t; \mathbf{x}_s^{(\mathbf{k})}, \mathbf{x}_2, t) \equiv \frac{\langle \hat{a}_{\mathbf{k}}^\dagger(\mathbf{x}_s^{(\mathbf{k})}, \mathbf{x}_1, t) \hat{a}_{\mathbf{k}}(\mathbf{x}_s^{(\mathbf{k})}, \mathbf{x}_2, t) \rangle}{\langle \hat{n}_{\mathbf{k}} \rangle} \quad (4.6)$$

Similar expression holds correct for the mode \mathbf{k}' . The expectation value in Eq. (4.6) is generally taken over the total state $\hat{\rho} = \hat{\rho}_{\text{gw}} \otimes \hat{\rho}_{\mathbf{k}} \otimes \hat{\rho}_{\mathbf{k}'}$, where $\hat{\rho}_{\text{gw}}$ describes the state of GWs, and $\hat{\rho}_{\mathbf{k}}$ and $\hat{\rho}_{\mathbf{k}'}$ stand for the density matrix of the EM field of modes \mathbf{k} and \mathbf{k}' . One may assume the emission of distant objects to be dominated by a thermal emission with a mean number of photons $\langle \hat{n}_{\mathbf{k}} \rangle = [\exp(\hbar\omega_{\mathbf{k}}/k_{\text{B}}T) - 1]^{-1}$. However, as it can be seen from Eq. (4.4) and (4.6), the state of the EM field does not play an important role and only the mean number of photons appears. This is one of the main features that makes spatial correlations favorable with respect to temporal correlations that drastically depend on the EM state. Thus, the degree of coherence depends *only* on the state of GWs, as indicated by Eq. (4.6). Assuming equal mean number of photons in each mode \mathbf{k} and \mathbf{k}' , Eq. (4.4) reduces to

$$I(\mathbf{x}_P, t) = |\mathcal{E}_{\mathbf{k}}|^2 \left\{ 2\langle \hat{n}_{\mathbf{k}}(\mathbf{x}_s^{(\mathbf{k})}) \rangle + 2\langle \hat{n}_{\mathbf{k}}(\mathbf{x}_s^{(\mathbf{k})}) \rangle \Re \left[g^{(1)}(\mathbf{x}_s^{(\mathbf{k})}, \mathbf{x}_1, t; \mathbf{x}_s^{(\mathbf{k})}, \mathbf{x}_2, t) e^{-i\mathbf{k} \cdot (\mathbf{x}_1 - \mathbf{x}_2)} + \mathbf{k} \longleftrightarrow \mathbf{k}' \right] \right\}. \quad (4.7)$$

where definition Eq. (4.6) is used. Note that, in the absence of GW background one has $g^{(1)}(\mathbf{x}_s^{(\mathbf{k})}, \mathbf{x}_1, t; \mathbf{x}_s^{(\mathbf{k})}, \mathbf{x}_2, t) \rightarrow 1$ and Eq. (4.7) reduces to the standard interference pattern in free space (see Eq. (4.1.24) of [132]).

In App. C, we generalize the expression Eq. (4.7) to the case that the emission from all point sources located on the planar disc is accounted in the intensity $I(\mathbf{x}_P, t)$. The intensity is then determined by

$$I(\mathbf{x}_P, t) = 2I \left\{ 1 + \Re \left[\frac{\int_{\mathbf{x}_s^{(\mathbf{k})} \in \sigma} d^2\sigma g^{(1)}(\mathbf{x}_s^{(\mathbf{k})}, \mathbf{x}_1, t; \mathbf{x}_s^{(\mathbf{k})}, \mathbf{x}_2, t) e^{-i\mathbf{k} \cdot (\mathbf{x}_1 - \mathbf{x}_2)}}{\int_{\mathbf{x}_s^{(\mathbf{k})} \in \sigma} d^2\sigma} \right] \right\}. \quad (4.8)$$

Here, $d^2\sigma = \rho d\rho d\varphi$ is the surface element with $0 \leq \rho \leq a$ and $0 \leq \varphi \leq 2\pi$, and the integration is performed over all surface elements that emit the radio wave. At first it seems that the degree of coherence $g^{(1)}$ depends on the location $\mathbf{x}_s^{(\mathbf{k})} \equiv (\rho \cos \phi, \rho \sin \phi)$ where the EM mode \mathbf{k} is emitted from. However, again we may profit from the adiabatic condition $K \ll k$ and show that indeed the function $g^{(1)}$ varies on large scales (proportional to K^{-1}) and can almost be considered as a constant over the planar disc of radius a (see App. C for the details of calculations). Consequently, we may consider the function $g^{(1)}$ equal to its value at the origin of the disc, $\mathbf{x}_s^{(\mathbf{k})} = 0$, and factorize it so that Eq. (4.8) read as

$$\begin{aligned} I(\mathbf{x}_P, t) &= 2I \left\{ 1 + \Re \left[g^{(1)}(\mathbf{x}_1, t; \mathbf{x}_2, t) \left(\frac{\int_{\mathbf{x}_s^{(\mathbf{k})} \in \sigma} d^2\sigma e^{-i\mathbf{k} \cdot (\mathbf{x}_1 - \mathbf{x}_2)}}{\int_{\mathbf{x}_s^{(\mathbf{k})} \in \sigma} d^2\sigma} \right) \right] \right\} \\ &= 2I \left\{ 1 + \Re \left[g^{(1)}(\mathbf{x}_1, t; \mathbf{x}_2, t) j(\mathbf{x}_1, \mathbf{x}_2) \right] \right\}. \end{aligned} \quad (4.9)$$

Here, $g^{(1)}(\mathbf{x}_1, t; \mathbf{x}_2, t)$ should be evaluated from Eq. (4.9), for an EM signal emitted from the center of the source, $\mathbf{x}_s^{(\mathbf{k})} = 0$, and observed at \mathbf{x}_1 and \mathbf{x}_2 with respect to \mathcal{O} (see panel (c) of Fig. 2). In the second line of Eq. (4.9), we have replaced the integral over the planar surface with the van Citter-Zernike correlations (see App. C for details), namely

$$j(\mathbf{x}_1, \mathbf{x}_2) \equiv \frac{\int_{\mathbf{x}_s^{(\mathbf{k})} \in \sigma} d^2\sigma e^{-i\mathbf{k} \cdot (\mathbf{x}_1 - \mathbf{x}_2)}}{\int_{\mathbf{x}_s^{(\mathbf{k})} \in \sigma} d^2\sigma}, \quad (4.10)$$

The function $j(\mathbf{x}_1, \mathbf{x}_2)$ is usually called the *mutual intensity* and bears spatial correlations in the absence of GWs background, and is described in Sec. 5.1 in details. In the rest of the paper, we obtain equal-time correlations $g^{(1)}(\mathbf{x}_1, t; \mathbf{x}_2, t)$ defined by Eq. (4.6) and the visibility of the EM field in the presence of GWs in two-mode squeezed state, as predicted by inflationary scenario. In the following calculations, we set $\mathbf{x}_s^{(\mathbf{k})} = 0$, $\mathbf{x}_1 = (-d/2, 0, L)$ and $\mathbf{x}_2 = (d/2, 0, L)$.

4.2 First-order degree of coherence in the presence of PGWs in two-mode squeezed state

In this section, we compute the expression of correlation function Eq. (4.6) when GWs are placed in the two-mode squeezed state $|\text{TS}(\eta_H)\rangle$, specified by Eq. (2.10). With the help of Eq. (3.24), the general expression of the two-point degree of coherence of the EM field, defined by Eq. (4.6), in the presence of two-mode squeezed can be written as

$$\begin{aligned} g_{\text{ts}}^{(1)}(1; 2) &= \prod_{\gamma, \mathbf{K} \in \mathfrak{R}^{3+}} \langle 0_{\mathbf{K}}, 0_{-\mathbf{K}} | \hat{R}_{\mathbf{K}}^\dagger \hat{S}_{\mathbf{K}}^\dagger \hat{D}_{\mathbf{K}, \gamma}^\dagger(-\kappa\eta_{\mathbf{K}}(1)) \hat{D}_{\mathbf{K}, \gamma}(-\kappa\eta_{-\mathbf{K}}(2)) \\ &\quad \times \hat{D}_{-\mathbf{K}, \gamma}^\dagger(-\kappa\eta_{-\mathbf{K}}(1)) \hat{D}_{-\mathbf{K}, \gamma}(-\kappa\eta_{-\mathbf{K}}(2)) \hat{S}_{\mathbf{K}} \hat{R}_{\mathbf{K}} | 0_{\mathbf{K}}, 0_{-\mathbf{K}} \rangle \\ &= e^{-i\sum_{\gamma} \int_{\mathbf{K} \in \mathfrak{R}^3} \kappa^2 \Im(\eta_{\mathbf{K}}(1)\eta_{\mathbf{K}}^*(2))} e^{-i\omega_{\mathbf{K}}(t_1 - t_2)} \\ &\quad \times \prod_{\gamma, \mathbf{K} \in \mathfrak{R}^{3+}} \langle 0_{\mathbf{K}}, 0_{-\mathbf{K}} | \hat{R}_{\mathbf{K}}^\dagger \hat{S}_{\mathbf{K}}^\dagger \hat{D}_{\mathbf{K}, \gamma}^\dagger(\kappa[\eta_{\mathbf{K}}(1) - \eta_{\mathbf{K}}(2)]) \hat{S}_{\mathbf{K}} \hat{R}_{\mathbf{K}} \\ &\quad \times \hat{R}_{-\mathbf{K}}^\dagger \hat{S}_{-\mathbf{K}}^\dagger \hat{D}_{-\mathbf{K}, \gamma}^\dagger(\kappa[\eta_{-\mathbf{K}}(1) - \eta_{-\mathbf{K}}(2)]) \hat{S}_{-\mathbf{K}} \hat{R}_{-\mathbf{K}} | 0_{\mathbf{K}}, 0_{-\mathbf{K}} \rangle. \end{aligned} \quad (4.11)$$

Here, for the sake of abbreviation, we used κ in place of $\kappa_{\gamma}(\mathbf{K}, \mathbf{k})$ and $(1, 2)$ in place of $(\mathbf{x}_s^{(\mathbf{k})}, \mathbf{x}_1, t_1)$ and $(\mathbf{x}_s^{(\mathbf{k})}, \mathbf{x}_2, t_2)$, respectively (note that $\kappa_{\gamma}(\mathbf{K}, \mathbf{k}) = \kappa_{\gamma}(-\mathbf{K}, \mathbf{k})$ for real polarization tensors). The opposite momenta \mathbf{K} and $-\mathbf{K}$ are independent in the half Fourier space \mathfrak{R}^{3+} , consequently their associated displacement operators commute. Using the multiplication property of the displacement operator \hat{D} , such that $\hat{D}(\alpha)\hat{D}(\beta) = e^{i\Im(\alpha\beta^*)}\hat{D}(\alpha + \beta)$, one has

$$\hat{D}_{\mathbf{K}}^\dagger(-\kappa\eta_{\mathbf{K}}(1))\hat{D}_{\mathbf{K}}(-\kappa\eta_{\mathbf{K}}(2)) = e^{-i\kappa^2\Im(\eta_{\mathbf{K}}(1)\eta_{\mathbf{K}}^*(2))}\hat{D}_{\mathbf{K}}(\kappa[\eta_{\mathbf{K}}(1) - \eta_{\mathbf{K}}(2)]). \quad (4.12)$$

together with similar expression for $-\mathbf{K}$. Here, we remind that \Im stands for the imaginary part. Moreover, the two-mode squeezing operator $\hat{S}_{\mathbf{K}}$ and the rotation operator $\hat{R}_{\mathbf{K}}$ involve opposite modes \mathbf{K} and $-\mathbf{K}$ (see the definitions in Eq. (2.11)), so in order to write Eq. (4.12) in a separated form, we may use the following identities

$$\begin{aligned} \hat{R}_{\mathbf{K}}^\dagger \hat{S}_{\mathbf{K}}^\dagger \hat{D}_{\mathbf{K}}(-\kappa\eta_{\mathbf{K}}) \hat{S}_{\mathbf{K}} \hat{R}_{\mathbf{K}} &= \hat{D}_{\mathbf{K}}(-\kappa\eta_{\mathbf{K}} u_{\mathbf{K}}^*(\eta_H)) \otimes \hat{D}_{-\mathbf{K}}(\kappa\eta_{\mathbf{K}}^* v_{\mathbf{K}}(\eta_H)), \\ \hat{R}_{-\mathbf{K}}^\dagger \hat{S}_{-\mathbf{K}}^\dagger \hat{D}_{-\mathbf{K}}(-\kappa\eta_{-\mathbf{K}}) \hat{S}_{-\mathbf{K}} \hat{R}_{-\mathbf{K}} &= \hat{D}_{-\mathbf{K}}(-\kappa\eta_{-\mathbf{K}} u_{\mathbf{K}}^*(\eta_H)) \otimes \hat{D}_{\mathbf{K}}(\kappa\eta_{-\mathbf{K}}^* v_{\mathbf{K}}(\eta_H)). \end{aligned} \quad (4.13)$$

where $u_K(\eta_H)$ and $v_K(\eta_H)$ are defined by Eq. (2.13). Note that the quantities related to the PGWs are evaluated at the present time η_H , however, we shall suppress η_H for the sake of abbreviation. With the help of Eq. (4.13), Eq. (4.11) can be written as follows

$$\begin{aligned}
g_{\text{ts}}^{(1)}(1; 2) &= e^{-i\sum_{\gamma} \int_{\mathbf{K} \in \mathbb{R}^3} \kappa^2 \mathfrak{S}(\eta_{\mathbf{K}}(1)\eta_{\mathbf{K}}^*(2))} e^{-i\omega_k(t_1-t_2)} \quad (4.14) \\
&\times \prod_{\gamma, \mathbf{K} \in \mathbb{R}^{3+}} \left\langle 0_{\mathbf{K}}, 0_{-\mathbf{K}} \left| \hat{D}_{\mathbf{K}}(\kappa u_K^*[\eta_{\mathbf{K}}(1) - \eta_{\mathbf{K}}(2)]) \otimes \hat{D}_{-\mathbf{K}}(-\kappa v_K[\eta_{\mathbf{K}}^*(1) - \eta_{\mathbf{K}}^*(2)]) \right. \right. \\
&\times \left. \left. \hat{D}_{-\mathbf{K}}(\kappa u_K^*[\eta_{-\mathbf{K}}(1) - \eta_{-\mathbf{K}}(2)]) \otimes \hat{D}_{\mathbf{K}}(-\kappa v_K[\eta_{-\mathbf{K}}^*(1) - \eta_{-\mathbf{K}}^*(2)]) \right| 0_{\mathbf{K}}, 0_{-\mathbf{K}} \right\rangle \\
&= e^{-i\sum_{\gamma} \int_{\mathbf{K} \in \mathbb{R}^3} \kappa^2 \mathfrak{S}(\eta_{\mathbf{K}}(1)\eta_{\mathbf{K}}^*(2))} e^{-i\omega_k(t_1-t_2)} \\
&\times \prod_{\gamma, \mathbf{K} \in \mathbb{R}^{3+}} \left\langle 0_{\mathbf{K}} \left| \hat{D}_{\mathbf{K}}^\dagger(-\kappa u_K^*[\eta_{\mathbf{K}}(1) - \eta_{\mathbf{K}}(2)]) \hat{D}_{\mathbf{K}}(-\kappa v_K[\eta_{-\mathbf{K}}^*(1) - \eta_{-\mathbf{K}}^*(2)]) \right| 0_{-\mathbf{K}} \right\rangle \\
&\times \left\langle 0_{-\mathbf{K}} \left| \hat{D}_{-\mathbf{K}}^\dagger(\kappa v_K[\eta_{\mathbf{K}}^*(1) - \eta_{\mathbf{K}}^*(2)]) \hat{D}_{-\mathbf{K}}(\kappa u_K^*[\eta_{-\mathbf{K}}(1) - \eta_{-\mathbf{K}}(2)]) \right| 0_{-\mathbf{K}} \right\rangle \\
&= e^{-i\sum_{\gamma} \int_{\mathbf{K} \in \mathbb{R}^3} \kappa^2 \mathfrak{S}(\eta_{\mathbf{K}}(1)\eta_{\mathbf{K}}^*(2))} e^{-i\omega_k(t_1-t_2)} \\
&\times \prod_{\gamma, \mathbf{K} \in \mathbb{R}^{3+}} \left\langle -\kappa u_K^*[\eta_{\mathbf{K}}(1) - \eta_{\mathbf{K}}(2)] \left| -\kappa v_K[\eta_{-\mathbf{K}}^*(1) - \eta_{-\mathbf{K}}^*(2)] \right. \right. \\
&\times \left. \left. \kappa v_K[\eta_{\mathbf{K}}^*(1) - \eta_{\mathbf{K}}^*(2)] \left| \kappa u_K^*[\eta_{-\mathbf{K}}(1) - \eta_{-\mathbf{K}}(2)] \right. \right. \right\rangle.
\end{aligned}$$

Now using the projection property of coherent states, $\langle \alpha | \alpha' \rangle = e^{-\frac{1}{2}|\alpha|^2 - \frac{1}{2}|\alpha'|^2 + \alpha^* \alpha'}$, Eq. (4.14) yields

$$\begin{aligned}
g_{\text{ts}}^{(1)}(1; 2) &= e^{-i\sum_{\gamma} \int_{\mathbf{K} \in \mathbb{R}^3} \kappa^2 \mathfrak{S}(\eta_{\mathbf{K}}(1)\eta_{\mathbf{K}}^*(2))} e^{-i\omega_k(t_1-t_2)} \quad (4.15) \\
&\times \prod_{\gamma, \mathbf{K} \in \mathbb{R}^{3+}} \exp\left[-\frac{1}{2}\kappa^2 |u_K|^2 \left| \eta_{\mathbf{K}}(1) - \eta_{\mathbf{K}}(2) \right|^2\right] \exp\left[-\frac{1}{2}\kappa^2 |v_K|^2 \left| \eta_{-\mathbf{K}}^*(1) - \eta_{-\mathbf{K}}^*(2) \right|^2\right] \\
&\times \exp\left[\kappa^2 u_K v_K \left(\eta_{\mathbf{K}}^*(1) - \eta_{\mathbf{K}}^*(2) \right) \left(\eta_{-\mathbf{K}}^*(1) - \eta_{-\mathbf{K}}^*(2) \right)\right] \\
&\times \exp\left[-\frac{1}{2}\kappa^2 |v_K|^2 \left| \eta_{\mathbf{K}}^*(1) - \eta_{\mathbf{K}}^*(2) \right|^2\right] \exp\left[-\frac{1}{2}\kappa^2 |u_K|^2 \left| \eta_{-\mathbf{K}}(1) - \eta_{-\mathbf{K}}(2) \right|^2\right] \\
&\times \exp\left[\kappa^2 u_K^* v_K^* \left(\eta_{\mathbf{K}}(1) - \eta_{\mathbf{K}}(2) \right) \left(\eta_{-\mathbf{K}}(1) - \eta_{-\mathbf{K}}(2) \right)\right] \\
&= e^{-i\sum_{\gamma} \int_{\mathbf{K} \in \mathbb{R}^3} \kappa^2 \mathfrak{S}(\eta_{\mathbf{K}}(1)\eta_{\mathbf{K}}^*(2))} e^{-i\omega_k(t_1-t_2)} \\
&\times \exp\left[-\frac{1}{2} \sum_{\gamma} \int_{\mathbf{K} \in \mathbb{R}^3} d^3\mathbf{K} \kappa^2 \left(|u_K|^2 + |v_K|^2 \right) \left| \eta_{\mathbf{K}}(1) - \eta_{\mathbf{K}}(2) \right|^2\right] \\
&\times \exp\left[\sum_{\gamma} \int_{\mathbf{K} \in \mathbb{R}^3} d^3\mathbf{K} \kappa^2 \Re\left\{ u_K v_K \left(\eta_{\mathbf{K}}^*(1)\eta_{-\mathbf{K}}^*(1) - \eta_{\mathbf{K}}^*(2)\eta_{-\mathbf{K}}^*(2) \right) \right\}\right].
\end{aligned}$$

In the last equality we transformed to the continuum notation, and used the normalization property $|u_K(\eta_H)|^2 - |v_K(\eta_H)|^2 = 1$ for two-mode squeezed states (see Eq. (2.13)). If one resumes the calculations for GWs in a vacuum state, namely $\hat{\rho}_{\text{vac}} = \prod_K |0_K\rangle\langle 0_K|$, it can be verified that the contribution of vacuum fluctuations are already involved in the contribution of two-mode squeezed state (see App. C.2). More precisely, one can factorize Eq. (4.15) as a

multiplication of the contribution of vacuum fluctuations of GWs, times a contribution due to the two-mode squeezed PGWs as follows

$$g_{\text{ts}}^{(1)}(1; 2) = e^{-i\mathcal{C}^{\text{vac}}(1;2)} e^{-\mathcal{D}^{\text{vac}}(1;2)} e^{-\mathcal{D}^{\text{ts}}(1;2)} \quad , \quad (4.16)$$

where the two-point kernels $\mathcal{C}^{\text{vac}}(1; 2)$, $\mathcal{D}^{\text{vac}}(1; 2)$ and $\mathcal{D}^{\text{ts}}(1; 2)$ are defined accordingly

$$\begin{aligned} \mathcal{C}^{\text{vac}}(1; 2) &\equiv \sum_{\gamma} \int_{\mathbf{K} \in \mathbb{R}^3} d^3\mathbf{K} \kappa_{\gamma}^2(\mathbf{K}, \mathbf{k}) \mathcal{C}_{\mathbf{K}}^{\text{vac}}(1; 2) \Big], \quad (4.17) \\ \mathcal{D}^{\text{vac}}(1; 2) &\equiv \frac{1}{2} \sum_{\gamma} \int_{\mathbf{k} \in \mathbb{R}^3} d^3\mathbf{K} \kappa_{\gamma}^2(\mathbf{K}, \mathbf{k}) \mathcal{D}_{\mathbf{K}}^{\text{vac}}(1; 2), \\ \mathcal{D}^{\text{ts}}(1; 2) &\equiv \sum_{\gamma} \int_{\mathbf{K} \in \mathbb{R}^3} d^3\mathbf{K} \kappa_{\gamma}^2(\mathbf{K}, \mathbf{k}) \left\{ |v_K(\eta_H)|^2 \mathcal{D}_{\mathbf{K}}^{\text{vac}}(1; 2) + \frac{1}{2} \mathcal{D}_{\mathbf{K}}^{\text{ts-corr}}(1; 2) \right\}. \end{aligned}$$

together with

$$\begin{aligned} \mathcal{C}_{\mathbf{K}}^{\text{vac}}(1; 2) &\equiv \Im \left[\eta_{\mathbf{K}}(1) \eta_{\mathbf{K}}^*(2) \right], \quad (4.18) \\ \mathcal{D}_{\mathbf{K}}^{\text{vac}}(1; 2) &\equiv |\eta_{\mathbf{K}}(1) - \eta_{\mathbf{K}}(2)|^2, \\ \mathcal{D}_{\mathbf{K}}^{\text{ts-corr}}(1; 2) &\equiv 2\Re \left[u_K^*(\eta_H) v_K^*(\eta_H) \left(\eta_{\mathbf{K}}(1) - \eta_{\mathbf{K}}(2) \right) \left(\eta_{-\mathbf{K}}(1) - \eta_{-\mathbf{K}}(2) \right) \right]. \end{aligned}$$

In the following, we analyze these kernels in detail, in the special case of $t_1 = t_2 \equiv t$.

4.2.1 Contribution of vacuum fluctuations of GWs in spatial incoherence

To proceed, we consider equal-time correlations by adopting $t_1 = t_2 \equiv t$. Moreover, we set $\mathbf{x}_s^{(\mathbf{k})} = 0$ as we previously explained in Sec. 4.1.2. The contribution of vacuum fluctuations in spatial correlations Eq. (4.15) is determined by (see App. C.2 for details)

$$g_{\text{vac}}^{(1)}(\mathbf{x}_1, t; \mathbf{x}_2, t) \equiv e^{-i\mathcal{C}^{\text{vac}}(\mathbf{x}_1, t; \mathbf{x}_2, t)} e^{-\mathcal{D}^{\text{vac}}(\mathbf{x}_1, t; \mathbf{x}_2, t)}, \quad (4.19)$$

where we have defined

$$\begin{aligned} \mathcal{C}^{\text{vac}}(\mathbf{x}_1, t; \mathbf{x}_2, t) &\equiv \sum_{\gamma} \int_{\mathbf{K} \in \mathbb{R}^3} d^3\mathbf{K} \kappa_{\gamma}^2(\mathbf{K}, \mathbf{k}) \mathcal{C}_{\mathbf{K}}^{\text{vac}}(\mathbf{x}_1, t; \mathbf{x}_2, t) \Big], \quad (4.20) \\ \mathcal{D}^{\text{vac}}(\mathbf{x}_1, t; \mathbf{x}_2, t) &\equiv \frac{1}{2} \sum_{\gamma} \int_{\mathbf{K} \in \mathbb{R}^3} d^3\mathbf{K} \kappa_{\gamma}^2(\mathbf{K}, \mathbf{k}) \mathcal{D}_{\mathbf{K}}^{\text{vac}}(\mathbf{x}_1, t; \mathbf{x}_2, t), \end{aligned}$$

together with

$$\begin{aligned} \mathcal{C}_{\mathbf{K}}^{\text{vac}}(\mathbf{x}_1, t; \mathbf{x}_2, t) &\equiv \Im \left[\eta_{\mathbf{K}}(\mathbf{x}_1, t) \eta_{\mathbf{K}}^*(\mathbf{x}_2, t) \right] \quad (4.21) \\ \mathcal{D}_{\mathbf{K}}^{\text{vac}}(\mathbf{x}_1, t; \mathbf{x}_2, t) &\equiv |\eta_{\mathbf{K}}(\mathbf{x}_1, t) - \eta_{\mathbf{K}}(\mathbf{x}_2, t)|^2. \end{aligned}$$

The kernels $\mathcal{C}^{\text{vac}}(\mathbf{x}_1, t; \mathbf{x}_2, t)$ and $\mathcal{D}^{\text{vac}}(\mathbf{x}_1, t; \mathbf{x}_2, t)$ represent the contribution of vacuum fluctuations in *coherent* and *incoherent* evolution of spatial correlations of the EM field, respectively. With the help of definitions Eq. (3.4) and Eq. (3.19) for $g(\mathbf{K} \cdot \mathbf{x})$ and $\eta_{\mathbf{K}}(\mathbf{x}, t)$, one obtains

$$\begin{aligned} \mathcal{C}^{\text{vac}}(\mathbf{x}_1, t; \mathbf{x}_2, t) &= \Im \left[\left(4 \sin^2 \frac{\Omega_K t}{2} \right) \prod_{i=1}^3 \frac{e^{-iK_i(x_1^i - x_2^i)} - e^{-iK_i x_1^i} - e^{-iK_i x_2^i} + 1}{K_i^2 x_1^i x_2^i} \right] \quad (4.22) \\ &= -8 \sin^2 \left(\frac{\Omega_K t}{2} \right) \prod_{i=1}^3 \frac{\sin^2 \left(\frac{K_i x_1^i}{2} \right) \sin(K_i x_2^i) - \sin^2 \left(\frac{K_i x_2^i}{2} \right) \sin(K_i x_1^i)}{(K_i x_1^i)(K_i x_2^i)} \quad , \end{aligned}$$

and

$$\mathcal{D}_{\mathbf{K}}^{\text{vac}}(\mathbf{x}_1, t; \mathbf{x}_2, t) = 4 \sin^2\left(\frac{\Omega_K t}{2}\right) \left\{ |g(\mathbf{K} \cdot \mathbf{x}_1)|^2 + |g(\mathbf{K} \cdot \mathbf{x}_2)|^2 - 2\Re[g^*(\mathbf{K} \cdot \mathbf{x}_1)g(\mathbf{K} \cdot \mathbf{x}_2)] \right\}. \quad (4.23)$$

Considering $\mathbf{x}_1 = (-\frac{d}{2}, 0, L)$ and $\mathbf{x}_2 = (\frac{d}{2}, 0, L)$ corresponding to the setup depicted in panel (c) of Fig. 2, geometrical factors containing $g(\mathbf{K} \cdot \mathbf{x}_i)$ can be evaluated. In particular, we have (remind that $\mathbf{x}_s = 0$)

$$\begin{aligned} & |g(\mathbf{K} \cdot \mathbf{x}_1)|^2 + |g(\mathbf{K} \cdot \mathbf{x}_2)|^2 - 2\Re[g^*(\mathbf{K} \cdot \mathbf{x}_1)g(\mathbf{K} \cdot \mathbf{x}_2)] \\ &= 2 \left(\frac{\sin(\frac{K_z L}{2})}{(\frac{K_z L}{2})} \right)^2 \times \left(\left(\frac{\sin(\frac{K_x d}{4})}{(\frac{K_x d}{4})} \right)^2 + \frac{\cos(K_x d) - 2 \cos(\frac{K_x d}{2}) + 1}{(\frac{K_x d}{2})^2} \right). \end{aligned} \quad (4.24)$$

For the largest possible interferometers on the Earth, the separation between detectors could be as long as the Earth's radius. Thus, for GWs of frequency $\Omega_K \ll c/d \sim c/R_{\oplus} \sim 50$ Hz, one may safely assume $Kd \ll 1$. Note that, the high-frequency part of the PGWs spectrum possesses the lowest graviton content as implied by Fig. 1, and practically does not make a significant contribution in the incoherence mechanism. As a result, we may proceed assuming $Kd \ll 1$ in our calculations. Expanding terms up to $\mathcal{O}(K_x d)^2$ yields

$$\begin{aligned} \left(\frac{\sin(\frac{K_x d}{4})}{(\frac{K_x d}{4})} \right)^2 &\simeq \left(\frac{(\frac{K_x d}{4}) - \frac{1}{3!}(\frac{K_x d}{4})^3}{(\frac{K_x d}{4})} \right)^2 = 1 - \frac{1}{3} \left(\frac{K_x d}{4} \right)^2, \\ \frac{\cos(K_x d) - 2 \cos(\frac{K_x d}{2}) + 1}{(\frac{K_x d}{2})^2} &= \frac{-(\frac{K_x d}{2})^2 + \frac{7}{192}(K_x d)^4}{(\frac{K_x d}{2})^2} = -1 + \frac{28}{192} (K_x d)^2. \end{aligned} \quad (4.25)$$

Plugging Eq. (4.25) into Eq. (4.24) yields

$$\begin{aligned} & |g(\mathbf{K} \cdot \mathbf{x}_1)|^2 + |g(\mathbf{K} \cdot \mathbf{x}_2)|^2 - 2\Re[g^*(\mathbf{K} \cdot \mathbf{x}_1)g(\mathbf{K} \cdot \mathbf{x}_2)] \\ &= \frac{1}{4} \left(\frac{\sin(\frac{K_z L}{2})}{(\frac{K_z L}{2})} \right)^2 \times K^2 \sin^2 \Theta_k \cos^2 \Phi_K d^2 \end{aligned} \quad (4.26)$$

up to $\mathcal{O}(Kd)^2$. The final expression of the two kernels defined in Eq. (4.22) and Eq. (4.24) recast to the following form

$$\begin{aligned} \mathcal{C}_{\mathbf{K}}^{\text{vac}}(d, L, t) &= 0, \\ \mathcal{D}_{\mathbf{K}}^{\text{vac}}(d, L, t) &= \left(\sin^2\left(\frac{\Omega_K t}{2}\right) \times \left(\frac{\sin(\frac{K_z L}{2})}{(\frac{K_z L}{2})} \right)^2 K^2 \sin^2 \Theta_K \cos^2 \Phi_K \right) d^2. \end{aligned} \quad (4.27)$$

Thus, the effect of vacuum fluctuations in *coherent dynamics* of the EM spatial correlation vanishes at $\mathcal{O}(Kd)^2$ order. On the other hand, one may show that (see App. C.3 for details of calculations)

$$\sum_{\gamma} \int_{\mathbf{K} \in \mathbb{R}^3} d^3 \mathbf{K} \kappa_{\gamma}^2(\mathbf{K}, \mathbf{k}) = \frac{1}{(2\pi)^2} \left(\frac{\hbar \omega_k}{E_{\text{Pl}}} \right)^2 \int_0^{2\pi} d\Phi_K \int_0^{\pi} d(\cos \Theta_K) \sin^4 \Theta_K \int_{K_E}^{K_1} \frac{dK}{K}, \quad (4.28)$$

By inserting Eq. (4.27) into Eq. (4.20) and using Eq. (4.28), one may identify *incoherent dynamics* induced by vacuum fluctuations, encapsulated in the kernel $\mathcal{D}^{\text{vac}}(d, L, t)$, as follows

$$\mathcal{D}_{\mathbf{K}}^{\text{vac}}(d, L, t) \equiv \left(\frac{d}{\xi^{\text{vac}}(L, t)} \right)^2, \quad (4.29)$$

where the incoherence-length induced by vacuum fluctuations $\xi^{\text{vac}}(L, t)$ is defined by

$$\begin{aligned} \xi^{\text{vac}}(L, t) = & \left[\frac{1}{2(2\pi)^2} \left(\frac{\hbar\omega_k}{E_{\text{Pl}}} \right)^2 \int d\Phi_K \cos^2 \Phi_K \int d(\cos \Theta_K) \sin^6 \Theta_K \right. \\ & \left. \times \int_{K_E}^{K_1} \frac{dK}{K} K^2 \left(\sin^2 \left(\frac{\Omega_K t}{2} \right) \right) \left(\frac{\sin \left(\frac{K_z L}{2} \right)}{\left(\frac{K_z L}{2} \right)} \right)^2 \right]^{-1/2}. \end{aligned} \quad (4.30)$$

Now, combining Eqs. (4.17 , 4.27 - 4.30), the contribution of vacuum fluctuations of GWs in *incoherent* dynamics of spatial correlations can be written in the following compact form

$$g_{\text{vac}}^{(1)}(d, L, t) = e^{-\left(\frac{d}{\xi^{\text{vac}}(L, t)} \right)^2}. \quad (4.31)$$

One can easily verify that for a vanishing time of flight, $t \rightarrow 0$, $\xi^{\text{vac}}(L, t)$ tends to infinity which yields $g_{\text{vac}}^{(1)}(d, L, t) \rightarrow 1$, as one expects. Due to the interaction with GW background during the time of flight t , the length-scale $\xi^{\text{vac}}(L, t)$ finds finite values. However, due to negligibly small coupling strength $\left(\frac{\hbar\omega_k}{E_{\text{Pl}}} \right)^2$, the length-scale $\xi^{\text{vac}}(L, t)$ is so large that practically does not ruin spatial coherence of the Em field. On the other hand, as we are going to investigate in the next section, amplified vacuum fluctuations that form the two-mode squeezed PGWs may completely affect the spatial coherence.

4.2.2 Contribution of gravitons in two-mode squeezed state in spatial incoherence

The two-point function $\mathcal{D}^{\text{ts}}(1; 2)$ introduced in Eq. (4.17) encapsulates the effect of gravitons in the two-mode squeezed state in the incoherence of EM correlations. In particular, the first term containing $|v_K(\eta_H)|^2$ represents the role of the *mean number of gravitons*, while the second term containing the kernel $\mathcal{D}^{\text{ts-corr}}(1; 2)$ bears the contribution of *correlations between gravitons* in two-mode squeezed, in the incoherence dynamics. In the special case of equal-time correlations, i.e., when $t_1 = t_2 \equiv t$, from Eq. (4.17) we obtain

$$\begin{aligned} \mathcal{D}^{\text{ts}}(\mathbf{x}_1, t; \mathbf{x}_2, t) \equiv & \sum_{\gamma} \int d^3\mathbf{K} \kappa_{\gamma}^2(\mathbf{K}, \mathbf{k}) \left\{ |v_K(\eta_H)|^2 \mathcal{D}_{\mathbf{K}}^{\text{vac}}(\mathbf{x}_1, t; \mathbf{x}_2, t) \right. \\ & \left. + \frac{1}{2} \mathcal{D}_{\mathbf{K}}^{\text{ts-corr}}(\mathbf{x}_1, t; \mathbf{x}_2, t) \right\}. \end{aligned} \quad (4.32)$$

With the help of Eq. (4.18), one has

$$\begin{aligned} \mathcal{D}_{\mathbf{K}}^{\text{ts-corr}}(\mathbf{x}_1, t; \mathbf{x}_2, t) = & 2\Re \left[u_K(\eta_H) v_K(\eta_H) \left(\eta_{\mathbf{K}}^*(\mathbf{x}_1, t) - \eta_{\mathbf{K}}^*(\mathbf{x}_2, t) \right) \left(\eta_{-\mathbf{K}}^*(\mathbf{x}_1, t) - \eta_{-\mathbf{K}}^*(\mathbf{x}_2, t) \right) \right] \\ = & \sinh 2r_K \Re \left\{ \left(e^{-2i\phi_K} - 2e^{i(\Omega_K t - 2\phi_K)} + e^{2i(\Omega_K t - \phi_K)} \right) \right. \\ & \left. \times \left(|g(\mathbf{K} \cdot \mathbf{x}_1)|^2 + |g(\mathbf{K} \cdot \mathbf{x}_2)|^2 - 2\Re \left[g^*(\mathbf{K} \cdot \mathbf{x}_1) g(\mathbf{K} \cdot \mathbf{x}_2) \right] \right) \right\}. \end{aligned} \quad (4.33)$$

Considering spatial points $\mathbf{x}_1 = (-\frac{d}{2}, 0, L)$ and $\mathbf{x}_2 = (\frac{d}{2}, 0, L)$ and by plugging Eq. (4.26) into Eq. (4.33), following expression for the kernel $\mathcal{D}^{\text{ts}}(d, L, t)$ is obtained

$$\begin{aligned}
\mathcal{D}^{\text{ts}}(d, L, t) &= \sum_{\gamma} \int d^3\mathbf{K} \kappa_{\gamma}^2(\mathbf{K}, \mathbf{k}) \left\{ \sinh^2 r_K \mathcal{D}^{\text{vac}}(d, L, t) + \frac{1}{2} \mathcal{D}^{\text{ts-corr}}(d, L, t) \right\} \quad (4.34) \\
&= \sum_{\gamma} \int d^3\mathbf{K} \kappa_{\gamma}^2(\mathbf{K}, \mathbf{k}) \left\{ \left[\sinh^2 r_K \left(4 \sin^2 \left(\frac{\Omega_K t}{2} \right) \right) + \frac{1}{2} \sinh 2r_K \right. \right. \\
&\quad \times \left. \left(\cos(2\phi_K) - 2 \cos(\Omega_K t - 2\phi_K) + \cos(2\Omega_K t - 2\phi_K) \right) \right] \\
&\quad \times \left. \left(|g(\mathbf{K} \cdot \mathbf{x}_1)|^2 + |g(\mathbf{K} \cdot \mathbf{x}_2)|^2 - 2\Re \left[g^*(\mathbf{K} \cdot \mathbf{x}_1) g(\mathbf{K} \cdot \mathbf{x}_2) \right] \right) \right\} \\
&= \left[\frac{1}{(2\pi)^2} \left(\frac{\hbar\omega_k}{E_{Pl}} \right)^2 \int d\Phi_K \cos^2 \Phi_K \int d(\cos \Theta_K) F_{\gamma}^2(\hat{\mathbf{K}}, \hat{\mathbf{k}}) \sin^2 \Theta_K \right. \\
&\quad \times \int dK K \left(\frac{\sin(\frac{K_z L}{2})}{(\frac{K_z L}{2})} \right)^2 \left\{ \sinh^2 r_K \left(\sin^2 \frac{\Omega_K t}{2} \right) + \frac{1}{8} \sinh 2r_K \right. \\
&\quad \times \left. \left. \left(\cos(2\phi_K) - 2 \cos(\Omega_K t - 2\phi_K) + \cos(2\Omega_K t - 2\phi_K) \right) \right\} \right] d^2 \\
&\equiv \left(\frac{d}{\xi^{\text{ts}}(L, t)} \right)^2.
\end{aligned}$$

Here, Eq.(4.27) for $\mathcal{D}^{\text{vac}}(d, L, t)$ and Eq. (4.28) are used. In the last line, the incoherence length induced by two-mode squeezed PGWs $\xi^{\text{ts}}(L, t)$ is defined by

$$\begin{aligned}
\xi^{\text{ts}}(L, t) &\equiv \left[\frac{1}{(2\pi)^2} \left(\frac{\hbar\omega_k}{E_{Pl}} \right)^2 \int d\Phi_K \cos^2 \Phi_K \int d(\cos \Theta_K) \sin^6 \Theta_K \right. \\
&\quad \times \int dK K \left(\frac{\sin(\frac{K_z L}{2})}{(\frac{K_z L}{2})} \right)^2 \left\{ \sinh^2 r_K \left(\sin^2 \left(\frac{\Omega_K t}{2} \right) \right) + \frac{1}{8} \sinh 2r_K \right. \\
&\quad \times \left. \left. \left(\cos(2\phi_K) - 2 \cos(\Omega_K t - 2\phi_K) + \cos(2\Omega_K t - 2\phi_K) \right) \right\} \right]^{-1/2}. \quad (4.35)
\end{aligned}$$

Again, one may easily check that for vanishing interaction time, $t \rightarrow 0$, $\xi^{\text{ts}}(L, t) \rightarrow \infty$ and the incoherence disappears.

With the help of Eqs. (4.31, 4.34, 4.35), the two-point degree of coherence Eq. (4.16) in the equal-time limit is rewritten as follows

$$g^{(1)}(d, L, t) = g_{\text{vac}}^{(1)}(d, L, t) e^{-\left(\frac{d}{\xi^{\text{ts}}(L, t)} \right)^2}. \quad (4.36)$$

4.3 The intensity and visibility

Having obtained the expression of $g^{(\text{ts})}(d, L, t)$, we can now identify the intensity $I(\mathbf{x}_P, t)$. Combining Eq. (4.9) and Eq. (4.36) yields

$$I(\mathbf{x}_P, t) = 2I \left\{ 1 + j(\mathbf{x}_1, \mathbf{x}_2) e^{-\left(\frac{d}{\xi^{\text{vac}}(L, t)} \right)^2} e^{-\left(\frac{d}{\xi^{\text{ts}}(L, t)} \right)^2} \right\}. \quad (4.37)$$

According to the definition, the *visibility*, which is a measure of the sharpness of the interference fringes, is defined by [133]

$$\mathcal{V}(\mathbf{x}_P, t) \equiv \frac{I_{\max}(\mathbf{x}_P, t) - I_{\min}(\mathbf{x}_P, t)}{I_{\max}(\mathbf{x}_P, t) + I_{\min}(\mathbf{x}_P, t)}. \quad (4.38)$$

Hence, with the help of Eq. (4.37), the visibility is determined by

$$\mathcal{V}_{\text{ts}}(d, L, t) = \left| j(\mathbf{x}_1, \mathbf{x}_2) e^{-\left(\frac{d}{\xi^{\text{vac}}(L, t)}\right)^2} e^{-\left(\frac{d}{\xi^{\text{ts}}(L, t)}\right)^2} \right|, \quad (4.39)$$

which explicitly shows the *blurring* of the visibility induced by PGWs.

Consequently, Eq. (4.39) suggests that in the presence of PGWs, the visibility is modulated by damping factors that can completely suppress the interference pattern. The incoherence effect depends on the interaction time t , as well as the distance of the source to the Earth L . In addition, the length-scale $\xi^{\text{ts}}(L, t)$ depends also on the squeezing parameters (r_K, ϕ_K) , which on their own depend on the inflationary parameters such as tensor-to-scalar ratio. Thus, the order of magnitude of the incoherence depends crucially on the level of generated PGWs during inflation. On the other hand, successful measurement of spatial correlations of most distant sources can be convincing evidence that spatial correlations have survived during their journey to the Earth. In the following, we describe how very long baseline interferometry can help us constrain the underlying PGWs background.

5 Implication of PGWs background on the VLBI measurements

In this section, we discuss how the van Citter-Zernike correlations are affected by the presence of quantum GWs. We then define coherence criteria based on the van Citter-Zernike theorem and realize it with the help of the angular size-redshift $\theta - z$ measurements made by VLBI means. As we shall see, the coherence criteria lead to a stringent constraint on the tensor-to-scalar ratio.

5.1 van Citter-Zernike theorem and Very Long Baseline Interferometry (VLBI)

In this section, we first ignore the presence of GW background and describe the way VLBI method measures the angular size of an object by exploiting the coherence length of a distant source. In this case, the van Citter-Zernike theorem expresses the field correlations at two points in space, generated by a spatially incoherent, quasi-monochromatic, planar source, according to [18]

$$j(\mathbf{x}_1, \mathbf{x}_2) = \frac{2J_1(\nu)}{\nu}. \quad (5.1)$$

The function $j(\mathbf{x}_1, \mathbf{x}_2)$ is previously defined in Eq. (4.10), and expresses the equal-time spatial correlations of EM field at two points \mathbf{x}_1 and \mathbf{x}_2 . In Eq. (5.1), the dimensionless parameter ν is defined as $\nu = k \left(\frac{a}{L}\right) d$ with k being the central wave number of the quasi-monochromatic radiation, d stands for the separation of two telescopes (as shown in panel (c) of Fig. 2), a the radius of the planar source σ and L its distance to the Earth. The behavior of the function $j(\mathbf{x}_1, \mathbf{x}_2)$ versus the dimensionless parameter ν is depicted in Fig. 3. Starting by complete coherence $j(\mathbf{x}_1, \mathbf{x}_2) = 1$ at zero separation distance, correlations decrease steadily by increasing the distance between the detectors from $d = 0$ to $d = (3.83)k^{-1}(x/a)$ where

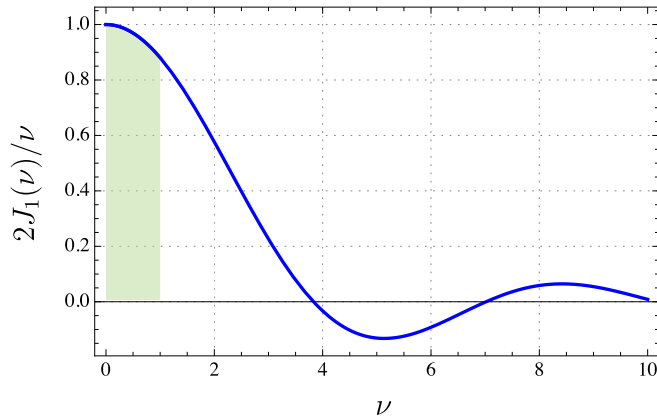


Figure 3. The mutual intensity $j(\mathbf{x}_1, \mathbf{x}_2) = 2J_1(\nu)/\nu$ versus the dimensionless parameter $\nu = k \left(\frac{a}{x}\right) d$. The colored region corresponds to the coherence length $0 \leq d \leq 2/k\theta$ where correlations decrease from unity to a value of 0.88. The mutual intensity vanishes for the first time for $\nu \simeq 3.83$.

complete incoherence $j(\mathbf{x}_1, \mathbf{x}_2) = 0$ happens for the first time. Then, the correlation increases again slightly, before vanishing for the second time. Practically, a drop from unity, which does not exceed about 12%, is not regarded as very significant [18]. This happens when $\nu < 1$, i.e., for a separation

$$d < \frac{1}{k} \left(\frac{L}{a}\right) = \frac{2}{k\theta}, \quad (5.2)$$

when correlations get a value 0.88. In the last equality, we replaced the ratio $\frac{a}{L}$ by $\frac{\theta}{2}$, where θ represents the angular diameter subtended by the source, when viewed from the Earth (see panel (c) of Fig. 2). Thus, *in the far zone and close to the direction normal to the source plane and parallel to it, the light produced by a spatially incoherent, quasi-monochromatic, uniform, circular source of radius a is approximately coherent over a circular area whose diameter is $\sim \frac{2}{k\theta}$* (see chapter 4 of [18]). Hence, one may regard the separation length $d_{\text{coh}} \equiv 2/(k\theta)$ as a threshold of coherence. For our purposes, we define the dimensionless *coherence parameter* as

$$\alpha_{\text{coh}} \equiv \log(k d_{\text{coh}}) = \log\left(\frac{2}{\theta}\right), \quad (5.3)$$

We remind that d is the transverse coherence length, namely the projected baseline of the VLBI apparatuses. For a general VLBI setup presented in panel (b) of Fig. 2, one has $d = b \sin \theta_s = \frac{2}{k\theta}$, where $\mathbf{b} = \mathbf{x}_1 - \mathbf{x}_2$ denotes the baseline and θ_s stands for the angle between the line of sight and the baseline of the interferometer. In the symmetric configuration as in panel (c) of Fig. 2, $d = b = |\mathbf{x}_1 - \mathbf{x}_2|$ corresponding to $\theta_s = 90^\circ$.

In practice, by varying the separation \mathbf{b} between two telescopes, one monitors the variation of the visibility which gives rise to the measurement of the angular size of the source. Successful measurement of the angular size of distant objects based on visibility implies that the correlation length of the source is at least equal to the projected baseline of the VLBI instrument.

5.2 VLBI measurement of the angular size of standard ruler

The angular size-redshift relation for an object of metric size ℓ_m located at angular diameter distance $L(z)$ in the flat Λ CDM model (neglecting the radiation fractional energy density Ω_r) is given by [116]

$$\theta(z) = \frac{\ell_m}{L(z)} = \frac{\ell_m H_0 (1+z)}{c} \left(\int_0^z \frac{dz'}{\sqrt{\Omega_m (1+z')^3 + (1-\Omega_m)}} \right)^{-1}, \quad (5.4)$$

where $\Omega_m \sim 0.3$ and $\Omega_\Lambda \sim 0.7$ denote the fractional matter and dark energy densities, respectively [110]. Combining Eq. (5.3) and Eq. (5.8) for the cosmological model of $\theta(z)$, the coherence parameter is identified by

$$\alpha_{\text{coh}}(z) \equiv \log \left(\frac{2}{\theta(z)} \right). \quad (5.5)$$

Recently, a set of 120 compact radio sources representing intermediate-luminosity quasars covering the redshift range $0.46 \leq z \leq 2.76$ have been investigated to check the possibility of using them as an independent cosmological probe. These quasars observed at 2.29 GHz show negligible dependence on redshift and intrinsic luminosity and thus represent a fixed comoving-length of a standard ruler. It is indeed found that compact structure in the intermediate-luminosity radio quasars could serve as a standard cosmological ruler and could thus provide valuable sources of angular diameter distances at high redshifts ($z \sim 3.0$) [95]. This new approach has recently been used to demonstrate that using these standard rulers could be helpful in understanding the current cosmological issues concerning the Hubble tension and cosmic curvature tension [97, 134], even if the precision is not yet sufficient compared to other standard ruler (CMB acoustic peak or baryon acoustic oscillations). What makes the use of these objects significant for us lies in the fact that these observations are made based on the VLBI technique, i.e., spatial correlations in the light coming from very distant radio quasars, observed on the Earth.

Using a compilation of angular size-redshift data for ultra-compact radio sources from a well-known VLBI survey, the linear size of this standard ruler turns out to be $\ell_m = 11.03 \pm 0.25$ pc, which is the typical radius at which AGN jets become opaque at the observed frequency $\omega_k \sim 2$ GHz. Here, we make use of the sample of 120 radio-quasars described in [95, 96, 135]. The scatter diagram of the observed angular size for 120 radio quasars is shown in panel (a) of Fig. 4. In this figure, the cyan line corresponds to fiducial Λ CDM model for $\theta(z)$, given by Eq. (5.8), with $H_0 = 67.4$ km s⁻¹ Mpc⁻¹ and $\Omega_m = 0.3$ adopted from the Planck results [110]. Moreover, the linear size of the standard ruler $\ell_m = 11.03$ pc is adopted [97]. Panel (b) of figure 4 is a representation of the coherence parameter $\alpha_{\text{coh}} = \log \left(\frac{2}{\theta(z)} \right)$ and the fit in cyan considering each quasar to be a standard ruler of size $\ell_m = 11.03$ pc.

5.3 Definition of the incoherence parameter $\alpha^{\text{ts}}(z)$ versus redshift

As we have seen in Sec. 4, the presence of PGWs can significantly change the visibility of VLBI measurements, defined by Eq. (5.1). Indeed, the visibility in the presence of PGWs changes according to Eq. (4.39). Substituting $j(\mathbf{x}_1, \mathbf{x}_2)$ from Eq. (5.1) into Eq. (4.39), we obtain

$$\mathcal{V}_{\text{ts}}(\mathbf{x}_P, t) = \left(\frac{2 J_1(k \theta d/2)}{(k \theta d/2)} \right) e^{-\left(\frac{d}{\xi^{\text{vac}}(L,t)}\right)^2} e^{-\left(\frac{d}{\xi^{\text{ts}}(L,t)}\right)^2}. \quad (5.6)$$

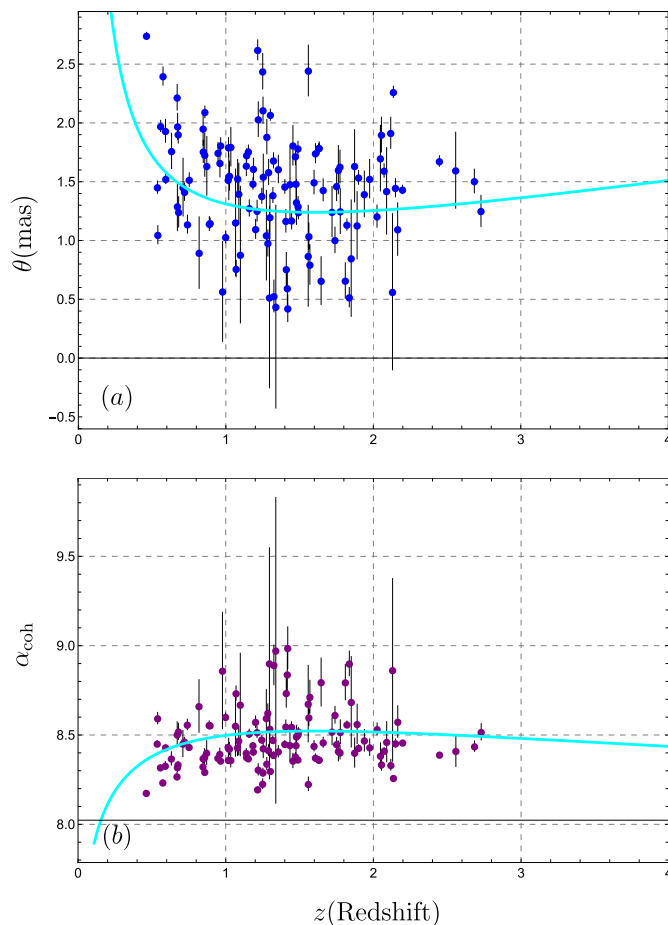


Figure 4. *Panel (a):* the scatter plot of angular sizes θ of 120 compact radio quasars based on the data given in Table. 1 of Cao et al [95]. The cyan line represents the fit $\theta(z)$ as given by Eq. (5.8) with a standard ruler given by $\ell_m = 11.03$ pc [97], as computed for a flat Λ CDM model with $H_0 = 67.4$ km s^{-1} Mpc $^{-1}$ and $\Omega_m = 0.3$ (adopted from the Planck results [110]). *Panel (b):* purple points show the coherence parameter α_{coh} based on $\theta - z$ data given in panel (a), and the cyan curve is a representation of the coherence parameter $\alpha_{\text{coh}}(z) = \log\left(\frac{2}{\theta(z)}\right)$ corresponding to panel (a).

Here, $\nu = k\theta d/2$ is plugged in. Thus, the presence of PGWs may significantly change the interference pattern. Due to negligibly small coupling strength $(\hbar\omega_k/E_{\text{Pl}})^2 \lll 1$, the incoherent dynamics induced by vacuum indicated by $\xi^{\text{vac}}(L, t)$ is too feeble to be sensed. For optical field of frequency $\sim 10^{15}$ Hz, one has $(\hbar\omega_k/E_{\text{Pl}})^2 \sim 10^{-58}$, thus $\xi^{\text{vac}}(L, t) \rightarrow \infty$, which implies that the vacuum fluctuations of GWs make no change in the visibility. Hence, the effect of two-mode squeezed PGWs appears only as the decaying exponential $e^{-(d/\xi^{\text{ts}}(L, t))^2}$ in the van Citter-Zernike correlations. To quantify the incoherence induced by PGWs and compare it with observational measurements, we define *incoherence parameter* as follows

$$\alpha^{\text{ts}}(L, t) \equiv \log\left(k\xi^{\text{ts}}(L, t)\right), \quad (5.7)$$

which is a dimensionless quantity, and is independent of the EM frequency (see definition Eq. (4.35) for $\xi^{\text{ts}}(L, t)$). This parameter contains the blurring of the interference pattern

induced by two-mode squeezed PGWs. Since we finally aim at considering objects located at a cosmological distance from the Earth, it seems natural to express time, distance, and frequency in terms of the redshift of the source z . The expression of the time of flight and distance in terms of the redshift, $t(z)$ and $L(z)$, in the flat Λ CDM spacetime is provided in App. C.4. Consequently, the incoherence parameter Eq. (5.6) in terms of the redshift of the source z is obtained as follows

$$\begin{aligned} \alpha^{\text{ts}}(z) &\equiv \log \left(k \xi^{\text{ts}}(z) \right) \\ &= \log \left(\left[\frac{1}{(2\pi)^2} \left(\frac{\hbar c}{E_{Pl}(1+z)} \right)^2 \int d\Phi_K \cos^2 \Phi_K \int d(\cos \Theta_K) \sin^6 \Theta_K \right. \right. \\ &\quad \times \int dK K \left(\frac{\sin(\frac{K_z L(z)}{2})}{(\frac{K_z L(z)}{2})} \right)^2 \left\{ \sinh^2 r_K \left(\sin^2 \frac{\Omega_K t(z)}{2} \right) + \frac{1}{8} \sinh 2r_K \right. \\ &\quad \left. \left. \times \left(\cos(2\phi_K) - 2 \cos(\Omega_K t(z) - 2\phi_K) + \cos(2\Omega_K t(z) - 2\phi_K) \right) \right\} \right]^{-1/2} \right). \end{aligned} \quad (5.8)$$

where $\omega_k \rightarrow \omega_k/(1+z)$ is substituted to account for the gravitational redshift of the EM frequency due to Universe expansion (see Sec. 3.1). If the PGWs background is too strong so that $\xi^{\text{ts}}(z)$ exceeds the transverse coherence length $d = 2/(k\theta(z))$, it renders the observation of the interference pattern and the measurement of the angular size of the source almost impossible. This will constitute a coherence criteria, which can be written as $d < \xi^{\text{ts}}(z)$, or equivalently $kd < k\xi^{\text{ts}}(z)$. In terms of the incoherence parameter, the coherence criteria is identified by

$$\alpha_{\text{coh}}(z) < \alpha^{\text{ts}}(z) \quad \Rightarrow \quad \alpha^{\text{ts}}(z) > \log \left(\frac{2}{\theta(z)} \right) \quad (5.9)$$

In the following, $\theta - z$ data of quasars at redshift range $0.46 \leq z \leq 2.73$, observed by VLBI means, are used to realize the coherence criteria Eq. (5.9). Consequently, we infer a new constraint on the tensor-to-scalar ratio r_{k_0} .

5.4 VLBI constraint on the tensor-to-scalar ratio r_{k_0}

The incoherence induced by two-mode squeezed PGWs is encapsulated in $\alpha^{\text{ts}}(z)$ given by the second equation in Eq. (5.7). To visualize the behavior of the incoherence parameter, we first assume that the PGWs modes are highly-squeezed, i.e., $r_K \gg 1$. Thus, one has $\bar{n}_{\text{ts}}(K) = \sinh^2 r_K \simeq e^{2r_K}/4$ and $\sinh 2r_K \simeq e^{2r_K}/2$. In this approximation, Eq. (5.8) reads

$$\begin{aligned} \alpha^{\text{ts}}(z) &= \log \left(\left[\frac{1}{(2\pi)^2} \left(\frac{\hbar c}{E_{Pl}(1+z)} \right)^2 \int d\Phi_K \cos^2 \Phi_K \int d(\cos \Theta_K) \sin^6 \Theta_K \right. \right. \\ &\quad \left. \left. \times \int dK K \left(\frac{\sin(\frac{K_z L(z)}{2})}{(\frac{K_z L(z)}{2})} \right)^2 \frac{e^{2r_K}}{4} \left\{ 2 \sin^2 \left(\frac{\Omega_K t(z)}{2} \right) \sin^2 \left(\frac{2\phi_K - \Omega_K t(z)}{2} \right) \right\} \right]^{-1/2} \right). \end{aligned} \quad (5.10)$$

Generally, for a given value of the redshift z , the term $\Omega_K t(z) = 2\phi_K$ happening for some specific values of Ω_K , leads the oscillating factor to vanish, so the contribution of those modes in integration. As a result, $\alpha^{\text{ts}}(z)$ might take a larger value when $\phi_K \neq 0$. In this way, the incoherence induced by two-mode squeezed PGWs may get attenuated as a result of non-vanishing ϕ_K . However, in the following discussion, we assume $\phi_K = 0$ which allows the contribution of all PGWs modes in the integrand Eq. (5.10) to be accounted for, hence leads to the most-stringent upper bound on tensor-to-scalar ratio. Thus, incorporating $\phi_K \neq 0$ may

relieve the following constraint. For vanishing squeezing phase $\phi_K = 0$, Eq. (5.10) further reduces to

$$\alpha_{\phi_K=0}^{\text{ts}}(z) = \log \left(\left[\frac{1}{(2\pi)^2} \left(\frac{\hbar c}{E_{\text{Pl}}(1+z)} \right)^2 \int d\Phi_K \cos^2 \Phi_K \int d(\cos \Theta_K) \sin^6 \Theta_K \right. \right. \\ \left. \left. \times \int dK K \left(\frac{\sin(\frac{K_z L(z)}{2})}{(\frac{K_z L(z)}{2})} \right)^2 \frac{e^{2r_K}}{2} \sin^4 \left(\frac{\Omega_K t(z)}{2} \right) \right]^{-1/2} \right). \quad (5.11)$$

Fig. 5 shows the plot of $\alpha_{\phi_K=0}^{\text{ts}}(z)$ versus redshift, based on Eq. (5.11). Here, the expression

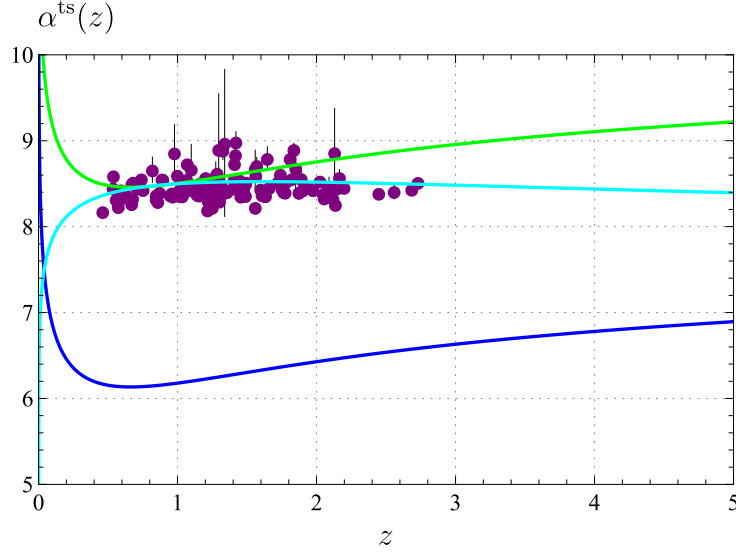


Figure 5. The incoherence parameter $\alpha^{\text{ts}}(z)$ versus redshift z in case of two-mode squeezed GWs based on Eq. (5.11). The purple points show the coherence parameter α_{coh} based on $\theta-z$ data, and the cyan curve represents the coherence parameter α_{coh} based on Eq. (5.5) for the standard ruler of size $\ell_m = 11.03$ pc (see panel (b) of Fig. 4). Here, blue and green curves correspond to $r_{k_0} = 0.032 \sim 10^{-1.5}$ and $r_{k_0} = 10^{-6.15}$, respectively. Other parameters are chosen as $\beta = -2, \beta_s = 1, T_{\text{reh}} = 10^8$ Gev. The coherence criteria $\alpha^{\text{ts}}(z) \geq \alpha_{\text{coh}}(z)$ is met for $r_{k_0} \lesssim 10^{-6.15}$.

Eq. (2.17) for $e^{r_K(\eta_H)}$ has been used, where $\beta = -2, \beta_s = 1$ and $T_{\text{reh}} = 10^8$ Gev are fixed. Different values of r_{k_0} are chosen as follows: the blue curve is plotted for $r_{k_0} = 0.032 \sim 10^{-1.5}$ corresponding to the improved constraint on this parameter made by *Planck PR4 (2020)* [136]; the green curve corresponds to a reduced value of the tensor-to-scalar ratio, $r_{k_0} = 10^{-6.15}$ for which the coherence criteria $\alpha^{\text{ts}}(z) \geq \alpha_{\text{coh}}(z)$ is met. It is only in this circumstance that the van Citter-Zernike correlations are detected, otherwise one has $\xi^{\text{ts}}(z) \leq d_{\text{coh}}(z)$ and the visibility Eq. (5.6) vanishes. The cyan curve shows the fit of the coherence parameter $\alpha_{\text{coh}}(z)$ for standard ruler with size $\ell_m = 11.03$ pc (see panel (b) of Fig. 4).

The coherence criteria $\alpha^{\text{ts}}(z) > \alpha_{\text{coh}}(z)$ (or equivalently $\xi^{\text{ts}}(z) > d_{\text{coh}}(z)$) is violated for the blue curve for which $r_{k_0} = 0.032 \sim 10^{-1.5}$. Changing other parameters such as $\beta, \beta_s, T_{\text{reh}}$ practically does not change the incoherence parameter $\alpha^{\text{ts}}(z)$. However, reducing and increasing the tensor-to-scalar ratio r_{k_0} drastically shifts the curve $\alpha^{\text{ts}}(z)$ up and down, respectively. Since $e^{2r_K} \propto A^2 \propto r_{k_0}$ (see Eq. (2.17) and (2.18)), Eq. (4.35) implies that $\xi^{\text{ts}} \propto r_{k_0}^{-1/2}$. Hence, this scaling implies that a reduction of the tensor-to-scalar ratio leads the

incoherence length $\xi^{\text{ts}}(z)$ to increase since PGWs leave a weaker effect on spatial correlations of the EM field.

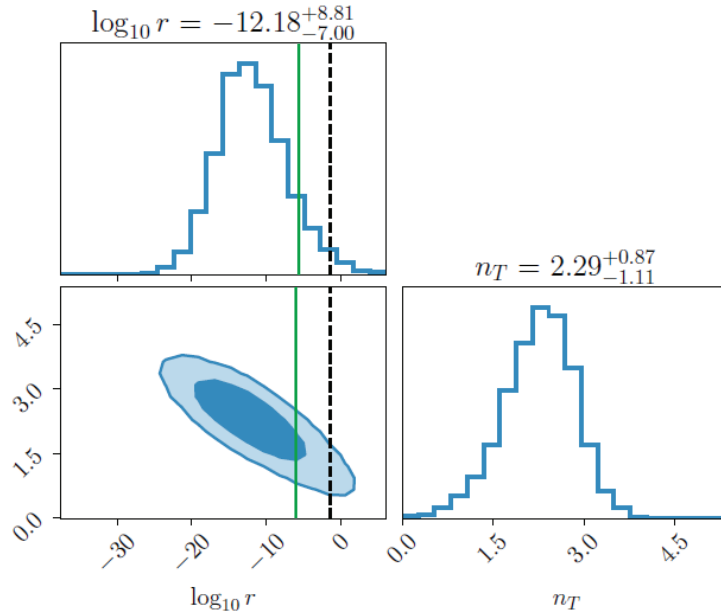


Figure 6. 2D posteriors of the tensor-to-scalar ratio (in \log_{10}) and the fractional energy density spectral index n_T in the PTA observations (figure extracted from [137]). The 68% and 95% credible regions are displayed. The black dashed line represents the tensor-to-scalar ratio upper bound $r_{k_0} = 0.032 \sim 10^{-1.5}$ found by Planck combined with BK18 and baryon-acoustic-oscillation [136] and the solid green line corresponds to the upper bound $r_{k_0} \sim 10^{-7}$ based on VLBI $\theta - z$ measurement, found in the present study.

The current constraint on the tensor-to-scalar ratio coming from the combination of Planck with BK18 and baryon-acoustic-oscillation is $r_{k_0} < 0.032$ [136]. However, recent measurements of the European pulsar timing array (EPTA) are compatible with excessively small values $r_{k_0} \sim 10^{-12.1}$ [137]. Figure 6 shows the 2D posteriors of the tensor-to-scalar ratio (in \log_{10}) and the fractional energy density spectral index n_T in the PTA observations at the nanohertz working frequency [137]. The 68% and 95% credible regions are displayed. The black dashed line represents the tensor-to-scalar ratio upper bound $r_{k_0} = 0.032 \sim 10^{-1.5}$ found by Planck combined with BK18 and baryon-acoustic-oscillation [136] assuming single-field slow-roll inflation. The solid green line corresponds to the upper bound $r_{k_0} = 10^{-6.15}$ based on VLBI $\theta - z$ measurement, found in this study. The present constraint $r_{k_0} \lesssim 10^{-6.15}$ based on VLBI $\theta - z$ measurements is compatible with the inferred value from EPTA if the detected GW background is indeed the primordial GW background.

6 Further discussion and results

6.1 Implications for the slow-roll framework

We have seen that PGWs induced-incoherence may put constraints on the inflationary parameter r_{k_0} while the reheating parameters such as $(\beta_s, \zeta_1, T_{\text{reh}})$ are not sensible by this method, as we explained before. Although we have presented the method in a model-independent manner, specific models describing the inflationary epoch can be addressed straightforwardly.

General inflationary parameters such as r_{k_0} , β , n_s and n_T are expressible in terms of the slow-roll parameters within a given inflationary model with specific potential $V(\phi)$. Hence, the coherence criteria based on $\theta - z$ observations may put constraints on the model parameters. However, the stringent upper bound $r_{k_0} \lesssim 10^{-6.15}$ which was obtained in a model-independent manner, holds correct and implies extremely small values for the (first order) slow-roll parameter ϵ_V .

Generally, under the first order slow-roll approximation, tensor and scalar spectral tilts are determined by $n_T \simeq -2\epsilon_V$ and $n_s - 1 \simeq 2\eta_V - 6\epsilon_V$, where ϵ_V and η_V are the slow-roll parameters which depend on the specific form of the inflationary potential $V(\phi)$. Assuming the initial tensor spectrum $h(k_0, \eta_i) = A(k_0/K_H)^{2+\beta}$ constitutes tensor perturbation at pivot scale, $A_T(k_0)$, one obtains the relation $n_T = 2\beta + 4$ [113]. Hence, a general (model-independent) result is the relation between ϵ_V and β given by $\epsilon_V = -\beta - 2$. Note that according to definition, $\epsilon_V > 0$ so that $\beta < -2$. Moreover, the single-field slow-roll inflation predicts $r = -8n_T = 16\epsilon_V = -16(\beta + 2)$. Hence, the constraint $r_{k_0} \lesssim 10^{-6.15}$ implies upper bound on the slow-roll parameter such that $\epsilon_V \lesssim 4.4 \times 10^{-8}$ and $|n_T| \lesssim 8.8 \times 10^{-8}$. Such small values for r_{k_0} and ϵ_V are compatible with the prediction of some specific inflationary models [138]. Hence, knowledge of upper bounds on slow-roll parameters based on VLBI method may rule out inflationary models or put stringent constraints on the model parameters. On the experimental side, while the Planck collaboration combined with BK18 and baryon-acoustic-oscillation place a limit on the tensor-to-scalar ratio $r_{k_0} \lesssim 0.032$ [136], recent measurements of the European pulsar timing array (EPTA) are compatible with much smaller values $r_{k_0} \sim 10^{-12.1}$ [137]. Consequently, the constraint $r_{k_0} \lesssim 10^{-6.15}$ stemming from VLBI is compatible with the possible detection of a relic GW background with EPTA [137].

6.2 Possible quantum-to-classical transition issue

So far, it turns out that the highly-correlated highly-populated two-mode squeezed PGWs leave a severe effect on the phase-correlations of the EM field, leading to a stringent constraint on r_{k_0} . However, possible decoherence of PGWs may change the result [121, 139]. Basically, in a given decoherence schema for PGWs, it is crucial to follow the dynamics of the *mean number of gravitons* and *quantum correlations between gravitons* in the course of Universe expansion. These information are encoded in the diagonal and off-diagonal elements (in the Fock space representation) of the density matrix describing the evolution of PGWs, namely $\rho_{\text{pgws}}^{mn}(\eta)$. Possible decaying of the density matrix elements due to the decoherence mechanism, especially in the ultra-low frequency band of PGWs, may significantly reduce the incoherence of the EM field that results in a less stringent upper bound on the tensor-to-scalar ratio r_{k_0} . In particular, the decay of the diagonal elements corresponds to the decay of the mean number of gravitons, which leads to weaker EM-GWs coupling, and relieves the constraint on r_{k_0} . Hence, investigating the effect of PGWs subjected to decoherence on the phase correlations of the EM field deserves further assay that can be addressed within the presented formalism. The main goal of the present study is to introduce and evaluate a new way to look forward quantum gravitational effects using the well-established VLBI techniques and to infer the corresponding model parameters based on that.

7 Summary and conclusion

In a nutshell, this work promotes the idea of using gravitational-induced spatial incoherence of the EM field radiated from distant objects, as a new approach to probe the inflationary

Universe. We theoretically investigated the spatial coherence of the EM field emitted from distant objects interacting with the background of primordial gravitational waves which encode historical features of the expanding Universe in itself. It turns out that spatial correlation of the EM field, which in the absence of PGWs is simply governed by the van Citter-Zernike theorem, is modified by the presence of PGWs such that the transverse separation d between two telescopes in the VLBI can not exceed a characteristic length-scale $\xi^{\text{ts}}(L, t)$ defined by Eq. (4.35), otherwise the interference vanishes. However, successful observation of the visibility pattern in VLBI experiments implies that $\xi^{\text{ts}}(z)$ must be larger than the projected baseline of the VLBI. A coherence criterion has been defined based on the van-Citter-Zernike theorem which relates the spatial coherence of the source, d_{coh} , to its angular size $\theta(z)$. We used the angular size-redshift relation $\theta-z$ of 120 radio AGNs located at redshift range $0.46 \leq z \leq 2.73$ to define the coherence parameter, $\alpha_{\text{coh}}(z) \equiv \log(\frac{2}{\theta(z)})$ (see Eq. (5.5)), based on which the two-mode squeezed PGWs induced-incoherence can be constrained. It turns out that the coherence criteria $\alpha^{\text{ts}}(z) > \alpha_{\text{coh}}(z)$ exerts stringent upper bound on the tensor-to-scalar ratio, $r_{k_0} \lesssim 10^{-6.15}$. Hence, it is found that the present method can be used to put a constraint on specific inflationary model parameters. The aim of the present study is to highlight the capability of the interferometric methods, in particular the very long baseline interferometry technique, to put constraints on the inflationary Universe by means of gravitationally induced incoherence of the electromagnetic field. Altogether, VLBI method seems promising to be used as a new observatory to search for quantum features of spacetime.

8 Supplementary materials

A PGWs spectrum and related parameters

A.1 Increase parameters $\zeta_E, \zeta_2, \zeta_s, \zeta_1$

In the Λ CDM framework, one can show that the increase parameter during Λ -dominated stage is given by

$$\zeta_E = 1 + z_E = (\Omega_\Lambda/\Omega_m)^{1/3} \simeq 1.33, \quad (\text{A.1})$$

given the current values $\Omega_\Lambda \sim 0.7$ and $\Omega_m \sim 0.3$. Here, z_E is the redshift at the matter-dark energy equality. The increase factor at matter-radiation equality is

$$\zeta_2 = (1 + z_{\text{eq}}) \zeta_E^{-1} \simeq 2547, \quad (\text{A.2})$$

where $z_{\text{eq}} = 3387$ [110]. The increase of scale factor during the reheating, namely ζ_s , depends on the reheating temperature T_{reh} through [113]

$$\zeta_s = \frac{T_{\text{reh}}}{T_{\text{CMB}}(1 + z_{\text{eq}})} \left(\frac{g_{*s}}{g_{*s}} \right)^{1/3}, \quad (\text{A.3})$$

where $T_{\text{CMB}} = 2.348 \cdot 10^{-13}$ GeV [140]. Here, g_{*s} and g_{*s} count the effective number of relativistic species contributing to the entropy during the reheating and recombination, respectively, and will be taken $g_{*s} \simeq 200$ and $g_{*s} = 3.91$ [141], as was also employed in [113]. Moreover, under the quantum normalization condition, the increase parameter ζ_1 is expressed in terms of $\zeta_s, \zeta_2, \zeta_E$ according to Eq. (2.19).

A.2 Spectral amplitude of PGWs

The dimensionless *spectral amplitude* of PGWs, $h(k, \eta)$ is usually defined by [103]

$$\int_{K_E}^{K_1} h^2(K, \eta) \frac{dK}{K} \equiv \langle \text{TS}(\eta) | \hat{h}_{ij}(\mathbf{x}, \eta_{\text{ini}}) \hat{h}^{ij}(\mathbf{x}, \eta_{\text{ini}}) | \text{TS}(\eta) \rangle, \quad (\text{A.4})$$

where the r.h.s is the variance of the field in the two-mode squeezed state and $\hat{h}_{ij}(\mathbf{x}, \eta_{\text{ini}})$ is given by Eq. (2.9). Note that, as we discussed in Sec. (2.2), in the Schrödinger picture the evolution of perturbations is included in the state of the system, while the field operator is given by its initial expression. Moreover, the lower and upper limits of the integral are considered as $K_{\text{low}} = K_E$ and $K_{\text{up}} = K_1$. Inserting Eq. (2.9) into Eq. (A.4) and with the help of Eqs. (2.10 - 2.13), one may straightforwardly show that

$$h(K, \eta) = \frac{4\ell_{\text{Pl}}}{\sqrt{\pi}a(\eta)} K \left(|u_K(\eta)|^2 + |v_K(\eta)|^2 + u_K(\eta)v_K(\eta) + u_K^*(\eta)v_K^*(\eta) \right)^{1/2}. \quad (\text{A.5})$$

where the functions $u_K(\eta)$ and $v_K(\eta)$ are given by Eq. (2.13) with the initial conditions $u_K(\eta_{\text{ini}}) = 1$ and $v_K(\eta_{\text{ini}}) = 0$ [115]. Thus, using the expression Eq. (A.5), one may find the evolution of the spectral amplitude $h(K, \eta)$ readily, as soon as the evolution of the functions $u_K(\eta)$ and $v_K(\eta)$ are determined. Another important application of Eq. (A.5) is to build the relationship between the squeezing parameters (r_k, ϕ_k) and the spectral amplitude $h(K, \eta)$. Especially, by substitution of Eq. (2.13) for the functions u_K and v_K into Eq. (A.5) and assuming $r_K \gg 1$ for super-Hubble modes ($K \leq 2\pi\mathcal{H}$), one obtains the following relationship

$$h(K, \eta) = 8\sqrt{\pi} \left(\frac{\ell_{\text{Pl}}}{\ell_H} \right) \left(\frac{K}{K_H} \right) e^{r_K(\eta)} \cos \phi_K(\eta). \quad (\text{A.6})$$

Eq. (A.6) is in accordance with Eq. (31) of [22]. Note that, according to Eq. (2.14), the variable ϕ_k is not an independent variable, and its dynamics are determined once the dynamics of r_K are specified. Hence, the evolution of $h(K, \eta)$ can be solely given by the evolution of the squeezing amplitude r_K . Inversely, one may obtain the approximate expression of the squeezing factor e^{r_K} from $h(K, \eta)$ according to

$$e^{r_K(\eta)} = \frac{1}{8\sqrt{\pi}} \left(\frac{\ell_H}{\ell_{\text{Pl}}} \right) \left(\frac{K_H}{K} \right) h(K, \eta). \quad (\text{A.7})$$

in the super-Hubble regime, where the oscillatory factor $\cos \phi_k$ tends to 1 (see Eq. (2.15)). On the other hand, one may show that $h(K, \eta)$ is related to the Fourier field amplitude $h_{\mathbf{K}}(\eta)$ (defined in Eq. (2.3)) by the following relation

$$h(K, \eta) = \frac{4\ell_{\text{Pl}}K}{\sqrt{\pi}} \sqrt{\frac{2K}{\hbar}} |h_{\mathbf{K}}(\eta)|. \quad (\text{A.8})$$

Note that, definition of $h_{\mathbf{K}}(\eta)$ is occasionally different with Eq. (2.3) in a $\sqrt{2K}$ factor. In some references, the prefactor $1/\sqrt{2K}$ is included in the field expansion Eq. (2.3), while in others this prefactor is implied in the temporal mode functions $h_{\mathbf{K}}^\gamma(\eta)$. Here, we adopted the second notation. As a result of Eq. (A.8), the spectral amplitude could also be found by solving the equation of motion for $h_{\mathbf{K}}(\eta)$ given by Eq. (2.7). Especially, one may show that during the long wavelength regime, the spectral amplitude $h_{\mathbf{K}}(\eta)$ (and $h(K, \eta)$) stay constant.

In this manner, approximate solutions for $h(K, \eta)$ are found in the super-Hubble regime. It turns out that the spectral amplitude is determined by [104]

$$h(K, \eta) = \begin{cases} A \left(\frac{K}{K_H} \right)^{2+\beta} & , \quad K \leq K_E \\ A \left(\frac{K}{K_H} \right)^{\beta-\gamma} \zeta_E^{-\frac{2+\gamma}{\gamma}} & , \quad K_E \leq K \leq K_H \\ A \left(\frac{K}{K_H} \right)^{\beta} \zeta_E^{-\frac{2+\gamma}{\gamma}} & , \quad K_H \leq K \leq K_2 \\ A \left(\frac{K}{K_H} \right)^{1+\beta} \left(\frac{K_H}{K_2} \right) \zeta_E^{-\frac{2+\gamma}{\gamma}} & , \quad K_2 \leq K \leq K_s \\ A \left(\frac{K}{K_H} \right)^{1+\beta-\beta_s} \left(\frac{K_s}{K_H} \right)^{\beta_s} \left(\frac{K_H}{K_2} \right) \zeta_E^{-\frac{2+\gamma}{\gamma}} & , \quad K_s \leq K \leq K. \end{cases} \quad (\text{A.9})$$

where the coefficient A is discussed in Sec. 2.3.

A.3 Characteristic wave numbers K_E, K_H, K_2, K_s and K_1

The conformal wave number at a given jointing time η_x is defined as $K_x \equiv K(\eta_x) = 2\pi\mathcal{H}(\eta)$, assuming the wave mode crosses the horizon when $\lambda = 1/\mathcal{H}$ with \mathcal{H} being the Hubble radius (this definition for horizon-crossing is also used in [22, 109]). Thus $K_H = 2\pi\mathcal{H}(\eta_H) = 2\pi\gamma$ is the conformal Hubble wave number. The physical wave number at present is related to the conformal wave number K according to $K^{\text{ph}} = K/a(\eta_H) = K/\ell_H$. Hence, $K_H^{\text{ph}} = 2\pi\gamma/\ell_H = 2\pi H_0/c$ with H_0 being today Hubble frequency. One can show that characteristic wave numbers at different jointing points η_1, η_s, η_2 and η_E are related to the increase parameters according to [103]

$$\frac{K_E}{K_H} = \zeta_E^{-\frac{1}{\gamma}} \quad , \quad \frac{K_2}{K_E} = \zeta_2^{\frac{1}{2}} \quad , \quad \frac{K_s}{K_2} = \zeta_s \quad , \quad \frac{K_1}{K_s} = \zeta_1^{\frac{1}{1+\beta_s}}. \quad (\text{A.10})$$

Similar expressions hold for the PGWs frequencies, $\Omega_K = cK$. Given $H_0 = 67.4 \text{ km s}^{-1} \text{ Mpc}^{-1}$ one has $K_H^{\text{ph}} \sim 4.52 \times 10^{-26}$, $K_E^{\text{ph}} = 3.4 \times 10^{-26}$ and $K_2 = 1.71 \times 10^{-24}$ in m^{-1} units. The values of K_s and K_1 , corresponding to waves that crossed the horizon at the end of the reheating and inflationary stages respectively, are determined by $(\zeta_s, \zeta_1, \beta_s)$. For $T_{\text{reh}} = 10^8 \text{ GeV}$, $K_s = 7.9 \text{ m}^{-1}$ and K_1 depends also on the values of (β, r_{k_0}) through Eq. (2.19). For $\beta = -2$ and $r_{k_0} = 10^{-1.5}$ adopted in this study, one has $K_1 = 0.08 \text{ m}^{-1}$.

Basically, β_s and T_{reh} determine characteristic features of the expanding Universe during the reheating stage, so they only affect the frequencies Ω_s and Ω_1 , e.g., waves re-entering the horizon during the reheating stage (see panel (a, b) of figure 1). However, the main contribution to the incoherence mechanism comes from ultra-low frequency PGWs, say $\Omega_K \leq \Omega_s$, which possess higher squeezing amplitudes. Throughout the paper, unless it is stated, we mostly take $\beta_s = 1$ and $T_{\text{reh}} = 10^8 \text{ GeV}$ in our calculations.

The value of the upper frequency of PGWs, $\Omega_{K_1} = cK_1$, depends on the choice of the increase parameter ζ_1 . Modes with frequency higher than Ω_{K_1} have been decayed by the expansion of the universe and have not been squeezed at all. In any case, the value of Ω_{K_1} should be below the constraint from the rate of the primordial nucleosynthesis, i.e., $\Omega_{K_1} \lesssim 10^{10} \text{ Hz}$ [113, 122], which is the case in our study.

B Hamiltonian formalism for description of EM-GWs interaction

In this section, we present a detailed derivation of the interaction Hamiltonian describing EM-GWs coupling, given by Eq. (3.3), within the adiabatic conditions where $K \ll k$ and

$\Omega_K \ll \omega_k$. The calculation is a generalization of the method introduced in [100] to the case where the small-detector approximation $KL \ll 1$ is abandoned, and spatial expansion of the probe can be arbitrarily large. In [100], the idea of using the optical medium analogy is promoted to derive the interaction Hamiltonian describing the EM-GWs coupling at the quantum level. Although, one should note that the resulting Hamiltonian is independent of the approach, and identical results could be obtained starting from the Einstein-Hilbert action $S_{\text{int}}^{\text{EH}} = -1/2 \int d^4x h_{\mu\nu} T^{\mu\nu}$, with $h_{\mu\nu}$ and $T^{\mu\nu}$ describing GWs perturbations field and the energy-momentum tensor of the EM field, respectively.

B.1 Derivation of the EM-GWs Hamiltonian $\hat{H}_{\text{em-gw}}$ in the adiabatic limit

As it is shown in [100], the vector potential \mathbf{A} of the EM field in the presence of GWs in Minkowski spacetime obeys the following generalized wave equation

$$\nabla \times [\bar{\mu}^{-1}(\mathbf{x}, t) \nabla \times \mathbf{A}(\mathbf{x}, t)] = -\bar{\varepsilon}(\mathbf{x}, t) \partial_t^2 \mathbf{A}(\mathbf{x}, t), \quad (\text{B.1})$$

such that the electromagnetic fields are determined by $\mathbf{E} = -\partial_t \mathbf{A}$ and $\mathbf{B} = \nabla \times \mathbf{A}$. Here, the (spacetime-dependent) permittivity and permeability tensors $\bar{\varepsilon}(\mathbf{x}, t)$ and $\bar{\mu}(\mathbf{x}, t)$ are characterized by [100]

$$\begin{aligned} \varepsilon_{ij}(\mathbf{x}, t)/\varepsilon_0 = \mu_{ij}(\mathbf{x}, t)/\mu_0 &= \delta_{ij} - h_{ij}(\mathbf{x}, t) \\ &= \delta_{ij} - \mathcal{C} \sum_{\gamma=+, \times} \int \frac{d^3\mathbf{K}}{(2\pi)^{3/2}} \frac{e_{ij}^\gamma[\hat{\mathbf{K}}]}{\sqrt{2\Omega_K}} \left(h_{\mathbf{K}}^\gamma e^{-i(\Omega t - \mathbf{K} \cdot \mathbf{x})} + h_{\mathbf{K}}^{\gamma*} e^{i(\Omega t - \mathbf{K} \cdot \mathbf{x})} \right), \end{aligned} \quad (\text{B.2})$$

Here, Eq. (3.6) is used for the expression of $h_{ij}(\mathbf{x}, t)$. For a general discussion, we have replaced quantum ladder operators $\hat{b}_{\mathbf{K}, \gamma}$ and $\hat{b}_{\mathbf{K}, \gamma}^\dagger$ by classical field amplitudes $h_{\mathbf{K}}^\gamma$ and $h_{\mathbf{K}}^{\gamma*}$. However, the following arguments and results hold correct, whether $h_{ij}(\mathbf{x}, t)$ is treated as classical or quantum entity.

In order to solve Eq. (B.1), one consider a plane-wave expansion of the vector potential $\mathbf{A}(\mathbf{x}, t)$ as follows

$$\mathbf{A}(\mathbf{x}, t) = \sum_k \sqrt{\frac{\hbar}{2}} \left(\alpha_k \nu_k(\mathbf{x}, t) \mathbf{f}_k(\mathbf{x}, t) + \alpha_k^* \nu_k^*(\mathbf{x}, t) \mathbf{f}_k^*(\mathbf{x}, t) \right). \quad (\text{B.3})$$

Here, $k \equiv (\lambda, \mathbf{k})$ denotes different modes of the EM field with wave vector \mathbf{k} and polarization λ , and α_k is the expansion coefficient. Although the quantum pre-factor \hbar is included intentionally, at the classical level one can substitute $\alpha_k \sqrt{\hbar} \rightarrow \mathcal{A}_k$. The time-harmonic behavior of $\mathbf{A}(\mathbf{x}, t)$ is included in the temporal mode function $\nu_k(\mathbf{x}, t)$ which recasts to $e^{\pm i\omega_k t}$ in the vacuum case, i.e., when there is no gravitational background. However, we let this function be \mathbf{x} -dependent as well since the gravitational background is \mathbf{x} -dependent through $h_{ij}(\mathbf{x}, t)$. That means, $\nu_k(\mathbf{x}, t)$ is a slowly varying function of \mathbf{x} . The spatial mode function $\mathbf{f}_k(\mathbf{x}, t)$ contains the spatial factor which recasts to the plane modes $e^{i\mathbf{k} \cdot \mathbf{x}}$ in the absence of GWs, and again we let it to have a slowly varying envelope as well since the gravitational medium is time-dependent. Thus we may consider $\mathbf{f}_k(\mathbf{x}, t) \equiv f(t) \hat{\mathbf{u}}_{\mathbf{k}} e^{i\mathbf{k} \cdot \mathbf{x}}$ with $f(t)$ being a slowly varying function of time and $\hat{\mathbf{u}}_{\mathbf{k}}$ a unit vector denoting the polarization of the electric field. The slowly varying envelope approximation (SVEA) implies that [142]

$$\left| \frac{\ddot{\mathbf{f}}_k}{\dot{\mathbf{f}}_k} \right| \ll \left| \frac{\dot{\mathbf{f}}_k}{\mathbf{f}_k} \right| \ll \omega_k, \quad \left| \frac{\nabla^2 \nu_k(\mathbf{x}, t)}{\nabla \nu_k(\mathbf{x}, t)} \right| \ll \left| \frac{\nabla \nu_k(\mathbf{x}, t)}{\nu_k(\mathbf{x}, t)} \right| \ll k. \quad (\text{B.4})$$

That means a temporal change of the spatial mode function due to the existence of GWs happens in a time scale much larger than the characteristic oscillatory behavior of the EM wave. Similarly, spatial change of the temporal mode functions induced by GW medium happens at scales much larger than the typical wavelength of the EM field. Inserting the field expansion Eq. (B.3) into the wave equation Eq. (B.1) results in

$$\left[\nabla \times \left(\bar{\mu}^{-1}(\mathbf{x}, t) \nabla \times \mathbf{f}_k(\mathbf{x}, t) \right) \right] \nu_k(\mathbf{x}, t) = -\ddot{\nu}_k(\mathbf{x}, t) \bar{\epsilon}(\mathbf{x}, t) \mathbf{f}_k(\mathbf{x}, t). \quad (\text{B.5})$$

In derivation of Eq. (B.5), we have neglected spatial derivative of $\bar{\mu}(\mathbf{x}, t)$ and $\nu_k(\mathbf{x}, t)$, as well as time derivative of $\mathbf{f}_k(\mathbf{x}, t)$ under the adiabatic approximation Eq. (B.4). Thus, Eq. (B.5) contains the second-order spatial derivative of $\mathbf{f}_k(\mathbf{x}, t)$ in the left-hand side, and second-order time derivative of $\nu_k(\mathbf{x}, t)$ in the right-hand side. To solve Eq. (B.5), we proceed by assuming the following time behavior for the temporal mode functions,

$$\ddot{\nu}_k(\mathbf{x}, t) \equiv -\omega_k^2(\mathbf{x}, t) \nu_k(\mathbf{x}, t). \quad (\text{B.6})$$

Firstly, note that the \mathbf{x} -dependence of temporal mode function $\nu_k(\mathbf{x}, t)$ must satisfy the SVEA condition Eq. (B.4). In the following, we shall see that this is indeed the case. On the other hand, in the proposed form Eq. (B.6) a friction term is absent in the time evolution of the EM field, while its frequency may be affected by the underlying GWs background. This assumption intuitively supports the fact that the GW background does not produce or annihilate photons, under the adiabatic approximation where $\Omega_K \ll \omega_k$. This means that the GW medium is not dispersive and absorptive in the optical range since the EM-GWs interaction is off-resonant. In the corresponding quantum field theory, this assumption implies that EM-GWs interaction does not create or annihilate photons, and the mean number of photons in the EM field is conserved. This point was first noted by Kip. Thorne [143] in the case of a slowly varying GW background.

Now, inserting Eq. (B.6) into the wave equation Eq. (B.5) yields

$$\nabla \times \left(\bar{\mu}^{-1}(\mathbf{x}, t) \nabla \times \mathbf{f}_k(\mathbf{x}, t) \right) = \omega_k^2(\mathbf{x}, t) \bar{\epsilon}(\mathbf{x}, t) \mathbf{f}_k(\mathbf{x}, t), \quad (\text{B.7})$$

which is an eigen-equation for $\mathbf{f}_k(\mathbf{x}, t)$ with eigen-values $\omega_k(\mathbf{x}, t)$. In the presence of anisotropic media, it is convenient to define the orthogonality equation of the spatial mode functions $\mathbf{f}_k(\mathbf{x}, t)$ according to

$$\int_V d^3\mathbf{x} \bar{\epsilon}_{ij}(\mathbf{x}, t) f_{\lambda, \mathbf{k}}^{*i}(\mathbf{x}, t) f_{\lambda', \mathbf{k}'}^j(\mathbf{x}, t) = \delta^{(3)}(\mathbf{k} - \mathbf{k}') \delta_{\lambda\lambda'}. \quad (\text{B.8})$$

(see [100] and references therein). Here, $f_{\lambda, \mathbf{k}}^i(\mathbf{x}, t)$ denote the i -th component of the spatial mode function of mode $k = (\lambda, \mathbf{k})$, namely $\mathbf{f}_{\lambda, \mathbf{k}}$. Note that since the medium is spacetime-dependent, in general, the integration in Eq. (B.8) does not produce the Dirac delta function $\delta^{(3)}(\mathbf{k} - \mathbf{k}')$. However, as we are going to see in the next section, the orthonormality relation Eq. (B.8) holds correct in the adiabatic limit $K \ll k$.

B.2 Orthogonality relation of the mode functions $\mathbf{f}_k(\mathbf{x}, t)$

Firstly note that our EM fields of interest have a frequency of radio to optical waves, which span from \sim GHz to 10^{15} Hz so that $10 \leq k \leq 10^7 \text{ m}^{-1}$. On the other hand, PGWs span a wide range of frequency $10^{-18} \leq \Omega_K \leq 10^{10}$ Hz, so that $10^{-26} \leq K \leq 10^2 \text{ m}^{-1}$. Thus,

the adiabatic condition $K \ll k$ is almost fulfilled for PGWs and radio waves. Moreover, the high-frequency part of PGWs has a negligible graviton content, and their effect on the EM observables is automatically vanishing due to the small coupling strength. Inserting the expression of $\mathbf{f}_k(\mathbf{x}, t) = f(t) \hat{\mathbf{u}}_{\mathbf{k}} e^{i\mathbf{k}\cdot\mathbf{x}}$ (where $f(t)$ is a slowly-varying function of time satisfying Eq. (B.4)) into Eq. (B.8), and with the help of Eq. (B.2), one obtains

$$\begin{aligned}
\langle \mathbf{f}_k | \mathbf{f}_{k'} \rangle &= \varepsilon_0 f^2(t) \int d^3\mathbf{x} (\delta_{ij} - h_{ij}(\mathbf{x}, t)) \hat{\mathbf{u}}_{\mathbf{k}i} \hat{\mathbf{u}}_{\mathbf{k}'j} e^{-i(\mathbf{k}-\mathbf{k}')\cdot\mathbf{x}}, \\
&= \varepsilon_0 f^2(t) (2\pi)^3 \delta_{ij} \hat{\mathbf{u}}_{\mathbf{k}i} \hat{\mathbf{u}}_{\mathbf{k}'j} \delta^{(3)}(\mathbf{k} - \mathbf{k}') \\
&\quad - \varepsilon_0 f^2(t) \hat{\mathbf{u}}_{\mathbf{k}i} \hat{\mathbf{u}}_{\mathbf{k}'j} \mathcal{C} \sum_{\gamma=+, \times} \int \frac{d^3\mathbf{K}}{(2\pi)^{3/2}} \frac{e_{ij}[\hat{\mathbf{K}}]}{\sqrt{2\Omega_K}} \left(h_{\mathbf{K}}^\gamma e^{-i\Omega t} \int d^3\mathbf{x} e^{i(\mathbf{K} - (\mathbf{k} - \mathbf{k}')\cdot\mathbf{x})} \right. \\
&\quad \left. + h_{\mathbf{K}}^{\gamma*} e^{i\Omega t} \int d^3\mathbf{x} e^{-i(\mathbf{K} + (\mathbf{k} - \mathbf{k}')\cdot\mathbf{x})} \right) \\
&= \varepsilon_0 f^2(t) (2\pi)^3 \\
&\quad - \varepsilon_0 f^2(t) (2\pi)^3 \hat{\mathbf{u}}_{\mathbf{k}i} \hat{\mathbf{u}}_{\mathbf{k}'j} \mathcal{C} \sum_{\gamma=+, \times} \int \frac{d^3\mathbf{K}}{(2\pi)^{3/2}} \frac{e_{ij}[\hat{\mathbf{K}}]}{\sqrt{2\Omega_K}} \left(h_{\mathbf{K}}^\gamma e^{-i\Omega t} \delta^{(3)}(\mathbf{K} - (\mathbf{k} - \mathbf{k}')) \right. \\
&\quad \left. + h_{\mathbf{K}}^{\gamma*} e^{i\Omega t} \delta^{(3)}(\mathbf{K} + (\mathbf{k} - \mathbf{k}')) \right). \tag{B.9}
\end{aligned}$$

Here, we used $\delta_{ij} \hat{\mathbf{u}}_{\mathbf{k}i} \hat{\mathbf{u}}_{\mathbf{k}j} = 1$, and assumed a real polarization vector $\hat{\mathbf{u}}_{\mathbf{k}}$ such that $\hat{\mathbf{u}}_{\mathbf{k}}^* = \hat{\mathbf{u}}_{\mathbf{k}} = \hat{\mathbf{u}}_{-\mathbf{k}}$. Thus, Eq. (B.9) explicitly shows the scattering of mode \mathbf{k} to \mathbf{k}' of the EM field due to the presence of GWs with momentum \mathbf{K} . Thus, the momentum conservation implies either $\mathbf{k}' = \mathbf{k} - \mathbf{K}$ or $\mathbf{k}' = \mathbf{k} + \mathbf{K}$ possibilities. Since $K \ll k$, each mode of the EM field scatters to itself, and we may set

$$\begin{aligned}
\delta^{(3)}(\mathbf{K} - (\mathbf{k} - \mathbf{k}')) &\simeq \delta^{(3)}(\mathbf{k} - \mathbf{k}') \\
\delta^{(3)}(\mathbf{K} + (\mathbf{k} - \mathbf{k}')) &\simeq \delta^{(3)}(\mathbf{k} - \mathbf{k}'). \tag{B.10}
\end{aligned}$$

Indeed, these conditions are fulfilled by almost all frequency parts of the PGWs spectrum, for which $K \ll k, k'$. For all GWs with $K \ll k$, the incoming EM field of mode \mathbf{k} scatters to itself so that $\mathbf{k} \simeq \mathbf{k}'$. So, we may proceed by retaining the contribution of all PGWs modes in the integral Eq. (B.9), such that

$$\begin{aligned}
\langle \mathbf{f}_k | \mathbf{f}_{k'} \rangle &= \varepsilon_0 f^2(t) (2\pi)^3 \delta^{(3)}(\mathbf{k} - \mathbf{k}') \left(1 - \hat{\mathbf{u}}_{\mathbf{k}i} \hat{\mathbf{u}}_{\mathbf{k}j} \mathcal{C} \sum_{\gamma=+, \times} \int \frac{d^3\mathbf{K}}{(2\pi)^{3/2}} \frac{e_{ij}[\hat{\mathbf{K}}]}{\sqrt{2\Omega_K}} \left(h_{\mathbf{K}}^\gamma e^{-i\Omega t} + h_{\mathbf{K}}^{\gamma*} e^{i\Omega t} \right) \right) \\
&= \varepsilon_0 f^2(t) (2\pi)^3 \delta^{(3)}(\mathbf{k} - \mathbf{k}') (1 - h_{ij}(t) \hat{\mathbf{u}}_{\mathbf{k}i} \hat{\mathbf{u}}_{\mathbf{k}j}) \\
&\equiv \varepsilon_0 f^2(t) (2\pi)^3 m(t) \delta^{(3)}(\mathbf{k} - \mathbf{k}'). \tag{B.11}
\end{aligned}$$

where in the last line a slowly-varying function of time $m(t)$ is defined according to $m(t) \equiv 1 - h_{ij}(t) \hat{\mathbf{u}}_{\mathbf{k}i} \hat{\mathbf{u}}_{\mathbf{k}j}$. Here, $h_{ij}(t)$ represents the GWs field $h_{ij}(\mathbf{x} = 0, t)$, based on Eq. (3.6). Consequently, the spatial mode functions \mathbf{f}_k are orthogonal, and the normalization factor $f(t)$ outcomes as

$$f^2(t) = \frac{1}{\varepsilon_0 (2\pi)^3 m(t)}, \tag{B.12}$$

and spatial mode functions are determined by

$$\mathbf{f}_k(\mathbf{x}, t) = \frac{\hat{\mathbf{u}}_k e^{i\mathbf{k}\cdot\mathbf{x}}}{\sqrt{\varepsilon_0(2\pi)^3 m(t)}}. \quad (\text{B.13})$$

Note that $m(t)$ is a slowly varying function of time, as it should be. Now, plugging the mode functions Eq. (B.13) into the eigen-equation Eq. (B.7) results in the following algebraic equation for $\omega_k(\mathbf{x}, t)$, \mathbf{k} and $\hat{\mathbf{u}}_k$

$$\mathbf{k} \times (\bar{\mu}^{-1}(\mathbf{x}, t) \mathbf{k} \times \hat{\mathbf{u}}_k) = -\omega_k^2(\mathbf{x}, t) \bar{\varepsilon}(\mathbf{x}, t) \hat{\mathbf{u}}_k, \quad (\text{B.14})$$

which can also be re-written in the following compact form

$$[\omega_k^2(\mathbf{x}, t) \varepsilon_{il}(\mathbf{x}, t) + \epsilon_{ijr} \epsilon_{mnl} k_j k_n \mu_{rm}^{-1}(\mathbf{x}, t)] \hat{\mathbf{u}}_{k,l} = 0, \quad (\text{B.15})$$

with $\hat{\mathbf{u}}_{k,l}$ being the l -th component of the polarization vector $\hat{\mathbf{u}}_k$ and ϵ_{ijr} representing the Levi-Civita symbol. Now, if we define a new quantity

$$n_k(\mathbf{x}, t) \equiv \frac{\omega_k}{\omega_k(\mathbf{x}, t)}, \quad (\text{B.16})$$

where $\omega_k = ck$ is the EM frequency in the vacuum (in the absence of GWs). Combining Eq. (B.15) and Eq. (B.16) yields

$$\left[\varepsilon_{il}(\mathbf{x}, t) + \frac{n_k^2(\mathbf{x}, t)}{c^2} \epsilon_{ijr} \epsilon_{mnl} \hat{\mathbf{k}}_j \hat{\mathbf{k}}_n \mu_{rm}^{-1}(\mathbf{x}, t) \right] \hat{\mathbf{u}}_{k,l} = 0, \quad (\text{B.17})$$

where we have substituted $k_j = |\mathbf{k}| \hat{\mathbf{k}}_j = \omega_k / c \hat{\mathbf{k}}_j$. Eq. (B.17) is also obtained in [144] where it turns out that the quantity $n_k(\mathbf{x}, t)$ is nothing but the refractive index of the GWs medium. The existence of eigen-solutions for $\hat{\mathbf{u}}_k$ leads to the *generalized Fresnel equation*

$$n_k^2(\mathbf{x}, t) \varepsilon_{ij}(\mathbf{x}, t) \hat{\mathbf{k}}_i \hat{\mathbf{k}}_j - \det(\bar{\varepsilon}(\mathbf{x}, t)) = 0. \quad (\text{B.18})$$

Eq. (B.18) identifies the refractive index of the effective medium according to

$$n_k(\mathbf{x}, t) = \sqrt{\frac{\det(\bar{\varepsilon}(\mathbf{x}, t))}{\varepsilon_{ij}(\mathbf{x}, t) \hat{\mathbf{k}}_i \hat{\mathbf{k}}_j}}, \quad (\text{B.19})$$

which is consistent with Eq. (14) of [144]. With the help of Eq. (B.2), one can check that $\det(\bar{\varepsilon}(\mathbf{x}, t)) = 1$ in the linear order $\mathcal{O}(h)$, and Eq. (B.19) simplifies to

$$n_k(\mathbf{x}, t) = \left(\varepsilon_{ij}(\mathbf{x}, t) \hat{\mathbf{k}}_i \hat{\mathbf{k}}_j \right)^{-1/2} = \left(\delta_{ij} \hat{\mathbf{k}}_i \hat{\mathbf{k}}_j - h_{ij}(\mathbf{x}, t) \hat{\mathbf{k}}_i \hat{\mathbf{k}}_j \right)^{-1/2} = 1 + \frac{1}{2} h_{ij}(\mathbf{x}, t) \hat{\mathbf{k}}_i \hat{\mathbf{k}}_j. \quad (\text{B.20})$$

Consequently, the EM frequency in the presence of GW background is determined by Eq. (B.16), namely

$$\omega_k(\mathbf{x}, t) = \omega_k \left(\delta_{ij} - \frac{1}{2} h_{ij}(\mathbf{x}, t) \right) \hat{\mathbf{k}}_i \hat{\mathbf{k}}_j, \quad (\text{B.21})$$

and the temporal mode functions $\nu_k(\mathbf{x}, t)$ are specified by Eq. (B.6).

Having identified the expression of $\mathbf{A}(\mathbf{x}, t)$ given by Eq. (B.3), in the following we construct the Hamiltonian of the EM-GWs system.

B.3 Derivation of the interaction Hamiltonian $\hat{H}_{\text{em-gw}}$ in the adiabatic limit

The following Lagrangian density

$$\mathcal{L}_{\text{em-gw}}(\mathbf{x}, t) = \frac{1}{2} \left(\varepsilon_{ij}(\mathbf{x}, t) E^i(\mathbf{x}, t) E^j(\mathbf{x}, t) - \mu_{ij}^{-1}(\mathbf{x}, t) B^i(\mathbf{x}, t) B^j(\mathbf{x}, t) \right). \quad (\text{B.22})$$

correctly reproduces Maxwell's equations in the adiabatic approximation, Eq. (B.1) (see also [100]). Following the standard second quantization procedure, one promotes the vector potential $\mathbf{A}(\mathbf{x}, t)$ to the Hermitian quantum field operator $\hat{\mathbf{A}}(\mathbf{x}, t)$. Thus, the expansion coefficients (α_k, α_k^*) in the field expansion Eq. (B.3) become bosonic operators $(\hat{a}_k, \hat{a}_k^\dagger)$ satisfying the bosonic commutation relation $[\hat{a}_k, \hat{a}_{k'}^\dagger] = \delta_{kk'}$. The canonical conjugate momentum of the canonical variable $\hat{A}_i(\mathbf{x}, t)$ is defined by

$$\begin{aligned} \hat{\Pi}_i(\mathbf{x}, t) &\equiv \frac{\partial \mathcal{L}_{\text{em-gw}}(\mathbf{x}, t)}{\partial \dot{\hat{A}}_i(\mathbf{x}, t)} = \varepsilon_{ij}(\mathbf{x}, t) \dot{\hat{A}}_j(\mathbf{x}, t) \\ &= \sum_k \sqrt{\frac{\hbar}{2}} \left(\hat{a}_k \dot{\nu}_k(\mathbf{x}, t) \varepsilon_{ij}(\mathbf{x}, t) f_{kj}(\mathbf{x}, t) + \hat{a}_k^\dagger \dot{\nu}_k^*(\mathbf{x}, t) \varepsilon_{ij}(\mathbf{x}, t) f_{kj}^*(\mathbf{x}, t) \right). \end{aligned} \quad (\text{B.23})$$

Note that $\nu_k(\mathbf{x}, t)$ and $\mathbf{f}_k(\mathbf{x}, t)$ satisfy the SVEA condition (see Eq. (B.4)). The Hamiltonian can be established by performing the Legendre transform on the Lagrangian $\mathcal{L}_{\text{em-gw}}(\mathbf{x}, t)$. The resulting Hamiltonian is

$$\begin{aligned} \hat{H}_{\text{em-gw}} &= \frac{1}{2} \int_V d^3\mathbf{x} \left[\varepsilon_{ij}^{-1}(\mathbf{x}, t) \hat{\Pi}_i(\mathbf{x}, t) \hat{\Pi}_j(\mathbf{x}, t) \right. \\ &\quad \left. + \mu_{ij}^{-1}(\mathbf{x}, t) \left(\nabla \times \hat{\mathbf{A}}(\mathbf{x}, t) \right)_i \left(\nabla \times \hat{\mathbf{A}}(\mathbf{x}, t) \right)_j \right], \end{aligned} \quad (\text{B.24})$$

where the identity $\varepsilon_{ik} \varepsilon_{kl}^{-1} = \delta_{il}$ is used. Here, spatial integration $\int d^3\mathbf{x}$ is performed over the volume V wherein the EM-GWs interaction takes place. Plugging the expressions of $\hat{\mathbf{A}}(\mathbf{x}, t)$ and $\hat{\Pi}(\mathbf{x}, t)$ from Eqs. (B.3, B.23) into the Hamiltonian Eq. (B.24) yields

$$\begin{aligned} \hat{H}_{\text{em-gw}} &= \frac{1}{2} \int_V d^3\mathbf{x} \left[\varepsilon_{ij}^{-1}(\mathbf{x}, t) \hat{\Pi}_i(\mathbf{x}, t) \hat{\Pi}_j(\mathbf{x}, t) \right. \\ &\quad \left. + \mu_{ij}^{-1}(\mathbf{x}, t) \left(\nabla \times \hat{\mathbf{A}}(\mathbf{x}, t) \right)_i \left(\nabla \times \hat{\mathbf{A}}(\mathbf{x}, t) \right)_j \right] \\ &= \frac{1}{2} \times \frac{\hbar}{2} \sum_{\mathbf{k}, \mathbf{k}'} \left\{ \int d^3\mathbf{x} \varepsilon_{ij}(\mathbf{x}, t) \left(\hat{a}_k \dot{\nu}_k f_k^i + \hat{a}_k^\dagger \dot{\nu}_k^* f_k^{*i} \right) \left(\hat{a}_{k'} \dot{\nu}_{k'} f_{k'}^j + \hat{a}_{k'}^\dagger \dot{\nu}_{k'}^* f_{k'}^{*j} \right) \right. \\ &\quad \left. + \int d^3\mathbf{x} \mu_{ij}^{-1}(\mathbf{x}, t) \left(\hat{a}_k \nu_k (\nabla \times \mathbf{f}_k)_i + \hat{a}_k^\dagger \nu_k^* (\nabla \times \mathbf{f}_k^*)_i \right) \right. \\ &\quad \left. \times \left(\hat{a}_{k'} \nu_{k'} (\nabla \times \mathbf{f}_{k'})_j + \hat{a}_{k'}^\dagger \nu_{k'}^* (\nabla \times \mathbf{f}_{k'}^*)_j \right) \right\}. \end{aligned} \quad (\text{B.25})$$

Note that $\nu_k(\mathbf{x}, t)$ is a slowly varying function of \mathbf{x} . Re-arranging the terms, there would be four terms in the Hamiltonian, as follows

$$\begin{aligned} \hat{H}_{em-gw}(\mathbf{x}_s, \mathbf{x}_r, t) = & \frac{1}{2} \times \frac{\hbar}{2} \sum_{k, k'} \quad (B.26) \\ & \times \left\{ \hat{a}_k \hat{a}_{k'} \int_{\mathbf{x}_s}^{\mathbf{x}_r} d^3 \mathbf{x} \left(\varepsilon_{ij}(\mathbf{x}, t) f_k^i f_{k'}^j \dot{\nu}_k \dot{\nu}_{k'} + \mu_{ij}^{-1}(\mathbf{x}, t) \nu_k \nu_{k'} (\nabla \times \mathbf{f}_k)_i (\nabla \times \mathbf{f}_{k'})_j \right) \right. \\ & + \hat{a}_k \hat{a}_{k'}^\dagger \int_{\mathbf{x}_s}^{\mathbf{x}_r} d^3 \mathbf{x} \left(\varepsilon_{ij}(\mathbf{x}, t) f_k^i f_{k'}^{*j} \dot{\nu}_k \dot{\nu}_{k'}^* + \mu_{ij}^{-1}(\mathbf{x}, t) \nu_k \nu_{k'}^* (\nabla \times \mathbf{f}_k)_i (\nabla \times \mathbf{f}_{k'}^*)_j \right) \\ & + \hat{a}_k^\dagger \hat{a}_{k'} \int_{\mathbf{x}_s}^{\mathbf{x}_r} d^3 \mathbf{x} \left(\varepsilon_{ij}(\mathbf{x}, t) f_k^{*i} f_{k'}^j \dot{\nu}_k^* \dot{\nu}_{k'} + \mu_{ij}^{-1}(\mathbf{x}, t) \nu_k^* \nu_{k'} (\nabla \times \mathbf{f}_k^*)_i (\nabla \times \mathbf{f}_{k'})_j \right) \\ & \left. + \hat{a}_k^\dagger \hat{a}_{k'}^\dagger \int_{\mathbf{x}_s}^{\mathbf{x}_r} d^3 \mathbf{x} \left(\varepsilon_{ij}(\mathbf{x}, t) f_k^{*i} f_{k'}^{*j} \dot{\nu}_k^* \dot{\nu}_{k'}^* + \mu_{ij}^{-1}(\mathbf{x}, t) \nu_k^* \nu_{k'}^* (\nabla \times \mathbf{f}_k^*)_i (\nabla \times \mathbf{f}_{k'}^*)_j \right) \right\}. \end{aligned}$$

Note that, the spatial integration should be taken over the whole region where the EM field interacts with GWs. If we denote by \mathbf{x}_s and \mathbf{x}_r the sending and receiving points of the EM field in the GWs background, then the interaction takes place within the volume encompassed between these points. The resulting Hamiltonian thus depends on the interaction time t , and the sender and receiver points in space. In the following, we compute each term using the adiabatic approximation $K \ll k$ and derive the interaction Hamiltonian, Eq. (3.7).

With the help of Eq. (B.2) for definition of $\varepsilon_{ij}(\mathbf{x}, t)$, the first term in Eq. (B.26) is contains a terms given by

$$\begin{aligned} & \int_{\mathbf{x}_s}^{\mathbf{x}_r} d^3 \mathbf{x} \varepsilon_{ij}(\mathbf{x}, t) f_k^i(\mathbf{x}, t) f_{k'}^j(\mathbf{x}, t) \dot{\nu}_k(\mathbf{x}, t) \dot{\nu}_{k'}(\mathbf{x}, t) \quad (B.27) \\ & = \frac{1}{(2\pi)^3 m(t)} \delta_{ij} \hat{\mathbf{u}}_{k_i} \hat{\mathbf{u}}_{k'_j} \int_{\mathbf{x}_s}^{\mathbf{x}_r} d^3 \mathbf{x} e^{i(\mathbf{k}+\mathbf{k}') \cdot \mathbf{x}} \dot{\nu}_k(\mathbf{x}, t) \dot{\nu}_{k'}(\mathbf{x}, t) \\ & - \frac{1}{(2\pi)^3 m(t)} \int_{\mathbf{x}_s}^{\mathbf{x}_r} d^3 \mathbf{x} e^{i(\mathbf{k}+\mathbf{k}') \cdot \mathbf{x}} h_{ij}(\mathbf{x}, t) \hat{\mathbf{u}}_{k_i} \hat{\mathbf{u}}_{k'_j} \dot{\nu}_k(\mathbf{x}, t) \dot{\nu}_{k'}(\mathbf{x}, t). \end{aligned}$$

In the second line, we used the expression of $\mathbf{f}_k(\mathbf{x}, t)$ given by Eq. (B.13). The function $e^{i(\mathbf{k}+\mathbf{k}') \cdot \mathbf{x}}$ is highly oscillating for large $(\mathbf{k} + \mathbf{k}') \cdot \mathbf{x}$, thus the integral averages to zero unless $(\mathbf{k} + \mathbf{k}')$ goes to zero so that $e^{i(\mathbf{k}+\mathbf{k}') \cdot \mathbf{x}} \sim 1$. Consequently, the result of the first integral can be approximately written as

$$\frac{\delta^{(3)}(\mathbf{k} + \mathbf{k}')}{\delta^{(3)}(0)} \int_{\mathbf{x}_s}^{\mathbf{x}_r} d^3 \mathbf{x} \dot{\nu}_k^2(\mathbf{x}, t) = (2\pi)^3 \frac{\delta^{(3)}(\mathbf{k} + \mathbf{k}')}{V} \int_{\mathbf{x}_s}^{\mathbf{x}_r} d^3 \mathbf{x} \dot{\nu}_k^2(\mathbf{x}, t), \quad (B.28)$$

Here, the factor $\frac{\delta^{(3)}(\mathbf{k}+\mathbf{k}')}{\delta^{(3)}(0)} = 1$ is explicitly inserted to show that the result of the integral exists for $(\mathbf{k} + \mathbf{k}') \sim 0$. Moreover, we have used the identity

$$\int_{\mathbf{x}_s}^{\mathbf{x}_r} d^3 \mathbf{x} e^{i(0) \cdot \mathbf{x}} = (2\pi)^3 \delta^{(3)}(0) = V \quad \rightarrow \quad \delta^{(3)}(0) = \frac{V}{(2\pi)^3}. \quad (B.29)$$

By inserting the expression of $h_{ij}(\mathbf{x}, t)$ from Eq. (3.6), the second term in Eq. (B.27) takes

the form

$$\begin{aligned}
& -\frac{1}{(2\pi)^3 m(t)} \mathcal{C} \sum_{\gamma} \int \frac{d^3 \mathbf{K}}{(2\pi)^{3/2}} \frac{e_{ij}[\hat{\mathbf{K}}]}{\sqrt{2\Omega_K}} \hat{\mathbf{u}}_{\mathbf{k}i} \hat{\mathbf{u}}_{\mathbf{k}'j} \left(h_{\mathbf{K}}^{\gamma} e^{-i\Omega_K t} \int_{\mathbf{x}_s}^{\mathbf{x}_r} d^3 \mathbf{x} e^{i(\mathbf{K}+(\mathbf{k}+\mathbf{k}')) \cdot \mathbf{x}} \dot{\nu}_k(\mathbf{x}, t) \dot{\nu}_{k'}(\mathbf{x}, t) \right. \\
& \left. + h_{\mathbf{K}}^{\gamma*} e^{i\Omega_K t} \int_{\mathbf{x}_s}^{\mathbf{x}_r} d^3 \mathbf{x} e^{i(-\mathbf{K}+(\mathbf{k}+\mathbf{k}')) \cdot \mathbf{x}} \dot{\nu}_k(\mathbf{x}, t) \dot{\nu}_{k'}(\mathbf{x}, t) \right). \tag{B.30}
\end{aligned}$$

Again, due to the highly oscillating factors $e^{i(\pm\mathbf{K}+(\mathbf{k}+\mathbf{k}')) \cdot \mathbf{x}}$ the integration over \mathbf{x} averages to zero unless $(\pm\mathbf{K}+(\mathbf{k}+\mathbf{k}')) \sim 0$, for which the value of the integral in Eq. (B.30) can be approximated by

$$\begin{aligned}
& -\frac{1}{(2\pi)^3 m(t)} \mathcal{C} \sum_{\gamma} \int \frac{d^3 \mathbf{K}}{(2\pi)^{3/2}} \frac{e_{ij}[\hat{\mathbf{K}}]}{\sqrt{2\Omega_K}} \hat{\mathbf{u}}_{\mathbf{k}i} \hat{\mathbf{u}}_{\mathbf{k}'j} \left(h_{\mathbf{K}}^{\gamma} e^{-i\Omega_K t} \frac{\delta^{(3)}(\mathbf{K}+(\mathbf{k}+\mathbf{k}'))}{\delta^{(3)}(0)} \int_{\mathbf{x}_s}^{\mathbf{x}_r} d^3 \mathbf{x} \dot{\nu}_k(\mathbf{x}, t) \dot{\nu}_{k'}(\mathbf{x}, t) \right. \\
& \left. + h_{\mathbf{K}}^{\gamma*} e^{i\Omega_K t} \frac{\delta^{(3)}(-\mathbf{K}+(\mathbf{k}+\mathbf{k}'))}{\delta^{(3)}(0)} \int_{\mathbf{x}_s}^{\mathbf{x}_r} d^3 \mathbf{x} \dot{\nu}_k(\mathbf{x}, t) \dot{\nu}_{k'}(\mathbf{x}, t) \right). \tag{B.31}
\end{aligned}$$

As before, the unit factors $\frac{\delta^{(3)}(\pm\mathbf{K}+(\mathbf{k}+\mathbf{k}'))}{\delta^{(3)}(0)}$ is inserted to show that the integrals are non-vanishing only when $(\pm\mathbf{K}+(\mathbf{k}+\mathbf{k}')) \sim 0$. In the adiabatic limit $K \ll k$, we may neglect \mathbf{K} in delta functions (similar to Eq. (B.10)) and Eq. (B.31) reduces to

$$\begin{aligned}
& -\frac{\delta^{(3)}(\mathbf{k}+\mathbf{k}')}{m(t)V} \mathcal{C} \sum_{\gamma} \int \frac{d^3 \mathbf{K}}{(2\pi)^{3/2}} \frac{e_{ij}[\hat{\mathbf{K}}]}{\sqrt{2\Omega_K}} \hat{\mathbf{u}}_{\mathbf{k}i} \hat{\mathbf{u}}_{\mathbf{k}'j} \left(h_{\mathbf{K}}^{\gamma} e^{-i\Omega t} + h_{\mathbf{K}}^{\gamma*} e^{i\Omega t} \right) \left(\int_{\mathbf{x}_s}^{\mathbf{x}_r} d^3 \mathbf{x} \dot{\nu}_k^2(\mathbf{x}, t) \right) \\
& = -\frac{\delta^{(3)}(\mathbf{k}+\mathbf{k}')}{m(t)V} h_{ij}(t) \hat{\mathbf{u}}_{\mathbf{k}i} \hat{\mathbf{u}}_{\mathbf{k}'j} \left(\int_{\mathbf{x}_s}^{\mathbf{x}_r} d^3 \mathbf{x} \dot{\nu}_k^2(\mathbf{x}, t) \right). \tag{B.32}
\end{aligned}$$

Inserting Eq. (B.28) and Eq. (B.32) into Eq. (B.27) leads to

$$\begin{aligned}
\int_{\mathbf{x}_s}^{\mathbf{x}_r} d^3 \mathbf{x} \varepsilon_{ij}(\mathbf{x}, t) f_k^i(\mathbf{x}, t) f_{k'}^j(\mathbf{x}, t) \dot{\nu}_k(\mathbf{x}, t) \dot{\nu}_{k'}(\mathbf{x}, t) & = \frac{\delta^{(3)}(\mathbf{k}+\mathbf{k}')}{m(t)V} \left(\int_{\mathbf{x}_s}^{\mathbf{x}_r} d^3 \mathbf{x} \dot{\nu}_k^2(\mathbf{x}, t) \right) \left(1 - h_{ij}(t) \hat{\mathbf{u}}_{\mathbf{k}i} \hat{\mathbf{u}}_{\mathbf{k}'j} \right) \\
& = \frac{\delta^{(3)}(\mathbf{k}+\mathbf{k}')}{V} \left(\int_{\mathbf{x}_s}^{\mathbf{x}_r} d^3 \mathbf{x} \dot{\nu}_k^2(\mathbf{x}, t) \right). \tag{B.33}
\end{aligned}$$

Here, we used definition $m(t) \equiv (\delta_{ij} - h_{ij}(t)) \hat{\mathbf{u}}_{\mathbf{k}i} \hat{\mathbf{u}}_{\mathbf{k}'j}$ as defined in Eq. (B.11). Similarly, one may show that

$$\begin{aligned}
\int_{\mathbf{x}_s}^{\mathbf{x}_r} d^3 \mathbf{x} \varepsilon_{ij}(\mathbf{x}, t) f_k^i(\mathbf{x}, t) f_{k'}^{*j}(\mathbf{x}, t) \dot{\nu}_k(\mathbf{x}, t) \dot{\nu}_{k'}^*(\mathbf{x}, t) & = \frac{\delta^{(3)}(\mathbf{k}-\mathbf{k}')}{V} \left(\int_{\mathbf{x}_s}^{\mathbf{x}_r} d^3 \mathbf{x} |\dot{\nu}_k(\mathbf{x}, t)|^2 \right) \\
\int_{\mathbf{x}_s}^{\mathbf{x}_r} d^3 \mathbf{x} \varepsilon_{ij}(\mathbf{x}, t) f_k^{*i}(\mathbf{x}, t) f_{k'}^j(\mathbf{x}, t) \dot{\nu}_k^*(\mathbf{x}, t) \dot{\nu}_{k'}(\mathbf{x}, t) & = \frac{\delta^{(3)}(\mathbf{k}-\mathbf{k}')}{V} \left(\int_{\mathbf{x}_s}^{\mathbf{x}_r} d^3 \mathbf{x} |\dot{\nu}_k^*(\mathbf{x}, t)| \right) \\
\int_{\mathbf{x}_s}^{\mathbf{x}_r} d^3 \mathbf{x} \varepsilon_{ij}(\mathbf{x}, t) f_k^{*i}(\mathbf{x}, t) f_{k'}^{*j}(\mathbf{x}, t) \dot{\nu}_k^*(\mathbf{x}, t) \dot{\nu}_{k'}^*(\mathbf{x}, t) & = \frac{\delta^{(3)}(\mathbf{k}+\mathbf{k}')}{V} \left(\int_{\mathbf{x}_s}^{\mathbf{x}_r} d^3 \mathbf{x} \dot{\nu}_k^{*2}(\mathbf{x}, t) \right). \tag{B.34}
\end{aligned}$$

Next, we compute the second term in the first line of Eq. (B.26), which is of the form

$$\begin{aligned}
& \int_{\mathbf{x}_s}^{\mathbf{x}_r} d^3\mathbf{x} \mu_{ij}^{-1}(\mathbf{x}, t) (\nabla \times \mathbf{f}_{\mathbf{k}}(\mathbf{x}, t))_i (\nabla \times \mathbf{f}_{\mathbf{k}'}(\mathbf{x}, t))_j \nu_k(\mathbf{x}, t) \nu_{k'}(\mathbf{x}, t) \quad (\text{B.35}) \\
&= \int_{\mathbf{x}_s}^{\mathbf{x}_r} d^3\mathbf{x} \mu_{ij}^{-1}(\mathbf{x}, t) \epsilon_{ilm} (\partial_l f_k^m(\mathbf{x}, t)) (\nabla \times \mathbf{f}_{\mathbf{k}'}(\mathbf{x}, t))_j \nu_k(\mathbf{x}, t) \nu_{k'}(\mathbf{x}, t) \\
&= \int_{\mathbf{x}_s}^{\mathbf{x}_r} d^3\mathbf{x} \epsilon_{ilm} \partial_l \left[\mu_{ij}^{-1}(\mathbf{x}, t) f_k^m(\mathbf{x}, t) (\nabla \times \mathbf{f}_{\mathbf{k}'}(\mathbf{x}, t))_j \nu_k(\mathbf{x}, t) \nu_{k'}(\mathbf{x}, t) \right] \\
&\quad - \int_{\mathbf{x}_s}^{\mathbf{x}_r} d^3\mathbf{x} \epsilon_{ilm} f_k^m(\mathbf{x}, t) \partial_l \left[\mu_{ij}^{-1}(\mathbf{x}, t) (\nabla \times \mathbf{f}_{\mathbf{k}'}(\mathbf{x}, t))_j \nu_k(\mathbf{x}, t) \nu_{k'}(\mathbf{x}, t) \right] \\
&= \int_{\mathbf{x}_s}^{\mathbf{x}_r} d^3\mathbf{x} \epsilon_{mli} \partial_l \left[\mu^{-1}(\mathbf{x}, t) \nabla \times \mathbf{f}_{\mathbf{k}'}(\mathbf{x}, t) \right]_i \nu_k(\mathbf{x}, t) \nu_{k'}(\mathbf{x}, t) f_k^m.
\end{aligned}$$

Here, ϵ_{ilm} stands for the Levi-Civita symbol. Note that, in the last line, the surface integral vanishes assuming the EM field vanishes at the boundaries. This assumption is practical, since usually the EM field emitted from a natural or an artificial source has a finite spatial extension. Moreover, in the derivation of the last line, we have used

$$\begin{aligned}
\partial_l \left[\mu_{ij}^{-1}(\mathbf{x}, t) (\nabla \times \mathbf{f}_{\mathbf{k}'}(\mathbf{x}, t))_j \nu_k(\mathbf{x}, t) \nu_{k'}(\mathbf{x}, t) \right] &= (\partial_l \mu_{ij}^{-1}(\mathbf{x}, t)) (\nabla \times \mathbf{f}_{\mathbf{k}'}(\mathbf{x}, t))_i \nu_k(\mathbf{x}, t) \nu_{k'}(\mathbf{x}, t) \\
&\quad + \mu_{ij}^{-1}(\mathbf{x}, t) \partial_l \left[(\nabla \times \mathbf{f}_{\mathbf{k}'}(\mathbf{x}, t))_j \right] \\
&\quad + \mu_{ij}^{-1}(\mathbf{x}, t) (\nabla \times \mathbf{f}_{\mathbf{k}'}(\mathbf{x}, t))_j \partial_l (\nu_k(\mathbf{x}, t) \nu_{k'}(\mathbf{x}, t)) \\
&= \mu_{ij}^{-1}(\mathbf{x}, t) \partial_l \left[(\nabla \times \mathbf{f}_{\mathbf{k}'}(\mathbf{x}, t))_j \right]. \quad (\text{B.36})
\end{aligned}$$

In the last line, we used the fact that the functions $\mu_{ij}^{-1}(\mathbf{x}, t)$ and $\nu_k(\mathbf{x}, t)$ are slowly varying functions of \mathbf{x} and their derivative are proportional to K , which is negligible with respect to k . Thus, Eq. (B.35) can be rewritten as

$$\begin{aligned}
& \int_{\mathbf{x}_s}^{\mathbf{x}_r} d^3\mathbf{x} \mu_{ij}^{-1}(\mathbf{x}, t) (\nabla \times \mathbf{f}_{\mathbf{k}}(\mathbf{x}, t))_i (\nabla \times \mathbf{f}_{\mathbf{k}'}(\mathbf{x}, t))_j \nu_k(\mathbf{x}, t) \nu_{k'}(\mathbf{x}, t) \quad (\text{B.37}) \\
&= \int_{\mathbf{x}_s}^{\mathbf{x}_r} d^3\mathbf{x} \left(\nabla \times [\mu^{-1}(\mathbf{x}, t) \nabla \times \mathbf{f}_{\mathbf{k}}(\mathbf{x}, t)] \right)_m f_k^m \nu_k(\mathbf{x}, t) \nu_{k'}(\mathbf{x}, t) \\
&= \int_{\mathbf{x}_s}^{\mathbf{x}_r} d^3\mathbf{x} \omega_{k'}^2(\mathbf{x}, t) \epsilon_{ml}(\mathbf{x}, t) f_k^m(\mathbf{x}, t) f_{k'}^l(\mathbf{x}, t) \nu_k(\mathbf{x}, t) \nu_{k'}(\mathbf{x}, t).
\end{aligned}$$

In the second line, we plugged in from the wave equation Eq. (B.7). Inserting $\mathbf{f}_{\mathbf{k}}(\mathbf{x}, t)$ from Eq. (B.13) into Eq. (B.37) yields

$$\begin{aligned}
& \int_{\mathbf{x}_s}^{\mathbf{x}_r} d^3\mathbf{x} \mu_{ij}^{-1}(\mathbf{x}, t) (\nabla \times \mathbf{f}_{\mathbf{k}}(\mathbf{x}, t))_i (\nabla \times \mathbf{f}_{\mathbf{k}'}(\mathbf{x}, t))_j \nu_k(\mathbf{x}, t) \nu_{k'}(\mathbf{x}, t) \quad (\text{B.38}) \\
&= \frac{1}{(2\pi)^3 m(t)} \int d^3\mathbf{x} e^{i(\mathbf{k}+\mathbf{k}')\cdot\mathbf{x}} (\delta_{ij} - h_{ij}(\mathbf{x}, t)) \hat{\mathbf{u}}_{ki} \hat{\mathbf{u}}_{k'j} \nu_k(\mathbf{x}, t) \nu_{k'}(\mathbf{x}, t).
\end{aligned}$$

A similar procedure as in Eqs. (B.27 - B.33) results in the following equation

$$\begin{aligned}
& \int_{\mathbf{x}_s}^{\mathbf{x}_r} d^3\mathbf{x} \mu_{ij}^{-1}(\mathbf{x}, t) (\nabla \times \mathbf{f}_{\mathbf{k}}(\mathbf{x}, t))_i (\nabla \times \mathbf{f}_{\mathbf{k}'}(\mathbf{x}, t))_j \nu_k(\mathbf{x}, t) \nu_{k'}(\mathbf{x}, t) \quad (\text{B.39}) \\
&= \frac{\delta^{(3)}(\mathbf{k} + \mathbf{k}')}{V} \int_{\mathbf{x}_s}^{\mathbf{x}_r} d^3\mathbf{x} \omega_k^2(\mathbf{x}, t) \nu_k^2(\mathbf{x}, t).
\end{aligned}$$

Similarly, one may show that

$$\begin{aligned}
\int_{\mathbf{x}_s}^{\mathbf{x}_r} d^3\mathbf{x} \mu_{ij}^{-1}(\mathbf{x}, t) (\nabla \times \mathbf{f}_{\mathbf{k}})_i (\nabla \times \mathbf{f}_{\mathbf{k}'})_j \nu_k \nu_{k'}^* &= \frac{\delta^{(3)}(\mathbf{k} - \mathbf{k}')}{V} \int_{\mathbf{x}_s}^{\mathbf{x}_r} d^3\mathbf{x} \omega_k^2(\mathbf{x}, t) |\nu_k(\mathbf{x}, t)|^2, \quad (\text{B.40}) \\
\int_{\mathbf{x}_s}^{\mathbf{x}_r} d^3\mathbf{x} \mu_{ij}^{-1}(\mathbf{x}, t) (\nabla \times \mathbf{f}_{\mathbf{k}}^*)_i (\nabla \times \mathbf{f}_{\mathbf{k}'})_j \nu_k^* \nu_{k'} &= \frac{\delta^{(3)}(\mathbf{k} - \mathbf{k}')}{V} \int_{\mathbf{x}_s}^{\mathbf{x}_r} d^3\mathbf{x} \omega_k^2(\mathbf{x}, t) |\nu_k(\mathbf{x}, t)|^2 \\
\int_{\mathbf{x}_s}^{\mathbf{x}_r} d^3\mathbf{x} \mu_{ij}^{-1}(\mathbf{x}, t) (\nabla \times \mathbf{f}_{\mathbf{k}}^*)_i (\nabla \times \mathbf{f}_{\mathbf{k}'})_j \nu_k^* \nu_{k'}^* &= \frac{\delta^{(3)}(\mathbf{k} + \mathbf{k}')}{V} \int_{\mathbf{x}_s}^{\mathbf{x}_r} d^3\mathbf{x} \omega_k^2(\mathbf{x}, t) \nu_k^{*2}(\mathbf{x}, t).
\end{aligned}$$

Combining Eqs. (B.33, B.34) and Eqs. (B.39, B.40) yields the following expression for the Hamiltonian Eq. (B.26)

$$\begin{aligned}
\hat{H}_{em-gw}(\mathbf{x}_s, \mathbf{x}_r, t) &= \frac{\hbar}{4} \sum_{\mathbf{k}, \mathbf{k}'} \left\{ \hat{a}_{\mathbf{k}} \hat{a}_{\mathbf{k}'} \left(\frac{\delta^{(3)}(\mathbf{k} + \mathbf{k}')}{V} \right) \int_{\mathbf{x}_s}^{\mathbf{x}_r} d^3\mathbf{x} \left(\dot{\nu}_{\mathbf{k}}^2(\mathbf{x}, t) + \omega_{\mathbf{k}}^2(\mathbf{x}, t) \nu_{\mathbf{k}}^2(\mathbf{x}, t) \right) \right. \\
&\quad + \hat{a}_{\mathbf{k}} \hat{a}_{\mathbf{k}'}^\dagger \left(\frac{\delta^{(3)}(\mathbf{k} - \mathbf{k}')}{V} \right) \int_{\mathbf{x}_s}^{\mathbf{x}_r} d^3\mathbf{x} \left(|\dot{\nu}_{\mathbf{k}}(\mathbf{x}, t)|^2 + \omega_{\mathbf{k}}^2(\mathbf{x}, t) |\nu_{\mathbf{k}}(\mathbf{x}, t)|^2 \right) \\
&\quad + \hat{a}_{\mathbf{k}}^\dagger \hat{a}_{\mathbf{k}'} \left(\frac{\delta^{(3)}(\mathbf{k} - \mathbf{k}')}{V} \right) \int_{\mathbf{x}_s}^{\mathbf{x}_r} d^3\mathbf{x} \left(|\dot{\nu}_{\mathbf{k}}(\mathbf{x}, t)|^2 + \omega_{\mathbf{k}}^2(\mathbf{x}, t) |\nu_{\mathbf{k}}(\mathbf{x}, t)|^2 \right) \\
&\quad \left. + \hat{a}_{\mathbf{k}}^\dagger \hat{a}_{\mathbf{k}'}^\dagger \left(\frac{\delta^{(3)}(\mathbf{k} + \mathbf{k}')}{V} \right) \int_{\mathbf{x}_s}^{\mathbf{x}_r} d^3\mathbf{x} \left(\dot{\nu}_{\mathbf{k}}^{*2}(\mathbf{x}, t) + \omega_{\mathbf{k}}^2(\mathbf{x}, t) \nu_{\mathbf{k}}^{*2}(\mathbf{x}, t) \right) \right\}, \quad (\text{B.41})
\end{aligned}$$

or equivalently

$$\begin{aligned}
\hat{H}_{em-gw}(\mathbf{x}_s, \mathbf{x}_r, t) &= \frac{\hbar}{4} \sum_{\lambda, \mathbf{k}} \left(\hat{a}_{\mathbf{k}, \lambda} \hat{a}_{-\mathbf{k}, \lambda} \left(\frac{1}{V} \int_{\mathbf{x}_s}^{\mathbf{x}_r} d^3\mathbf{x} \left[\dot{\nu}_{\mathbf{k}}^2(\mathbf{x}, t) + \omega_{\mathbf{k}}^2(\mathbf{x}, t) \nu_{\mathbf{k}}^2(\mathbf{x}, t) \right] \right) \right. \\
&\quad + \hat{a}_{\mathbf{k}, \lambda}^\dagger \hat{a}_{-\mathbf{k}, \lambda}^\dagger \left(\frac{1}{V} \int_{\mathbf{x}_s}^{\mathbf{x}_r} d^3\mathbf{x} \left[\dot{\nu}_{\mathbf{k}}^{*2}(\mathbf{x}, t) + \omega_{\mathbf{k}}^2(\mathbf{x}, t) \nu_{\mathbf{k}}^{*2}(\mathbf{x}, t) \right] \right) \\
&\quad \left. + \left(\hat{a}_{\mathbf{k}, \lambda}^\dagger \hat{a}_{\mathbf{k}, \lambda} + \hat{a}_{\mathbf{k}, \lambda} \hat{a}_{\mathbf{k}, \lambda}^\dagger \right) \left(\frac{1}{V} \int_{\mathbf{x}_s}^{\mathbf{x}_r} d^3\mathbf{x} \left[|\dot{\nu}_{\mathbf{k}}(\mathbf{x}, t)|^2 + \omega_{\mathbf{k}}^2(\mathbf{x}, t) |\nu_{\mathbf{k}}(\mathbf{x}, t)|^2 \right] \right) \right). \quad (\text{B.42})
\end{aligned}$$

The first two terms represent the scattering of photons to their opposite momenta, mediated by long wavelength GWs (since $K \ll k$ is assumed). These terms correspond to the photon creation by the GWs field. However, the last two terms represent the scattering of mode \mathbf{k} to itself in the presence of GWs. The temporal mode functions $\nu_{\mathbf{k}}(\mathbf{x}, t)$ are already specified by Eq. (B.6) and Eq. (B.21) (in the adiabatic approximation $\Omega_K \ll \omega_k$). One can easily show that the following mode functions

$$\begin{aligned}
\nu_{\mathbf{k}}(\mathbf{x}, t) &= \frac{1}{\sqrt{\omega_{\mathbf{k}}(\mathbf{x}, t)}} e^{-i \int_0^t \omega_{\mathbf{k}}(\mathbf{x}, t') dt'}, \quad (\text{B.43}) \\
\dot{\nu}_{\mathbf{k}}(\mathbf{x}, t) &= \frac{1}{\sqrt{\omega_{\mathbf{k}}(\mathbf{x}, t)}} \frac{d}{dt} e^{-i \int_0^t \omega_{\mathbf{k}}(\mathbf{x}, t') dt'} = \frac{1}{\sqrt{\omega_{\mathbf{k}}(\mathbf{x}, t)}} \left(-i \frac{d}{dt} \left[\int_0^t \omega_{\mathbf{k}}(\mathbf{x}, t') dt' \right] \right) e^{-i \int_0^t \omega_{\mathbf{k}}(\mathbf{x}, t') dt'} \\
&= -i \omega_{\mathbf{k}}(\mathbf{x}, t) \nu_{\mathbf{k}}(\mathbf{x}, t).
\end{aligned}$$

satisfy Eq. (B.6). Note that, this solution is valid within the adiabatic approximation $\Omega_K \ll \omega_k$. Substitution of the mode functions Eq. (B.43) into the Hamiltonian Eq. (B.42) resets the

contribution of $\hat{a}_{\mathbf{k},\lambda}\hat{a}_{-\mathbf{k},\lambda}$ and $\hat{a}_{\mathbf{k},\lambda}^\dagger\hat{a}_{-\mathbf{k},\lambda}^\dagger$ to zero, and Eq. (B.42) reduces to

$$\begin{aligned}\hat{H}_{em-gw}(\mathbf{x}_s, \mathbf{x}_r, t) &= \hbar \sum_{\lambda, \mathbf{k}} \left(\frac{1}{V} \int_{\mathbf{x}_s}^{\mathbf{x}_r} d^3\mathbf{x} \omega_k(\mathbf{x}, t) \right) \left(\hat{a}_{\mathbf{k},\lambda}^\dagger \hat{a}_{\mathbf{k},\lambda} + \frac{1}{2} \right) \\ &= \sum_{\lambda, \mathbf{k}} \hbar \omega_k \left(\frac{1}{V} \int_{\mathbf{x}_s}^{\mathbf{x}_r} d^3\mathbf{x} \left[1 - \frac{1}{2} h_{ij}(\mathbf{x}, t) \hat{\mathbf{k}}_i \hat{\mathbf{k}}_j \right] \right) \left(\hat{a}_{\mathbf{k},\lambda}^\dagger \hat{a}_{\mathbf{k},\lambda} + \frac{1}{2} \right),\end{aligned}\quad (\text{B.44})$$

Consequently, under the adiabatic condition $\Omega_K \ll \omega_k$ (and $K \ll k$), particle creation by GWs background is negligible, and the EM-GW coupling is intensity-dependent, i.e., proportional to $\hat{a}_{\mathbf{k},\lambda}^\dagger \hat{a}_{\mathbf{k},\lambda}$.

One could equivalently derive the Hamiltonian Eq. (B.44) by energy consideration. Indeed, Eq. (B.42) implies that the Hamiltonian of the system is explicitly time-dependent and, in the corresponding quantum field theory, the vacuum state of the system is not well-defined. Nevertheless, still one may define *instantaneous* vacuum, by finding suitable mode functions $\nu_k(\mathbf{x}, t)$ such that the energy of the system, determined by the mean value of the Hamiltonian Eq. (B.42), is minimized at each moment. Hence, it follows that the adiabatic mode functions Eq. (B.43) indeed minimize the Hamiltonian Eq. (B.42), and are the preferred mode functions (see [145] for details).

In order to obtain the interaction Hamiltonian $\hat{H}_{\text{int}}(\mathbf{x}_s, \mathbf{x}_r, t)$ defined by Eq. (3.3), one can split the Hamiltonian Eq. (B.44) into two parts, as follows

$$\begin{aligned}\hat{H}_{em-gw}(\mathbf{x}_s, \mathbf{x}_r, t) &= \sum_{\lambda, \mathbf{k}} \hbar \omega_k \left(\hat{a}_{\mathbf{k},\lambda}^\dagger \hat{a}_{\mathbf{k},\lambda} + \frac{1}{2} \right) \\ &\quad - \frac{1}{2} \sum_{\lambda, \mathbf{k}} \hbar \omega_k \left(\frac{1}{V} \int_{\mathbf{x}_s}^{\mathbf{x}_r} d^3\mathbf{x} h_{ij}(\mathbf{x}, t) \hat{\mathbf{k}}_i \hat{\mathbf{k}}_j \right) \left(\hat{a}_{\mathbf{k},\lambda}^\dagger \hat{a}_{\mathbf{k},\lambda} + \frac{1}{2} \right).\end{aligned}\quad (\text{B.45})$$

The first term describes the free evolution of the EM field, while the second term shows the EM-GWs interaction Hamiltonian. Considering a single mode EM field of mode $k = (\lambda, \mathbf{k})$, the interaction Hamiltonian is specified by

$$\hat{H}_{\text{int}}(\mathbf{x}_s, \mathbf{x}_r, t)/\hbar = -\frac{1}{2} \omega_k \hat{\mathbf{k}}_i \hat{\mathbf{k}}_j \left(\frac{1}{V} \int_{\mathbf{x}_s}^{\mathbf{x}_r} d^3\mathbf{x} \hat{h}_{ij}(\mathbf{x}, t) \right) \left(\hat{a}_{\mathbf{k},\lambda}^\dagger \hat{a}_{\mathbf{k},\lambda} + \frac{1}{2} \right). \quad (\text{B.46})$$

Here, the classical field $h_{ij}(\mathbf{x}, t)$ is promoted to quantum field operator $\hat{h}_{ij}(\mathbf{x}, t)$, and the Hamiltonian Eq. (B.46) presents a fully-quantum mechanical description of the interaction between EM field and GWs. With the help of Eq. (3.6) we have

$$\begin{aligned}\frac{1}{V} \int_{\mathbf{x}_s}^{\mathbf{x}_r} d^3\mathbf{x} \hat{h}_{ij}(\mathbf{x}, t) &= \frac{\mathcal{C}}{(2\pi)^{3/2}} \sum_{\gamma=+, \times} \int d^3\mathbf{K} \frac{e_{ij}^\gamma[\hat{K}]}{\sqrt{2\Omega_K}} \left\{ \hat{b}_{\mathbf{K},\gamma} e^{-i\Omega_K t} \left(\frac{1}{V} \int_{\mathbf{x}_s}^{\mathbf{x}_r} d^3\mathbf{x} e^{i\mathbf{K}\cdot\mathbf{x}} \right) \right. \\ &\quad \left. + \hat{b}_{\mathbf{K},\gamma}^\dagger e^{i\Omega_K t} \left(\frac{1}{V} \int_{\mathbf{x}_s}^{\mathbf{x}_r} d^3\mathbf{x} e^{-i\mathbf{K}\cdot\mathbf{x}} \right) \right\},\end{aligned}\quad (\text{B.47})$$

With the help of the definition of $g(\mathbf{K} \cdot (\mathbf{x}_r - \mathbf{x}_s))$ given by Eq. (3.4), namely

$$g(\mathbf{K} \cdot (\mathbf{x}_r - \mathbf{x}_s)) \equiv \frac{1}{V} \int_{\mathbf{x}_s}^{\mathbf{x}_r} d^3\mathbf{x} e^{i\mathbf{K}\cdot\mathbf{x}}, \quad (\text{B.48})$$

Eq. (B.47) is re-written as

$$\frac{1}{V} \int_{\mathbf{x}} d^3 \mathbf{x} \hat{h}_{ij}(\mathbf{x}, t) = \frac{\mathcal{C}}{(2\pi)^{3/2}} \sum_{\gamma=+, \times} \int d^3 \mathbf{K} \frac{e_{ij}^{\gamma}[\hat{K}]}{\sqrt{2\Omega_{\mathbf{K}}}} \left\{ \hat{b}_{\mathbf{K}, \gamma} e^{-i\Omega_{\mathbf{K}} t} g(\mathbf{K} \cdot (\mathbf{x}_r - \mathbf{x}_s)) \right. \\ \left. + \hat{b}_{\mathbf{K}, \gamma}^{\dagger} e^{i\Omega_{\mathbf{K}} t} g^*(\mathbf{K} \cdot (\mathbf{x}_r - \mathbf{x}_s)) \right\}, \quad (\text{B.49})$$

Plugging $\mathcal{C} = \sqrt{16\pi c} \ell_{\text{Pl}} = \sqrt{16\pi c^3} (\hbar/E_{\text{Pl}})$ and Eq. (B.49) into Eq. (B.46), the interaction Hamiltonian Eq. (3.3) is recovered.

C Preliminaries for evaluation of $g^{(1)}(\mathbf{x}_1, t; \mathbf{x}_2, t)$

In this section, we generalize Eq. (4.7) to the case that all EM modes $\mathbf{k} \in \sigma$ emitted from the planar source σ contribute to the intensity $I(\mathbf{x}_P, t)$. This generalization gives rise to a modification of the van Citter-Zernike correlations.

C.1 Mutual intensity of a planar source in the presence of PGWs

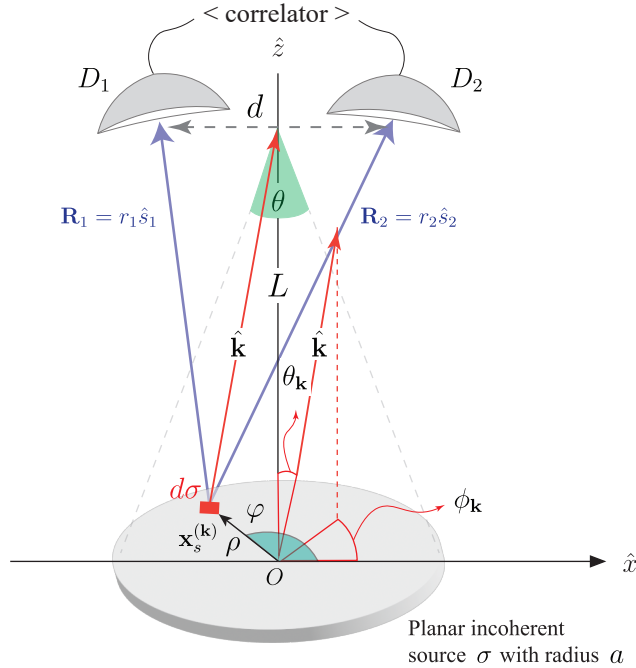


Figure 7. An infinitesimal surface element $d^2\sigma$ on the planar source located at $\mathbf{x}_s^{(\mathbf{k})} = (\rho \cos \varphi, \rho \sin \varphi)$ from the origin \mathcal{O} , sends EM radiation with a wave vector $\hat{\mathbf{k}} = k (\sin \theta_{\mathbf{k}} \cos \phi_{\mathbf{k}}, \sin \theta_{\mathbf{k}} \sin \phi_{\mathbf{k}}, \cos \theta_{\mathbf{k}})$ to the Earth. Here, $\theta_{\mathbf{k}}$ and $\phi_{\mathbf{k}}$ show spatial angles of the EM wave vector. The vectors $\mathbf{R}_i = r_i \hat{\mathbf{s}}_i$ with $i = 1, 2$ represents the position of the detector D_i from the surface element $d\sigma$. Here, $\hat{\mathbf{s}}_i$ stands for the unit vector in the direction of \mathbf{R}_i .

If one denotes by $dI(\mathbf{x}_P, t)$ the intensity element at point \mathbf{x}_P formed by a differential surface element $d\sigma$ located at $\mathbf{x}_s^{(\mathbf{k})}$ on the source and possessing the wave vector \mathbf{k} , Eq. (4.7)

may be generalized according to

$$dI(\mathbf{x}_P, t) = |\mathcal{E}_{\mathbf{k}}|^2 \left\{ 4 dI_{\mathbf{k}}(\mathbf{x}_s^{(\mathbf{k})}) + 2 dI_{\mathbf{k}}(\mathbf{x}_s^{(\mathbf{k})}) \Re[g^{(1)}(\mathbf{x}_s^{(\mathbf{k})}, \mathbf{x}_1, t; \mathbf{x}_s^{(\mathbf{k})}, \mathbf{x}_2, t) e^{-i\mathbf{k}\cdot(\mathbf{x}_1 - \mathbf{x}_2)}] \right\}. \quad (\text{C.1})$$

(see Fig. 7). Note that, as it is explained in Eq. (4.5), the mean number of photons is conserved, hence the mean intensity emitted by the source element located at $\mathbf{x}_s^{(\mathbf{k})}$ can be considered as

$$dI_{\mathbf{k}}(\mathbf{x}_s^{(\mathbf{k})}) \equiv |\mathcal{E}_{\mathbf{k}}|^2 \langle \hat{n}_{\mathbf{k}}(\mathbf{x}_s^{(\mathbf{k})}) \rangle. \quad (\text{C.2})$$

One may also define the surface intensity density of the source, $i(\mathbf{x}_s^{(\mathbf{k})})$, according to

$$i(\mathbf{x}_s^{(\mathbf{k})}) \equiv \frac{dI_{\mathbf{k}}(\mathbf{x}_s^{(\mathbf{k})})}{d^2\sigma}. \quad (\text{C.3})$$

Assuming a constant intensity density over the surface of the source, $i(\mathbf{x}_s^{(\mathbf{k})}) \equiv cte$, the whole intensity radiated from the source may be written as $I \equiv \int_{\sigma} dI_{\mathbf{k}}(\mathbf{x}_s^{(\mathbf{k})}) = \int_{\sigma} i(\mathbf{x}_s^{(\mathbf{k})}) d^2\sigma$. The total intensity at point \mathbf{x}_P can now be found by integrating over all surface elements. Hence, Eq. (C.1) gives rise to

$$I(\mathbf{x}_P, t) = 2I + 2I \Re \left[\frac{\int_{x_s^{(\mathbf{k})} \in \sigma} d^2\sigma g^{(1)}(\mathbf{x}_s^{(\mathbf{k})}, \mathbf{x}_1, t; \mathbf{x}_s^{(\mathbf{k})}, \mathbf{x}_2, t) e^{-i\mathbf{k}\cdot(\mathbf{x}_1 - \mathbf{x}_2)}}{\int_{x_s^{(\mathbf{k})} \in \sigma} d^2\sigma} \right]. \quad (\text{C.4})$$

In the next step, we show that the effect of PGWs on all modes \mathbf{k} leaving the source is identical and determined by Eq. (4.11). Hence, the two-point degree of coherence $g^{(1)}(\mathbf{x}_s^{(\mathbf{k})}, \mathbf{x}_1, t; \mathbf{x}_s^{(\mathbf{k})}, \mathbf{x}_2, t)$ in the integrand Eq. (C.4) can be factorized.

C.2 Separating different scales k and K in the expression of $g^{(1)}(\mathbf{x}_s^{(\mathbf{k})}, \mathbf{x}_1, t; \mathbf{x}_s^{(\mathbf{k})}, \mathbf{x}_2, t)$

In this section we show that the two-point correlation function $g^{(1)}(\mathbf{x}_s^{(\mathbf{k})}, \mathbf{x}_1, t; \mathbf{x}_s^{(\mathbf{k})}, \mathbf{x}_2, t)$ defined in Eq. (4.6) is indeed independent from $\mathbf{x}_s^{(\mathbf{k})}$, in the adiabatic approximation $K \ll k$. Here, \mathbf{x}_1 and \mathbf{x}_2 are the locations at which the EM field is observed, measured from the origin \mathcal{O} , as shown in Figure. 7. In the integral Eq. (C.4), the surface element is $d\sigma = \rho d\rho d\phi$, $0 \leq \rho \leq a$ and $0 \leq \phi \leq 2\pi$. First consider the exponential factor, which can be rewritten as

$$\begin{aligned} e^{-i\mathbf{k}\cdot(\mathbf{x}_1 - \mathbf{x}_2)} &= e^{-i\mathbf{k}\cdot(\mathbf{x}_s^{(\mathbf{k})} + \mathbf{R}_{1s} - \mathbf{x}_s^{(\mathbf{k})} - \mathbf{R}_{2s})} \\ &= e^{-i\mathbf{k}\cdot(\mathbf{R}_{1s} - \mathbf{R}_{2s})} = e^{-ik(R_{1s} - R_{2s})} \\ &= e^{-ik(r_1 - \hat{s}_1 \cdot \mathbf{x}_s^{(\mathbf{k})} - r_2 + \hat{s}_2 \cdot \mathbf{x}_s^{(\mathbf{k})})} \\ &= e^{-ik(r_1 - r_2)} e^{-ik(\hat{s}_2 - \hat{s}_1) \cdot \mathbf{x}_s^{(\mathbf{k})}}. \end{aligned} \quad (\text{C.5})$$

where we have replaced (see Fig. 7)

$$\begin{aligned} \mathbf{x}_1 &= \mathbf{x}_s^{(\mathbf{k})} + \mathbf{R}_{1s}, \\ \mathbf{x}_2 &= \mathbf{x}_s^{(\mathbf{k})} + \mathbf{R}_{2s}. \end{aligned} \quad (\text{C.6})$$

Here, $\mathbf{R}_i = r_i \hat{s}_i$ with $i = 1, 2$ represents the position of the detectors D_i with respect to the surface element $d\sigma$, and \hat{s}_i stands for the unit vector in the direction of \mathbf{R}_i . Note that in the far zone one has $\mathbf{k} \parallel \mathbf{R}_{1s}, \mathbf{R}_{2s}$. Moreover, we have used $R_{1s} \simeq r_1 - \hat{s}_1 \cdot \mathbf{x}_s^{(\mathbf{k})}$ and

$R_{2s} \simeq r_2 - \hat{s}_2 \cdot \mathbf{x}_s^{(\mathbf{k})}$. Now, since the integration is taken over the surface of the planar source, only the orthogonal component of the unit vector $\hat{s}_2 - \hat{s}_1$ has a contribution. So, one defines (see [18])

$$\begin{aligned} \mathbf{x}_s^{(\mathbf{k})} &\equiv (\rho \cos \varphi, \rho \sin \varphi), \\ \hat{s}_{2\perp} - \hat{s}_{1\perp} &\equiv (w \cos \psi, w \sin \psi) \end{aligned} \quad (\text{C.7})$$

where ρ and ϕ are integration variables, while w and ψ are two new variables which identify the projection of $\hat{s}_2 - \hat{s}_1$ onto the plane of the disc. Thus, we have

$$(\hat{s}_2 - \hat{s}_1) \cdot \mathbf{x}_s^{(\mathbf{k})} = (\hat{s}_{2\perp} - \hat{s}_{1\perp}) \cdot \mathbf{x}_s^{(\mathbf{k})} = \rho w \cos(\varphi - \psi). \quad (\text{C.8})$$

Since $r_1 \simeq r_2$, Eq. (C.8) reduces to [18]

$$e^{-i\mathbf{k} \cdot (\mathbf{x}_1 - \mathbf{x}_2)} = e^{-ik\rho w \cos(\varphi - \psi)} \quad (\text{C.9})$$

and the integration will be taken over ρ and ϕ .

Now, take a look at $g_{\mathbf{k}}(\mathbf{x}_s^{(\mathbf{k})}, \mathbf{x}_1, t; \mathbf{x}_s^{(\mathbf{k})}, \mathbf{x}_2, t)$. In the following arguments, we consider the case of vacuum fluctuations of GWs, but similar arguments hold correct for any state of GWs, such as the squeezed state. From the definition Eq. (4.6) and with the help of Eq. (3.24), for GWs in vacuum state we have

$$\begin{aligned} g_{\text{vac}}^{(1)}(\mathbf{x}_s^{(\mathbf{k})}, \mathbf{x}_1, t; \mathbf{x}_s^{(\mathbf{k})}, \mathbf{x}_2, t) &= \prod_{\gamma, \mathbf{K} \in \mathbb{R}^{3+}} \langle 0_{\mathbf{K}}, 0_{-\mathbf{K}} | \hat{D}_{\mathbf{K}}^\dagger(-\kappa\eta_{\mathbf{K}}(\mathbf{x}_s^{(\mathbf{k})}, \mathbf{x}_1, t)) \hat{D}_{\mathbf{K}}(-\kappa\eta_{\mathbf{K}}(\mathbf{x}_s^{(\mathbf{k})}, \mathbf{x}_2, t)) \\ &\quad \times \hat{D}_{-\mathbf{K}}^\dagger(-\kappa\eta_{-\mathbf{K}}(\mathbf{x}_s^{(\mathbf{k})}, \mathbf{x}_1, t)) \hat{D}_{-\mathbf{K}}(-\kappa\eta_{-\mathbf{K}}(\mathbf{x}_s^{(\mathbf{k})}, \mathbf{x}_2, t)) | 0_{\mathbf{K}}, 0_{-\mathbf{K}} \rangle \\ &= \prod_{\gamma, \mathbf{K} \in \mathbb{R}^{3+}} \langle 0_{\mathbf{K}} | \hat{D}_{\mathbf{K}}^\dagger(-\kappa\eta_{\mathbf{K}}(\mathbf{x}_s^{(\mathbf{k})}, \mathbf{x}_1, t)) \hat{D}_{\mathbf{K}}(-\kappa\eta_{\mathbf{K}}(\mathbf{x}_s^{(\mathbf{k})}, \mathbf{x}_2, t)) | 0_{\mathbf{K}} \rangle \\ &\quad \times \langle 0_{-\mathbf{K}} | \hat{D}_{-\mathbf{K}}^\dagger(-\kappa\eta_{-\mathbf{K}}(\mathbf{x}_s^{(\mathbf{k})}, \mathbf{x}_1, t)) \hat{D}_{-\mathbf{K}}(-\kappa\eta_{-\mathbf{K}}(\mathbf{x}_s^{(\mathbf{k})}, \mathbf{x}_2, t)) | 0_{-\mathbf{K}} \rangle. \end{aligned} \quad (\text{C.10})$$

With the help of the property $\hat{D}^\dagger(\alpha)\hat{D}(\beta) = e^{-i\Im\alpha\beta^*} \hat{D}(\beta - \alpha)$ for displacement operator, Eq. (C.10) is rewritten as

$$\begin{aligned} g_{\text{vac}}^{(1)}(\mathbf{x}_s^{(\mathbf{k})}, \mathbf{x}_1, t; \mathbf{x}_s^{(\mathbf{k})}, \mathbf{x}_2, t) &= \prod_{\gamma, \mathbf{K} \in \mathbb{R}^{3+}} \langle 0_{\mathbf{K}} | e^{-i\kappa^2 \Im} (\eta_{\mathbf{K}}(\mathbf{x}_s^{(\mathbf{k})}, \mathbf{x}_1, t) \eta_{\mathbf{K}}^*(\mathbf{x}_s^{(\mathbf{k})}, \mathbf{x}_2, t)) \\ &\quad \times \hat{D}_{\mathbf{K}}(\kappa[\eta_{\mathbf{K}}(\mathbf{x}_s^{(\mathbf{k})}, \mathbf{x}_1, t) - \eta_{\mathbf{K}}(\mathbf{x}_s^{(\mathbf{k})}, \mathbf{x}_2, t)]) | 0_{\mathbf{K}} \rangle \\ &\quad \times \langle 0_{-\mathbf{K}} | e^{-i\kappa^2 \Im} (\eta_{-\mathbf{K}}(\mathbf{x}_s^{(\mathbf{k})}, \mathbf{x}_1, t) \eta_{-\mathbf{K}}^*(\mathbf{x}_s^{(\mathbf{k})}, \mathbf{x}_2, t)) \\ &\quad \times \hat{D}_{-\mathbf{K}}(\kappa[\eta_{-\mathbf{K}}(\mathbf{x}_s^{(\mathbf{k})}, \mathbf{x}_1, t) - \eta_{-\mathbf{K}}(\mathbf{x}_s^{(\mathbf{k})}, \mathbf{x}_2, t)]) | 0_{-\mathbf{K}} \rangle \\ &= \prod_{\gamma, \mathbf{K} \in \mathbb{R}^{3+}} e^{-i\kappa^2 \Im} (\eta_{\mathbf{K}}(\mathbf{x}_s^{(\mathbf{k})}, \mathbf{x}_1, t) \eta_{\mathbf{K}}^*(\mathbf{x}_s^{(\mathbf{k})}, \mathbf{x}_2, t) + \eta_{-\mathbf{K}}(\mathbf{x}_s^{(\mathbf{k})}, \mathbf{x}_1, t) \eta_{-\mathbf{K}}^*(\mathbf{x}_s^{(\mathbf{k})}, \mathbf{x}_2, t)) \\ &\quad \times \exp\left[-\frac{1}{2}\kappa^2 |\eta_{\mathbf{K}}(\mathbf{x}_s^{(\mathbf{k})}, \mathbf{x}_1, t) - \eta_{\mathbf{K}}(\mathbf{x}_s^{(\mathbf{k})}, \mathbf{x}_2, t)|^2\right] \\ &\quad \times \exp\left[-\frac{1}{2}\kappa^2 |\eta_{-\mathbf{K}}(\mathbf{x}_s^{(\mathbf{k})}, \mathbf{x}_1, t) - \eta_{-\mathbf{K}}(\mathbf{x}_s^{(\mathbf{k})}, \mathbf{x}_2, t)|^2\right]. \end{aligned} \quad (\text{C.11})$$

Note that, in the above equations, we have used κ in place of $\kappa_\gamma(\mathbf{K}, \mathbf{k})$ for simplicity. Moreover, from definition Eq. (3.10), one has $\kappa_\gamma(\mathbf{K}, \mathbf{k}) = \kappa_\gamma(-\mathbf{K}, \mathbf{k})$. Using the continuous notation,

Eq. (C.11) becomes

$$g_{\text{vac}}^{(1)}(\mathbf{x}_s^{(\mathbf{k})}, \mathbf{x}_1, t; \mathbf{x}_s^{(\mathbf{k})}, \mathbf{x}_2, t) = e^{-i \sum_{\gamma} \int_{\mathbf{K} \in \mathbb{R}^3} d^3 \mathbf{K} \kappa_{\gamma}^2(\mathbf{K}, \mathbf{k}) \Im(\eta_{\mathbf{K}}(\mathbf{x}_s^{(\mathbf{k})}, \mathbf{x}_1, t) \eta_{\mathbf{K}}^*(\mathbf{x}_s^{(\mathbf{k})}, \mathbf{x}_2, t))} \quad (\text{C.12})$$

$$\times \exp \left[-\frac{1}{2} \sum_{\gamma} \int_{\mathbf{K} \in \mathbb{R}^3} d^3 \mathbf{K} \kappa_{\gamma}^2(\mathbf{K}, \mathbf{k}) |\eta_{\mathbf{K}}(\mathbf{x}_s^{(\mathbf{k})}, \mathbf{x}_1, t) - \eta_{\mathbf{K}}(\mathbf{x}_s^{(\mathbf{k})}, \mathbf{x}_2, t)|^2 \right].$$

With the help of definitions Eq. (4.17), we may now rewrite Eq. (C.12) as follows

$$g_{\text{vac}}^{(1)}(\mathbf{x}_s^{(\mathbf{k})}, \mathbf{x}_1, t; \mathbf{x}_s^{(\mathbf{k})}, \mathbf{x}_2, t) = e^{-i \mathcal{C}^{\text{vac}}(\mathbf{x}_s^{(\mathbf{k})}, \mathbf{x}_1, t; \mathbf{x}_s^{(\mathbf{k})}, \mathbf{x}_2, t)} e^{-\mathcal{D}^{\text{vac}}(\mathbf{x}_s^{(\mathbf{k})}, \mathbf{x}_1, t; \mathbf{x}_s^{(\mathbf{k})}, \mathbf{x}_2, t)}. \quad (\text{C.13})$$

Inserting Eqs. (C.9, C.13) into Eq. (C.4) results

$$I(\mathbf{x}_P, t) \propto \int_{\mathbf{x}_s^{(\mathbf{k})} \in \sigma} d^2 \sigma g_{\text{vac}}^{(1)}(\mathbf{x}_s^{(\mathbf{k})}, \mathbf{x}_1, t; \mathbf{x}_s^{(\mathbf{k})}, \mathbf{x}_2, t) e^{-i \mathbf{k} \cdot (\mathbf{x}_1 - \mathbf{x}_2)} \quad (\text{C.14})$$

$$= \int_{\mathbf{x}_s^{(\mathbf{k})} \in \sigma} \rho d\rho d\varphi e^{-\mathcal{D}^{\text{vac}}(\mathbf{x}_s^{(\mathbf{k})}, \mathbf{x}_1, t; \mathbf{x}_s^{(\mathbf{k})}, \mathbf{x}_2, t)} e^{-i \mathcal{C}^{\text{vac}}(\mathbf{x}_s^{(\mathbf{k})}, \mathbf{x}_1, t; \mathbf{x}_s^{(\mathbf{k})}, \mathbf{x}_2, t)} e^{-i k \rho w \cos(\varphi - \psi)}$$

$$= \int_{\mathbf{x}_s^{(\mathbf{k})} \in \sigma} \rho d\rho d\varphi \exp \left(- \sum_{\gamma = +, \times} \int d^3 \mathbf{K} \kappa_{\gamma}^2(\mathbf{K}, \mathbf{k}) \left[\frac{1}{2} \mathcal{D}_{\mathbf{K}}^{\text{vac}}(\mathbf{x}_s^{(\mathbf{k})}, \mathbf{x}_1, t; \mathbf{x}_s^{(\mathbf{k})}, \mathbf{x}_2, t) \right. \right.$$

$$\left. \left. + i \mathcal{C}_{\mathbf{K}}^{\text{vac}}(\mathbf{x}_s^{(\mathbf{k})}, \mathbf{x}_1, t; \mathbf{x}_s^{(\mathbf{k})}, \mathbf{x}_2, t) \right] \right) e^{-i k \rho w \cos(\varphi - \psi)}$$

$$= \prod_{\gamma, \mathbf{K} \in \mathbb{R}^3} \int_{\mathbf{x}_s^{(\mathbf{k})} \in \sigma} \rho d\rho d\varphi e^{-\kappa^2(\mathbf{K}, \mathbf{k}) \left[\frac{1}{2} \mathcal{D}_{\mathbf{K}}^{\text{vac}}(\mathbf{x}_s^{(\mathbf{k})}, \mathbf{x}_1, t; \mathbf{x}_s^{(\mathbf{k})}, \mathbf{x}_2, t) + i \mathcal{C}_{\mathbf{K}}^{\text{vac}}(\mathbf{x}_s^{(\mathbf{k})}, \mathbf{x}_1, t; \mathbf{x}_s^{(\mathbf{k})}, \mathbf{x}_2, t) \right]}$$

$$\times e^{-i k \rho w \cos(\varphi - \psi)}.$$

In the last line, we transformed from continuous to discrete notation. According to definition of the kernels $\mathcal{C}^{\text{vac}}(1; 2)$ and $\mathcal{D}^{\text{vac}}(1; 2)$ given by Eqs. (4.17, 4.18) and with the help of Eq. (3.19) for $\eta_{\mathbf{K}}(\mathbf{x}_s^{(\mathbf{k})}, \mathbf{x}_i, t)$, we obtain

$$I(\mathbf{x}_P, t) \propto \prod_{\gamma, \mathbf{K} \in \mathbb{R}^3} \int_{\mathbf{x}_s^{(\mathbf{k})} \in \sigma} \rho d\rho d\varphi \exp \left(-\kappa^2(\mathbf{K}, \mathbf{k}) \left[\frac{1}{2} (4 \sin^2 \frac{\Omega_K t}{2}) (|g(\mathbf{K} \cdot (\mathbf{x}_1 - \mathbf{x}_s^{(\mathbf{k})}))|^2 \right. \right. \quad (\text{C.15})$$

$$\left. \left. + |g(\mathbf{K} \cdot (\mathbf{x}_2 - \mathbf{x}_s^{(\mathbf{k})}))|^2 - 2 \Re \left\{ g^*(\mathbf{K} \cdot (\mathbf{x}_1 - \mathbf{x}_s^{(\mathbf{k})})) g(\mathbf{K} \cdot (\mathbf{x}_2 - \mathbf{x}_s^{(\mathbf{k})})) \right\} \right] \right)$$

$$+ i (4 \sin^2 \frac{\Omega_K t}{2}) \Im \left\{ g^*(\mathbf{K} \cdot (\mathbf{x}_1 - \mathbf{x}_s^{(\mathbf{k})})) g(\mathbf{K} \cdot (\mathbf{x}_2 - \mathbf{x}_s^{(\mathbf{k})})) \right\} \Big] \Big] e^{-i k \rho w \cos(\varphi - \psi)}$$

$$= \prod_{\gamma, \mathbf{K} \in \mathbb{R}^3} \int_{\mathbf{x}_s^{(\mathbf{k})} \in \sigma} \rho d\rho d\varphi \exp \left(-\kappa^2(\mathbf{K}, \mathbf{k}) (4 \sin^2 \frac{\Omega_K t}{2}) \left[\frac{1}{2} |g(\mathbf{K} \cdot (\mathbf{x}_1 - \mathbf{x}_s^{(\mathbf{k})}))|^2 \right. \right.$$

$$+ \frac{1}{2} |g(\mathbf{K} \cdot (\mathbf{x}_2 - \mathbf{x}_s^{(\mathbf{k})}))|^2 - \Re \left\{ g^*(\mathbf{K} \cdot (\mathbf{x}_1 - \mathbf{x}_s^{(\mathbf{k})})) g(\mathbf{K} \cdot (\mathbf{x}_2 - \mathbf{x}_s^{(\mathbf{k})})) \right\}$$

$$\left. \left. + i \Im \left\{ g^*(\mathbf{K} \cdot (\mathbf{x}_1 - \mathbf{x}_s^{(\mathbf{k})})) g(\mathbf{K} \cdot (\mathbf{x}_2 - \mathbf{x}_s^{(\mathbf{k})})) \right\} \right] - i k \rho w \cos(\varphi - \psi) \right).$$

Firstly, note that the factor $\kappa_{\gamma}^2(\hat{\mathbf{K}}, \hat{\mathbf{k}})$ does not depend on the location of the surface element $\mathbf{x}_s^{(\mathbf{k})} = (\rho \cos \varphi, \rho \sin \varphi)$. However, this factor depends on the orientation of the wave vector, namely $\mathbf{k} = k (\sin \theta_{\mathbf{k}} \cos \phi_{\mathbf{k}}, \sin \theta_{\mathbf{k}} \sin \phi_{\mathbf{k}}, \cos \theta_{\mathbf{k}})$, as depicted in Fig. (7). In App. C.3, we show that this factor is identical for all wave vectors \mathbf{k} up to $\mathcal{O}(\theta^2) \sim 10^{-16}$, where $\theta = 2a/L$ stands

for the angular diameter of the source. Secondly, in the exponential term in Eq. (C.15), we have integrals of the form

$$\begin{aligned} g^*(\mathbf{K} \cdot (\mathbf{x}_1 - \mathbf{x}_s^{(\mathbf{k})})) g(\mathbf{K} \cdot (\mathbf{x}_2 - \mathbf{x}_s^{(\mathbf{k})})) &= \frac{1}{V^2} \int_{\mathbf{x}_s^{(\mathbf{k})}}^{\mathbf{x}_1} d^3 \mathbf{x} \int_{\mathbf{x}_s^{(\mathbf{k})}}^{\mathbf{x}_2} d^3 \mathbf{x}' e^{-i\mathbf{K} \cdot \mathbf{x}} e^{i\mathbf{K} \cdot \mathbf{x}'} \quad (\text{C.16}) \\ &\equiv A(K_i x_s^{(\mathbf{k})^i}, K_i x_1^i, K_i x_2^i).. \end{aligned}$$

Note that, in the first line we have used the definition Eq. (3.4) for $g(\mathbf{K} \cdot (\mathbf{x} - \mathbf{x}_s^{(\mathbf{k})}))$. In the second line, we have introduced a new function that depends on three scales $K_i x_s^{(\mathbf{k})^i}$, $K_i x_1^i$, and $K_i x_2^i$ with $i = 1, 2, 3$. There are similar expressions for other terms in the integrand Eq. (C.16). In order to analyze different scales in the integral, let us rewrite Eq. (C.15) with the help of Eq. (C.16) in the following form

$$\begin{aligned} I(\mathbf{x}_P, t) \propto \prod_{\gamma, \mathbf{K} \in \mathbb{R}^3} \int_{\mathbf{x}_s^{(\mathbf{k})} \in \sigma} \rho d\rho d\varphi \exp \left(-\kappa^2(\mathbf{K}, \mathbf{k}) \left(4 \sin^2 \frac{\Omega_K t}{2} \right) \mathcal{A}_{\mathbf{K}}(K_i x_s^{(\mathbf{k})^i}, K_i x_1^i, K_i x_2^i) \right. \\ \left. - ik\rho w \cos(\varphi - \psi) \right), \quad (\text{C.17}) \end{aligned}$$

where we have defined

$$\begin{aligned} \mathcal{A}_{\mathbf{K}}(K_i x_s^{(\mathbf{k})^i}, K_i x_1^i, K_i x_2^i) &= \frac{1}{2} |g(\mathbf{K} \cdot (\mathbf{x}_1 - \mathbf{x}_s^{(\mathbf{k})}))|^2 + \frac{1}{2} |g(\mathbf{K} \cdot (\mathbf{x}_2 - \mathbf{x}_s^{(\mathbf{k})}))|^2 \\ &\quad - \Re \left\{ g^*(\mathbf{K} \cdot (\mathbf{x}_1 - \mathbf{x}_s^{(\mathbf{k})})) g(\mathbf{K} \cdot (\mathbf{x}_2 - \mathbf{x}_s^{(\mathbf{k})})) \right\} \\ &\quad + i \Im \left\{ g^*(\mathbf{K} \cdot (\mathbf{x}_1 - \mathbf{x}_s^{(\mathbf{k})})) g(\mathbf{K} \cdot (\mathbf{x}_2 - \mathbf{x}_s^{(\mathbf{k})})) \right\}. \quad (\text{C.18}) \end{aligned}$$

Now, in Eq. (C.17) the integration is performed over $\mathbf{x}_s^{(\mathbf{k})} = (\rho \cos \varphi, \rho \sin \varphi)$. The first term in the exponential factor acts on large scales K^{-1} while the second term contains small scales k^{-1} . As long as the adiabatic condition $K \ll k$ is concerned, one may assume that the function $\mathcal{A}_{\mathbf{K}}(K_i x_s^{(\mathbf{k})^i}, K_i x_1^i, K_i x_2^i)$ is practically constant over the surface of the planar source and, it is equal to its value at the center of the disc, where $\mathbf{x}_s^{(\mathbf{k})} = 0$. Thus, the integral in Eq. (C.17) can be factorized as following

$$I(\mathbf{x}_P, t) \propto \prod_{\gamma, \mathbf{K} \in \mathbb{R}^3} e^{-\kappa^2(\mathbf{K}, \mathbf{k}) \left(4 \sin^2 \frac{\Omega_K t}{2} \right) \mathcal{A}_{\mathbf{K}}(K_i x_s^{(\mathbf{k})^i}, K_i x_1^i, K_i x_2^i)} \int_{\mathbf{x}_s^{(\mathbf{k})} \in \sigma} \rho d\rho d\varphi e^{-ik\rho w \cos(\varphi - \psi)}. \quad (\text{C.19})$$

The integral appearing in Eq. (C.19) is nothing but the van Citter-Zernike correlation function $j(\mathbf{x}_1, \mathbf{x}_2)$ given by Eqs. (4.10,5.1) (see [18]). Thus, Eq. (C.19) can be factorized according to

$$I(\mathbf{x}_P, t) \propto g_{\text{vac}}^{(1)}(\mathbf{x}_1, t; \mathbf{x}_2, t) j(\mathbf{x}_1, \mathbf{x}_2). \quad (\text{C.20})$$

and Eq. (4.9) is obtained. Thus, all calculations can be done by setting $\mathbf{x}_s^{(\mathbf{k})} = 0$ and assuming the center of the planar source as the origin of coordinates.

C.3 Evaluation of the integral $\int d^3 \mathbf{K} \kappa_{\gamma}^2(\mathbf{K}, \mathbf{k})$

One of the main quantities that appear frequently in our calculations is the expression

$$\sum_{\gamma} \int d^3 \mathbf{K} \kappa_{\gamma}^2(\mathbf{K}, \mathbf{k}) \quad (\text{C.21})$$

To evaluate Eq. (C.21) in our context, we consider a surface element $d^2\sigma$ that emits EM radiation in direction

$$\hat{\mathbf{k}} = (\sin \theta_{\mathbf{k}} \cos \phi_{\mathbf{k}}, \sin \theta_{\mathbf{k}} \sin \phi_{\mathbf{k}}, \cos \theta_{\mathbf{k}}), \quad (\text{C.22})$$

where $\theta_{\mathbf{k}}$ and $\phi_{\mathbf{k}}$ represent spatial angles of the EM wave vector as shown in Fig. 7, with a range $0 \leq \theta_{\mathbf{k}} \leq \theta/2$ and $0 \leq \phi_{\mathbf{k}} \leq 2\pi$ where $\theta = 2a/L$ stands for the angular diameter of the source. The detector pattern function Eq. (3.5) thus becomes

$$\begin{aligned} F_\gamma(\hat{\mathbf{K}}, \hat{\mathbf{k}}) &= e_{ij}^\gamma[\hat{\mathbf{K}}] \hat{\mathbf{k}}_i \hat{\mathbf{k}}_j \\ &= e_{11}^\gamma[\hat{\mathbf{K}}] \sin^2 \theta_{\mathbf{k}} \cos^2 \phi_{\mathbf{k}} + e_{12}^\gamma[\hat{\mathbf{K}}] \sin^2 \theta_{\mathbf{k}} \sin 2\phi_{\mathbf{k}} + e_{13}^\gamma[\hat{\mathbf{K}}] \sin 2\theta_{\mathbf{k}} \cos \phi_{\mathbf{k}} \\ &\quad + e_{22}^\gamma[\hat{\mathbf{K}}] \sin^2 \theta_{\mathbf{k}} \sin^2 \phi_{\mathbf{k}} + e_{23}^\gamma[\hat{\mathbf{K}}] \sin 2\theta_{\mathbf{k}} \sin \phi_{\mathbf{k}} + e_{33}^\gamma[\hat{\mathbf{K}}] \cos^2 \theta_{\mathbf{k}}. \end{aligned} \quad (\text{C.23})$$

Typical angular size of distant quasars is of order $\mathcal{O}(\theta) \sim 10^{-8}$ [95]. The quantity of interest is $F_\gamma^2(\mathbf{K}, \mathbf{k})$. Calculations up to $\mathcal{O}(\theta^2)$ yields

$$\begin{aligned} F_\gamma(\hat{\mathbf{K}}, \hat{\mathbf{k}}) &= e_{33}^\gamma[\hat{\mathbf{K}}] + 2\theta_{\mathbf{k}} \left(e_{13}^\gamma[\hat{\mathbf{K}}] \cos \phi_{\mathbf{k}} + e_{23}^\gamma[\hat{\mathbf{K}}] \sin \phi_{\mathbf{k}} \right) \\ &\quad + \theta_{\mathbf{k}}^2 \left(e_{11}^\gamma[\hat{\mathbf{K}}] \cos^2 \phi_{\mathbf{k}} + e_{12}^\gamma[\hat{\mathbf{K}}] \sin 2\phi_{\mathbf{k}} + e_{22}^\gamma[\hat{\mathbf{K}}] \sin^2 \phi_{\mathbf{k}} - e_{33}^\gamma[\hat{\mathbf{K}}] \right). \end{aligned} \quad (\text{C.24})$$

Consequently, one has

$$\begin{aligned} F_\gamma^2(\hat{\mathbf{K}}, \hat{\mathbf{k}}) &= (e_{33}^\gamma[\hat{\mathbf{K}}])^2 + 4\theta_{\mathbf{k}} e_{33}^\gamma[\hat{\mathbf{K}}] \left(e_{13}^\gamma[\hat{\mathbf{K}}] \cos \phi_{\mathbf{k}} + e_{23}^\gamma[\hat{\mathbf{K}}] \sin \phi_{\mathbf{k}} \right) + 4\theta_{\mathbf{k}}^2 \left[\left(e_{13}^\gamma[\hat{\mathbf{K}}] \cos \phi_{\mathbf{k}} + e_{23}^\gamma[\hat{\mathbf{K}}] \sin \phi_{\mathbf{k}} \right)^2 \right. \\ &\quad \left. + \frac{1}{2} e_{33}^\gamma[\hat{\mathbf{K}}] \left(e_{11}^\gamma[\hat{\mathbf{K}}] \cos^2 \phi_{\mathbf{k}} + e_{12}^\gamma[\hat{\mathbf{K}}] \sin 2\phi_{\mathbf{k}} + e_{22}^\gamma[\hat{\mathbf{K}}] \sin^2 \phi_{\mathbf{k}} - e_{33}^\gamma[\hat{\mathbf{K}}] \right) \right]. \end{aligned} \quad (\text{C.25})$$

Hence the detector pattern function for given wave vectors \mathbf{k} and \mathbf{K} , up to $\mathcal{O}(\theta_{\mathbf{k}}^2)$, is determined by Eq. (C.25). According to definition of the polarization tensors $e_{ij}^\gamma[\hat{\mathbf{K}}]$ given by Eqs. (2.5, 2.6) one has

$$\begin{cases} e_{13}^+ = -\sin \Theta_K \cos \Theta_K \cos \Phi_K \\ e_{13}^\times = \sin \Theta_K \sin \Phi_K \end{cases}, \quad \begin{cases} e_{23}^+ = -\sin \Theta_K \cos \Theta_K \sin \Phi_K \\ e_{23}^\times = -\sin \Theta_K \cos \Phi_K \end{cases}, \quad \begin{cases} e_{33}^+ = \sin^2 \Theta_K \\ e_{33}^\times = 0. \end{cases} \quad (\text{C.26})$$

Integration over the azimuthal angle Φ_K yields

$$\int_0^{2\pi} d\Phi_K e_{13}^\gamma[\hat{\mathbf{K}}] e_{33}^\gamma[\hat{\mathbf{K}}] = 0 = \int_0^{2\pi} d\Phi_K e_{23}^\gamma[\hat{\mathbf{K}}] e_{33}^\gamma[\hat{\mathbf{K}}]. \quad (\text{C.27})$$

Thus, the contribution of the second term in Eq. (C.25) vanishes. On the other hand, the last term is proportional to $\theta_{\mathbf{k}}^2 \sim \mathcal{O}(10^{-16})$ and can be ignored safely. Consequently, one has $F_\gamma^2(\hat{\mathbf{K}}, \hat{\mathbf{k}}) \rightarrow (e_{33}^+[\hat{\mathbf{K}}])^2 = \sin^4 \Theta_K$, hence

$$\begin{aligned} \int_0^{2\pi} d\Phi_K \int_0^\pi d \cos(\Theta_K) F_\gamma^2(\hat{\mathbf{K}}, \hat{\mathbf{k}}) &\rightarrow \int_0^{2\pi} d\Phi_K \int_0^\pi d \cos(\Theta_K) F_+^2(\hat{\mathbf{K}}, \hat{\mathbf{k}}) \\ &= \int_0^{2\pi} d\Phi_K \int_0^\pi d \cos(\Theta_K) \sin^4 \Theta_K. \end{aligned} \quad (\text{C.28})$$

By inserting definition of $\kappa_\gamma(\mathbf{K}, \mathbf{k})$ from Eq. (3.10) into Eq. (3.21) and using Eq. (C.28), the integration over $d^3\mathbf{K}$ is simplified as follows

$$\sum_\gamma \int_{\mathbf{K} \in \mathfrak{R}^3} d^3\mathbf{K} \kappa_\gamma^2(\mathbf{K}, \mathbf{k}) = \frac{1}{(2\pi)^2} \left(\frac{\hbar\omega_{\mathbf{k}}}{E_{\text{Pl}}} \right)^2 \int_0^{2\pi} d\Phi_K \int_0^\pi d \cos(\Theta_K) \sin^4 \Theta_K \int_{K_E}^{K_1} \frac{dK}{K} \quad (\text{C.29})$$

C.4 Expression of the time of flight t and distance L versus redshift z

Typical quasars detected by VLBI means are located at cosmological distances. Hence, it seems necessary to express physical quantities in terms of the redshift of the source, z , rather than the time of flight t . These objects are located at the redshift range $0.46 \leq z \leq 2.73$, so during their journey to the Earth, they have been affected not only by PGWs background but also by the expansion of the Universe. One may incorporate the Universe expansion by expressing time, distance, and frequency in terms of redshift. In particular, one may replace the redshifted EM frequency according to $\omega_k \rightarrow \omega_k/(1+z)$. The light detected today was emitted at some earlier time. The time of flight $t(z)$, i.e., the time interval between emission at time $t_{\text{em}}(z)$, corresponding to the redshift z , and detection at present t_{z_H} , is determined by [116],

$$t(z) = t_{z_H} - t_{\text{em}}(z) = \int_{z_H}^z \frac{dz'}{(1+z')H(z')}, \quad (\text{C.30})$$

where $H(z')$ is the Hubble parameter at redshift z and $z_H = 0$ is the redshift at present time. We proceed assuming a flat Universe comprising only cold dark matter and a cosmological constant, so that $\Omega_\Lambda + \Omega_m = 1$. The Hubble parameter versus redshift is thus determined by

$$H(z) = H_0 \sqrt{(1 - \Omega_m) + \Omega_m(1+z)^3}. \quad (\text{C.31})$$

By plugging Eq. (C.31) into Eq. (C.30) and setting $z_H = 0$, the time of flight $t(z)$ turns out

$$t(z) = H_0^{-1} \int_0^z \frac{dz'}{\sqrt{(1 - \Omega_m)(1+z')^2 + \Omega_m(1+z')^5}}, \quad (\text{C.32})$$

Moreover, from Eq. (5.4) it is obvious that the angular diameter distance $L(z)$ of an object located at redshift z is determined by [116]

$$L(z) = \frac{c}{H_0(1+z)} \left(\int_0^z \frac{dz'}{\sqrt{\Omega_m(1+z')^3 + (1 - \Omega_m)}} \right). \quad (\text{C.33})$$

References

- [1] Peter R Saulson. *Fundamentals of interferometric gravitational wave detectors*. World Scientific, 1994.
- [2] Barry C Barish and Rainer Weiss. Ligo and the detection of gravitational waves. *Physics Today*, 52:44–50, 1999.
- [3] Li Ju, DG Blair, and Chunnong Zhao. Detection of gravitational waves. *Reports on Progress in Physics*, 63(9):1317, 2000.
- [4] Thimothée Accadia, F Acernese, M Alshourbagy, P Amico, F Antonucci, S Aoudia, N Arnaud, C Arnault, KG Arun, P Astone, et al. Virgo: a laser interferometer to detect gravitational waves. *Journal of Instrumentation*, 7(03):P03012, 2012.
- [5] David G Blair, Eric J Howell, Li Ju, and Chunnong Zhao. *Advanced gravitational wave detectors*. Cambridge University Press, 2012.
- [6] AAe Abdo, Markus Ackermann, Marco Ajello, K Asano, William B Atwood, Magnus Axelsson, Luca Baldini, Jean Ballet, Guido Barbiellini, Matthew G Baring, et al. A limit on the variation of the speed of light arising from quantum gravity effects. *Nature*, 462(7271):331–334, 2009.

- [7] Fabrizio Tamburini, Carmine Cuofano, Massimo Della Valle, and Roberto Gilmozzi. No quantum gravity signature from the farthest quasars. *Astronomy & Astrophysics*, 533:A71, 2011.
- [8] Luis J Garay. Spacetime foam as a quantum thermal bath. *Physical Review Letters*, 80(12):2508, 1998.
- [9] Achim Kempf. On the three short-distance structures which can be described by linear operators. *Reports on Mathematical Physics*, 43(1-2):171–177, 1999.
- [10] Carlo Rovelli. Loop quantum gravity. *Living reviews in relativity*, 11:1–69, 2008.
- [11] Giovanni Amelino-Camelia. Gravity-wave interferometers as probes of a low-energy effective quantum gravity. *Physical Review D*, 62(2):024015, 2000.
- [12] Richard Lieu and Lloyd W Hillman. The phase coherence of light from extragalactic sources: Direct evidence against first-order planck-scale fluctuations in time and space. *The Astrophysical Journal*, 585(2):L77, 2003.
- [13] Roberto Ragazzoni, Massimo Turatto, and Wolfgang Gaessler. The lack of observational evidence for the quantum structure of spacetime at planck scales. *The Astrophysical Journal*, 587(1):L1, 2003.
- [14] C Lämmerzahl. Interferometry as a universal tool in physics. In *Planck Scale Effects in Astrophysics and Cosmology*, pages 161–198. Springer, 2005.
- [15] Claus Lämmerzahl. The search for quantum gravity effects. *Quantum Gravity: Mathematical Models and Experimental Bounds*, pages 15–39, 2007.
- [16] Mohsen Khodadi, Kouros Nozari, Anha Bhat, and Sina Mohsenian. Probing planck-scale spacetime by cavity opto-atomic rb interferometry. *Progress of Theoretical and Experimental Physics*, 2019(5):053E03, 2019.
- [17] Y Jack Ng, Wayne A Christiansen, and Henrik van Dam. Probing planck-scale physics with extragalactic sources? *The Astrophysical Journal*, 591(2):L87, 2003.
- [18] Leonard Mandel and Emil Wolf. *Optical coherence and quantum optics*. Cambridge university press, 1995.
- [19] DH Coule. Planck scale still safe from stellar images. *Classical and Quantum Gravity*, 20(14):3107, 2003.
- [20] LP Grishchuk. Graviton creation in the early universe. *Annals of the New York Academy of Sciences*, 302(1):439–444, 1977.
- [21] LP Grishchuk. The implications of microwave background anisotropies for laser-interferometer-tested gravitational waves. *Classical and Quantum Gravity*, 14(6):1445, 1997.
- [22] Leonid P Grishchuk. Relic gravitational waves and their detection. In *Gyros, Clocks, Interferometers...: Testing Relativistic Gravity in Space*, pages 167–192. Springer, 2001.
- [23] Leonid P Grishchuk. Discovering relic gravitational waves in cosmic microwave background radiation. *General Relativity and John Archibald Wheeler*, pages 151–199, 2010.
- [24] VA Rubakov, M Verjaskin Sazhin, and AV Veryaskin. Graviton creation in the inflationary universe and the grand unification scale. *Physics Letters B*, 115(3):189–192, 1982.
- [25] R Fabbri and MD Pollock. The effect of primordially produced gravitons upon the anisotropy of the cosmological microwave background radiation. *Physics Letters B*, 125(6):445–448, 1983.
- [26] Laurence F Abbott and Mark B Wise. Constraints on generalized inflationary cosmologies. *Nuclear physics B*, 244(2):541–548, 1984.

- [27] Bruce Allen. Stochastic gravity-wave background in inflationary-universe models. *Physical Review D*, 37(8):2078, 1988.
- [28] Varun Sahni. Energy density of relic gravity waves from inflation. *Physical Review D*, 42(2):453, 1990.
- [29] Hiroyuki Tashiro, Takeshi Chiba, and Misao Sasaki. Reheating after quintessential inflation and gravitational waves. *Classical and Quantum Gravity*, 21(7):1761, 2004.
- [30] Alfredo B Henriques. The stochastic gravitational-wave background and the inflation to radiation transition in the early universe. *Classical and Quantum Gravity*, 21(12):3057, 2004.
- [31] Wen Zhao and Yang Zhang. Relic gravitational waves and their detection. *Physical Review D*, 74(4):043503, 2006.
- [32] Michele Maggiore. Gravitational waves constrained. *Nature*, 447(7145):651–652, 2007.
- [33] <http://www.ligo.caltech.edu/>.
- [34] <http://www.ligo.caltech.edu/advLIGO/>.
- [35] SJ Waldman. The advanced ligo gravitational wave detector. *arXiv preprint arXiv:1103.2728*, 2011.
- [36] <http://www.virgo.infn.it/>.
- [37] Fausto Acernese, Paolo Amico, M Al-Shourbagy, S Aoudia, S Avino, D Babusci, G Ballardín, R Barillé, F Barone, L Barsotti, et al. Status of virgo. *Classical and Quantum Gravity*, 22(18):S869, 2005.
- [38] <http://www.geo600.uni-hannover.de/geocurves/>.
- [39] Benno Willke, Peter Aufmuth, Carsten Aulbert, Stanislav Babak, Ramachandran Balasubramanian, BW Barr, S Berukoff, Sukanta Bose, G Cagnoli, Morag M Casey, et al. The geo 600 gravitational wave detector. *Classical and Quantum Gravity*, 19(7):1377, 2002.
- [40] Jérôme Degallaix, Bram Slagmolen, Chunnong Zhao, Li Ju, and David Blair. Thermal lensing compensation principle for the aciga’s high optical power test facility test 1. *General Relativity and Gravitation*, 37:1581–1589, 2005.
- [41] Pablo Barriga, Chunnong Zhao, and DG Blair. Optical design of a high power mode-cleaner for aigo. *General Relativity and Gravitation*, 37:1609–1619, 2005.
- [42] K Kuroda, on behalf of the LCGT Collaboration, et al. Status of lcgt. *Classical and Quantum Gravity*, 27(8):084004, 2010.
- [43] M Punturo, M Abernathy, F Acernese, B Allen, Nils Andersson, K Arun, F Barone, B Barr, M Barsuglia, M Beker, et al. The einstein telescope: a third-generation gravitational wave observatory. *Classical and Quantum Gravity*, 27(19):194002, 2010.
- [44] S Hild, M Abernathy, F ea Acernese, P Amaro-Seoane, N Andersson, K Arun, F Barone, B Barr, M Barsuglia, M Beker, et al. Sensitivity studies for third-generation gravitational wave observatories. *Classical and Quantum gravity*, 28(9):094013, 2011.
- [45] Shane L Larson, William A Hiscock, and Ronald W Hellings. Sensitivity curves for spaceborne gravitational wave interferometers. *Physical Review D*, 62(6):062001, 2000.
- [46] Shane L Larson, Ronald W Hellings, and William A Hiscock. Unequal arm space-borne gravitational wave detectors. *Physical Review D*, 66(6):062001, 2002.
- [47] Jeff Crowder and Neil J Cornish. Beyond lisa: Exploring future gravitational wave missions. *Physical Review D*, 72(8):083005, 2005.
- [48] Neil J Cornish and Jeff Crowder. Lisa data analysis using markov chain monte carlo methods. *Physical Review D*, 72(4):043005, 2005.

- [49] Curt Cutler and Jan Harms. Big bang observer and the neutron-star-binary subtraction problem. *Physical Review D*, 73(4):042001, 2006.
- [50] Seiji Kawamura, Takashi Nakamura, Masaki Ando, Naoki Seto, Kimio Tsubono, Kenji Numata, Ryuichi Takahashi, Shigeo Nagano, Takehiko Ishikawa, Mitsuru Musha, et al. The japanese space gravitational wave antenna—decigo. *Classical and Quantum Gravity*, 23(8):S125, 2006.
- [51] Hideaki Kudoh, Atsushi Taruya, Takashi Hiramatsu, and Yoshiaki Himemoto. Detecting a gravitational-wave background with next-generation space interferometers. *Physical Review D*, 73(6):064006, 2006.
- [52] Gabriella Agazie, Akash Anumalapudi, Anne M Archibald, Zaven Arzoumanian, Paul T Baker, Bence Bécsy, Laura Blecha, Adam Brazier, Paul R Brook, Sarah Burke-Spolaor, et al. The nanograv 15 yr data set: Evidence for a gravitational-wave background. *The Astrophysical Journal Letters*, 951(1):L8, 2023.
- [53] J Antoniadis, S Babak, A-S Bak Nielsen, CG Bassa, A Berthereau, M Bonetti, E Bortolas, PR Brook, MARTA Burgay, RN Caballero, et al. The second data release from the european pulsar timing array-i. the dataset and timing analysis. *Astronomy & Astrophysics*, 678:A48, 2023.
- [54] Andrew Zic, Daniel J Reardon, Agastya Kapur, George Hobbs, Rami Mandow, Małgorzata Curyło, Ryan M Shannon, Jacob Askew, Matthew Bailes, ND Ramesh Bhat, et al. The parkes pulsar timing array third data release. *Publications of the Astronomical Society of Australia*, 40:e049, 2023.
- [55] Daniel J Reardon, Andrew Zic, Ryan M Shannon, George B Hobbs, Matthew Bailes, Valentina Di Marco, Agastya Kapur, Axl F Rogers, Eric Thrane, Jacob Askew, et al. Search for an isotropic gravitational-wave background with the parkes pulsar timing array. *The Astrophysical Journal Letters*, 951(1):L6, 2023.
- [56] Heng Xu, Siyuan Chen, Yanjun Guo, Jinchun Jiang, Bojun Wang, Jiangwei Xu, Zihan Xue, R Nicolas Caballero, Jianping Yuan, Yonghua Xu, et al. Searching for the nano-hertz stochastic gravitational wave background with the chinese pulsar timing array data release i. *Research in Astronomy and Astrophysics*, 23(7):075024, 2023.
- [57] G Hobbs. Gravitational wave detection using high precision pulsar observations. *Classical and Quantum Gravity*, 25(11):114032, 2008.
- [58] RN Manchester. The parkes pulsar timing array. *Chinese Journal of Astronomy and Astrophysics*, 6(S2):139, 2006.
- [59] Frederick A Jenet, George B Hobbs, W Van Straten, Richard N Manchester, Matthew Bailes, JPW Verbiest, Russell T Edwards, Aidan W Hotan, John M Sarkissian, and Stephen M Ord. Upper bounds on the low-frequency stochastic gravitational wave background from pulsar timing observations: Current limits and future prospects. *The Astrophysical Journal*, 653(2):1571, 2006.
- [60] Michael Kramer, DC Backer, JM Cordes, TJW Lazio, BW Stappers, and S Johnston. Strong-field tests of gravity using pulsars and black holes. *New Astronomy Reviews*, 48(11-12):993–1002, 2004.
- [61] AM Cruise. An electromagnetic detector for very-high-frequency gravitational waves. *Classical and Quantum Gravity*, 17(13):2525, 2000.
- [62] AM Cruise and Richard MJ Ingle. A correlation detector for very high frequency gravitational waves. *Classical and Quantum Gravity*, 22(10):S479, 2005.
- [63] AM Cruise and RMJ Ingle. A prototype gravitational wave detector for 100 mhz. *Classical and Quantum Gravity*, 23(22):6185, 2006.

- [64] Ming-Lei Tong and Yang Zhang. Detecting very-high-frequency relic gravitational waves by a waveguide. *Chinese Journal of Astronomy and Astrophysics*, 8(3):314, 2008.
- [65] Fang-Yu Li, Meng-Xi Tang, and Dong-Ping Shi. Electromagnetic response of a gaussian beam to high-frequency relic gravitational waves in quintessential inflationary models. *Physical Review D*, 67(10):104008, 2003.
- [66] Fangyu Li, Robert ML Baker Jr, Zhenyun Fang, Gary V Stephenson, and Zhenya Chen. Perturbative photon fluxes generated by high-frequency gravitational waves and their physical effects. *The European Physical Journal C*, 56:407–423, 2008.
- [67] ML Tong, Yang Zhang, and Fang-Yu Li. Using a polarized maser to detect high-frequency relic gravitational waves. *Physical Review D*, 78(2):024041, 2008.
- [68] Tomotada Akutsu, Seiji Kawamura, Atsushi Nishizawa, Koji Arai, Kazuhiro Yamamoto, Daisuke Tatsumi, Shigeo Nagano, Erina Nishida, Takeshi Chiba, Ryuichi Takahashi, et al. Search for a stochastic background of 100-mhz gravitational waves with laser interferometers. *Physical review letters*, 101(10):101101, 2008.
- [69] Matias Zaldarriaga and Uroš Seljak. All-sky analysis of polarization in the microwave background. *Physical Review D*, 55(4):1830, 1997.
- [70] Marc Kamionkowski, Arthur Kosowsky, and Albert Stebbins. Statistics of cosmic microwave background polarization. *Physical Review D*, 55(12):7368, 1997.
- [71] Brian Keating, Peter Timbie, Alexander Polnarev, and Julia Steinberger. Large angular scale polarization of the cosmic microwave background radiation and the feasibility of its detection. *The Astrophysical Journal*, 495(2):580, 1998.
- [72] Jonathan R Pritchard and Marc Kamionkowski. Cosmic microwave background fluctuations from gravitational waves: An analytic approach. *Annals of Physics*, 318(1):2–36, 2005.
- [73] Wen Zhao and Yang Zhang. Analytic approach to the cmb polarization generated by relic gravitational waves. *Physical Review D*, 74(8):083006, 2006.
- [74] TY Xia and Y Zhang. Approximate analytic spectra of reionized cmb anisotropies and polarization generated by relic gravitational waves. *Physical Review D*, 79(8):083002, 2009.
- [75] W Zhao and D Baskaran. Detecting relic gravitational waves in the cmb: Optimal parameters and their constraints. *Physical Review D*, 79(8):083003, 2009.
- [76] Neil Bevis, Mark Hindmarsh, Martin Kunz, and Jon Urrestilla. Fitting cosmic microwave background data with cosmic strings and inflation. *Physical Review Letters*, 100(2):021301, 2008.
- [77] Eiichiro Komatsu, J Dunkley, MR Nolta, CL Bennett, B Gold, G Hinshaw, N Jarosik, D Larson, M Limon, L Page, et al. Five-year wilkinson microwave anisotropy probe* observations: cosmological interpretation. *The Astrophysical Journal Supplement Series*, 180(2):330, 2009.
- [78] J Dunkley, Eiichiro Komatsu, MR Nolta, DN Spergel, D Larson, G Hinshaw, L Page, CL Bennett, B Gold, N Jarosik, et al. Five-year wilkinson microwave anisotropy probe* observations: Likelihoods and parameters from the wmap data. *The Astrophysical Journal Supplement Series*, 180(2):306, 2009.
- [79] N Jarosik, CL Bennett, J Dunkley, B Gold, MR Greason, M Halpern, RS Hill, G Hinshaw, A Kogut, Eiichiro Komatsu, et al. Seven-year wilkinson microwave anisotropy probe (wmap*) observations: sky maps, systematic errors, and basic results. *The Astrophysical Journal Supplement Series*, 192(2):14, 2011.
- [80] Gary Hinshaw, D Larson, Eiichiro Komatsu, David N Spergel, CLaa Bennett, Joanna Dunkley, MR Nolta, M Halpern, RS Hill, N Odegard, et al. Nine-year wilkinson microwave

anisotropy probe (wmap) observations: cosmological parameter results. *The Astrophysical Journal Supplement Series*, 208(2):19, 2013.

- [81] Planck Collaboration et al. The scientific programme of planck. *arXiv preprint astro-ph/0604069*, 2006.
- [82] <http://www.rssd.esa.int/index.php?project=Planck>.
- [83] A Suzuki, Peter AR Ade, Yoshiki Akiba, D Alonso, K Arnold, J Aumont, C Baccigalupi, D Barron, S Basak, S Beckman, et al. The litebird satellite mission: Sub-kelvin instrument. *Journal of Low Temperature Physics*, 193(5):1048–1056, 2018.
- [84] Michael D Niemack, Peter AR Ade, J Aguirre, F Barrientos, JA Beall, JR Bond, J Britton, HM Cho, S Das, MJ Devlin, et al. Actpol: a polarization-sensitive receiver for the atacama cosmology telescope. In *Millimeter, Submillimeter, and Far-Infrared Detectors and Instrumentation for Astronomy V*, volume 7741, pages 537–557. SPIE, 2010.
- [85] J Dunkley, A Amblard, C Baccigalupi, M Betoule, D Chuss, A Cooray, J Delabrouille, C Dickinson, G Dobler, J Dotson, et al. Prospects for polarized foreground removal. In *AIP Conference Proceedings*, volume 1141, pages 222–264. American Institute of Physics, 2009.
- [86] Marshall Harris Cohen. Introduction to very-long-baseline interferometry. *Proceedings of the IEEE*, 61(9):1192–1197, 1973.
- [87] Heino Falcke, Neil M Nagar, Andrew S Wilson, and James S Ulvestad. Radio sources in low-luminosity active galactic nuclei. ii. very long baseline interferometry detections of compact radio cores and jets in a sample of liners. *The Astrophysical Journal*, 542(1):197, 2000.
- [88] AB Pushkarev and YY Kovalev. Milky way scattering properties and intrinsic sizes of active galactic nuclei cores probed by very long baseline interferometry surveys of compact extragalactic radio sources. *Monthly Notices of the Royal Astronomical Society*, 452(4):4274–4282, 2015.
- [89] T An, BW Sohn, and H Imai. Capabilities and prospects of the east asia very long baseline interferometry network. *Nature Astronomy*, 2(2):118–125, 2018.
- [90] JC Algaba. High-frequency very long baseline interferometry rotation measure of eight active galactic nuclei. *Monthly Notices of the Royal Astronomical Society*, 429(4):3551–3563, 2013.
- [91] Freek Roelofs, Christian M Fromm, Yosuke Mizuno, Jordy Davelaar, Michael Janssen, Ziri Younsi, Luciano Rezzolla, and Heino Falcke. Black hole parameter estimation with synthetic very long baseline interferometry data from the ground and from space. *Astronomy & Astrophysics*, 650:A56, 2021.
- [92] Raúl Carballo-Rubio, Vitor Cardoso, and Ziri Younsi. Toward very large baseline interferometry observations of black hole structure. *Physical Review D*, 106(8):084038, 2022.
- [93] DW Pesce, JA Braatz, MJ Reid, AG Riess, D Scolnic, JJ Condon, F Gao, C Henkel, CMV Impellizzeri, CY Kuo, et al. The megamaser cosmology project. xiii. combined hubble constant constraints. *The Astrophysical Journal Letters*, 891(1):L1, 2020.
- [94] CY Kuo, James A Braatz, Mark J Reid, KY Lo, James J Condon, Caterina MV Impellizzeri, and Christian Henkel. The megamaser cosmology project. v. an angular-diameter distance to ngc 6264 at 140 mpc. *The Astrophysical Journal*, 767(2):155, 2013.
- [95] Shuo Cao, Xiaogang Zheng, Marek Biesiada, Jingzhao Qi, Yun Chen, and Zong-Hong Zhu. Ultra-compact structure in intermediate-luminosity radio quasars: building a sample of standard cosmological rulers and improving the dark energy constraints up to $z \sim 3$. *Astronomy & Astrophysics*, 606:A15, 2017.

- [96] Tonghua Liu, Ziqiang Liu, Jiamin Wang, Shengnan Gong, Man Li, and Shuo Cao. Revisiting friedmann-like cosmology with torsion: newest constraints from high-redshift observations. *arXiv preprint arXiv:2304.06425*, 2023.
- [97] Tonghua Liu, Shuo Cao, Marek Biesiada, Yilong Zhang, and Jieci Wang. Model-independent way to determine the hubble constant and the curvature from the phase shift of gravitational waves with decigo. *The Astrophysical Journal Letters*, 965(1):L11, 2024.
- [98] IH Park, K-Y Choi, J Hwang, S Jung, DH Kim, MH Kim, C-H Lee, KH Lee, SH Oh, M-G Park, et al. Stellar interferometry for gravitational waves. *Journal of Cosmology and Astroparticle Physics*, 2021(11):008, 2021.
- [99] Michalis Lagouvardos and Charis Anastopoulos. Gravitational decoherence of photons. *Classical and Quantum Gravity*, 38(11):115012, 2021.
- [100] Fateme Shojaei Arani, Malek Bagheri Harouni, Brahim Lamine, and Alain Blanchard. Sensing quantum nature of primordial gravitational waves using electromagnetic probes. *Physica Scripta*, 2023.
- [101] Brahim Lamine, Rémy Hervé, Astrid Lambrecht, and Serge Reynaud. Ultimate decoherence border for matter-wave interferometry. *Physical review letters*, 96(5):050405, 2006.
- [102] Sugumi Kanno, Jiro Soda, and Junsei Tokuda. Noise and decoherence induced by gravitons. *Physical Review D*, 103(4):044017, 2021.
- [103] Ming-Lei Tong, Yang Zhang, Wen Zhao, Jin-Zhong Liu, Cheng-Shi Zhao, and Ting-Gao Yang. Using pulsar timing arrays and the quantum normalization condition to constrain relic gravitational waves. *Classical and Quantum Gravity*, 31(3):035001, 2013.
- [104] Minglei Tong. Revisit relic gravitational waves based on the latest cmb observations. *Classical and Quantum Gravity*, 29(15):155006, 2012.
- [105] Y Zhang, ML Tong, and ZW Fu. Constraints upon the spectral indices of relic gravitational waves by ligo s5. *Physical Review D*, 81(10):101501, 2010.
- [106] Ming-Lei Tong and Yang Zhang. Relic gravitational waves with a running spectral index and its constraints at high frequencies. *Physical Review D*, 80(8):084022, 2009.
- [107] Yashar Akrami, Frederico Arroja, M Ashdown, J Aumont, Carlo Baccigalupi, M Ballardini, Anthony J Banday, RB Barreiro, Nicola Bartolo, S Basak, et al. Planck 2018 results-x. constraints on inflation. *Astronomy & Astrophysics*, 641:A10, 2020.
- [108] Alexei A Starobinsky. A new type of isotropic cosmological models without singularity. *Physics Letters B*, 91(1):99–102, 1980.
- [109] HX Miao and Yang Zhang. Analytic spectrum of relic gravitational waves modified by neutrino free streaming and dark energy. *Physical Review D*, 75(10):104009, 2007.
- [110] Planck Collaboration, N Aghanim, Y Akrami, MIR Alves, M Ashdown, J Aumont, C Baccigalupi, M Ballardini, AJ Banday, RB Barreiro, et al. Planck 2018 results. *A&A*, 641:A12, 2020.
- [111] Jerome Martin and Christophe Ringeval. First cmb constraints on the inflationary reheating temperature. *Physical Review D*, 82(2):023511, 2010.
- [112] Sean Bailly, Ki-Young Choi, Karsten Jedamzik, and Leszek Roszkowski. A re-analysis of gravitino dark matter in the constrained mssm. *Journal of High Energy Physics*, 2009(05):103, 2009.
- [113] Minglei Tong. Relic gravitational waves in the frame of slow-roll inflation with a power-law potential, and their detection. *Classical and Quantum Gravity*, 30(5):055013, 2013.
- [114] LP Grishchuk. Quantum effects in cosmology. *Classical and Quantum Gravity*, 10(12):2449, 1993.

- [115] Jérôme Martin and Vincent Vennin. Quantum discord of cosmic inflation: Can we show that cmb anisotropies are of quantum-mechanical origin? *Physical Review D*, 93(2):023505, 2016.
- [116] Viatcheslav F Mukhanov. *Physical foundations of cosmology*. Cambridge university press, 2005.
- [117] Michele Maggiore. *Gravitational waves: Volume 1: Theory and experiments*. OUP Oxford, 2007.
- [118] Yang Zhang, XinZhong Er, TianYang Xia, Wen Zhao, and HaiXing Miao. An exact analytic spectrum of relic gravitational waves in an accelerating universe. *Classical and Quantum Gravity*, 23(11):3783, 2006.
- [119] Ling-An Wu, HJ Kimble, JL Hall, and Huifa Wu. Generation of squeezed states by parametric down conversion. *Physical review letters*, 57(20):2520, 1986.
- [120] Girish S Agarwal. *Quantum optics*. Cambridge University Press, 2012.
- [121] Jérôme Martin, Amaury Micheli, and Vincent Vennin. Discord and decoherence. *Journal of Cosmology and Astroparticle Physics*, 2022(04):051, 2022.
- [122] Yang Zhang, Yefei Yuan, Wen Zhao, and Ying-Tian Chen. Relic gravitational waves in the accelerating universe. *Classical and Quantum Gravity*, 22(7):1383, 2005.
- [123] Nabila Aghanim, Yashar Akrami, Mark Ashdown, J Aumont, C Baccigalupi, M Ballardini, AJ Banday, RB Barreiro, N Bartolo, S Basak, et al. Planck 2018 results-vi. cosmological parameters. *Astronomy & Astrophysics*, 641:A6, 2020.
- [124] Francesco Coradeschi, Antonia Micol Frassino, Thiago Guerreiro, Jennifer Rittenhouse West, and Enrico Junior Schioppa. Can we detect the quantum nature of weak gravitational fields? *Universe*, 7(11):414, 2021.
- [125] C Anastopoulos and BL Hu. A master equation for gravitational decoherence: probing the textures of spacetime. *Classical and Quantum Gravity*, 30(16):165007, 2013.
- [126] Luca Abrahao, Francesco Coradeschi, Antonia Micol Frassino, Thiago Guerreiro, Jennifer Rittenhouse West, and Enrico Junior Schioppa. The quantum optics of gravitational waves. *Classical and Quantum Gravity*, 41(1):015029, 2023.
- [127] Belinda Pang and Yanbei Chen. Quantum interactions between a laser interferometer and gravitational waves. *Physical Review D*, 98(12):124006, 2018.
- [128] Markus Aspelmeyer, Tobias J Kippenberg, and Florian Marquardt. Cavity optomechanics. *Reviews of Modern Physics*, 86(4):1391, 2014.
- [129] S Bose, K Jacobs, and PL Knight. Preparation of nonclassical states in cavities with a moving mirror. *Physical Review A*, 56(5):4175, 1997.
- [130] Thiago Guerreiro. Quantum effects in gravity waves. *Classical and Quantum Gravity*, 37(15):155001, 2020.
- [131] Liju Philip. Calibration and wide field imaging with paper: a catalogue of compact sources. 2016.
- [132] Marlan O Scully and M Suhail Zubairy. *Quantum optics*, 1999.
- [133] Marlan O Scully and M Suhail Zubairy. *Quantum optics*. Cambridge university press, 1997.
- [134] Tonghua Liu, Xiyang Yang, Zisheng Zhang, Jieci Wang, and Marek Biesiada. Measurements of the hubble constant from combinations of supernovae and radio quasars. *Physics Letters B*, 845:138166, 2023.
- [135] Tonghua Liu, Shuo Cao, Shuai Ma, Yuting Liu, Chenfa Zheng, and Jieci Wang. What are recent observations telling us in light of improved tests of distance duality relation? *Physics Letters B*, 838:137687, 2023.

- [136] Matthieu Tristram, Anthony J Banday, Krzysztof M Górski, Reijo Keskitalo, CR Lawrence, Kristian Joten Andersen, R Belén Barreiro, J Borrill, LPL Colombo, HK Eriksen, et al. Improved limits on the tensor-to-scalar ratio using bicep and p l a n c k data. *Physical Review D*, 105(8):083524, 2022.
- [137] J Antoniadis, P Arumugam, S Arumugam, S Babak, M Bagchi, A-S Bak Nielsen, CG Bassa, A Bathula, A Berthereau, M Bonetti, et al. The second data release from the european pulsar timing array-iv. implications for massive black holes, dark matter, and the early universe. *Astronomy & Astrophysics*, 685:A94, 2024.
- [138] Jerome Martin, Christophe Ringeval, and Vincent Vennin. How well can future cmb missions constrain cosmic inflation? *Journal of Cosmology and Astroparticle Physics*, 2014(10):038, 2014.
- [139] CP Burgess, R Holman, Greg Kaplanek, Jérôme Martin, and Vincent Vennin. Minimal decoherence from inflation. *Journal of Cosmology and Astroparticle Physics*, 2023(07):022, 2023.
- [140] DJ Fixsen. The temperature of the cosmic microwave background. *The Astrophysical Journal*, 707(2):916, 2009.
- [141] Yuki Watanabe and Eiichiro Komatsu. Improved calculation of the primordial gravitational wave spectrum in the standard model. *Physical Review D*, 73(12):123515, 2006.
- [142] Wolfgang P Schleich, Marlan Scully, et al. General relativity and modern optics. *Tendances actuelles en physique atomique= new trends in atomic physics*, 1982:995–1124, 1984.
- [143] Kip S Thorne, Charles W Misner, and John Archibald Wheeler. *Gravitation*. Freeman San Francisco, 2000.
- [144] Donato Bini, Pierluigi Fortini, Andrea Geralico, Maria Haney, and Antonello Ortolan. Light scattering by radiation fields: The optical medium analogy. *Europhysics Letters*, 102(2):20006, 2013.
- [145] Viatcheslav Mukhanov and Sergei Winitzki. *Introduction to quantum effects in gravity*. Cambridge university press, 2007.